The Role of Age and Model Severity on Cortical Vascular Response Following Traumatic Brain Injury

Thomas R. Brickler

Dissertation submitted to the faculty of the Virginia Polytechnic Institute and State University in partial fulfillment of the requirements for the degree of

Doctor of Philosophy

in

Biomedical and Veterinary Sciences

Michelle H. Theus, Chair

Willard H. Eyestone

John H. Rossmeisl

John B. Matson

April 26, 2017

Blacksburg, Virginia

Keywords: traumatic brain injury, arteriole vessels,

Angiopoietin, endothelial cell, blood brain barrier, juvenile TBI

The Role of Age and Model Severity on Cortical Vascular Response Following Traumatic Brain Injury

Thomas R. Brickler

Abstract

Traumatic brain injury (TBI) is a growing health concern worldwide that affects a broad range of the population. As TBI is the leading cause of disability and mortality in children, several pre-clinical models have been developed using rodents at a variety of different ages; however, key brain maturation events are overlooked that leave some age groups more or less vulnerable to injury. Thus, there has been a large emphasis on producing relevant animal models to elucidate molecular pathways that could be of therapeutic potential to help limit neuronal injury and improve behavioral outcome. TBI involves a host of different biochemical events, including disruption of the cerebral vasculature and breakdown of the blood brain barrier (BBB) that exacerbate secondary injuries. A better of understanding of the mechanism(s) underlying cerebral vascular regulation will aid in establishing more effective treatment strategies aimed at improving cerebral blood flow restoration and preventing further neuronal loss. Our studies reveal an age-at- injury dependence on the Angiopoetin-Tie2 axis, which mediates neuroprotection in a model of juvenile TBI following cortical controlled impact (CCI) that is not seen in adult mice. The protection observed was mediated, in part, by the microvascular response to CCI injury and prompted further detailed analysis of the larger arteriole network across several mouse strains and models of TBI. Our second study revealed both a model and species dependent effect on a specialized network of arteriole vessels, called collaterals after trauma. We demonstrated that a repetitive mild TBI (rmTBI) can induce collateral remodeling in C57BL/6 but not CD1 mice; however, CCI injury had no effect on collateral changes in either strain. Together, these findings demonstrate an age-dependent and

species/model dependent effect on vascular remodeling that highlights the importance of individualized therapeutics to TBI.

General Audience Abstract

Traumatic brain injury (TBI) is the most frequent cause of death in adults and children in the developed world and children are at the greatest risk of injury. In the United States alone there is a reported incidence of 1.7 million injuries a year and about half of these injuries are to children. Patients that survive TBI experience long-term neurological disabilities as there is not an effective treatment available. While the initial brain trauma cannot be treated, preventing further damage of delayed secondary responses of injury has garnered attention from researchers to better understand how the injury progresses. In order to mimic TBI in the lab, scientist use animal models of TBI to better understand the mechanism(s) involved in injury with the purpose of creating pharmacological targets to mitigate the effects of further tissue damage. While there are many cell types within the brain that are affected after TBI, our studies focus on endothelial cells that line the vascular system and allow for the circulatory function of blood to supply energy to the neurons of the brain. Our mouse model mimics the effects of sustaining a focal brain injury and we are interested in how the juvenile brain responds to this injury. We have found that juvenile mice are better protected after brain injury as they have less tissue damage compared to adult mice and we attribute this protection to better blood vessel numbers and function. While we observed changes to the vascular network in the juvenile model, this prompted studies to focus on other models of TBI to understand how blood vessels respond to a concussive-like injury. In these studies, we found that a particular species of mouse and the less severe injury prompted a special type of blood vessels to increase their diameter that was not seen in the more severe model of TBI. Taken together our findings demonstrate an age-dependent and species/model dependent effect on blood vessel remodeling.

Dedication

I would like to dedicate this dissertation to my parents, my brother Tyler, and Blake who have taught me the most about loving, thinking, learning, and living.

Acknowledgements

I feel blessed and honored to be at the point where I can thank others for the great success that has befallen on me so far and continues as I pursue my love of science.

Dr. Laurence Daheron, I have deep admiration for you as a scientist with great knowledge that you are able to share in an intense lab that always feels laid back and conducive to learning. Your wisdom and concern for me has been like an invisible hand always guiding and providing curiosity as I pursue my studies. Thank you for all you have done and continue to do as I advance in science.

The synergy of team lab work under the guise of directed leadership allows discovery and knowledge regardless of results. There is always a result and something to be learned from every experiment. One thing I have learned throughout my life in academia is that the association of and comradery of scientific friendships and teams can excel one to great works and discoveries that would be difficult to accomplish alone. My committee, comprised of Dr. Will Eyestone, Dr. John Rossmeisl, and Dr. John Matson, has worked in synergy and made the scientific process not only more rapidly successful, but fun in the group process of experimentation.

To the Theus Lab, we are a team where results positive and negative can be shared together and provides a stronger direction to the common goal. It was a privilege to be a part of this team and we should all work to the success we had with any future team we work with.

Dr. Michelle Theus, when I came to Virginia Tech, it was an exciting opportunity to once again enter academia with a purpose, a job, and an eye to the future. Honestly, I was anxious and inquisitive on how this would all work out. Dr. Theus, you literally understood my passion and drive as a scientist and was able to foster and nurture my convictions to a meaningful and understandable method of scientific study. Whenever I am in lab and feel stressed or tired from

working a long day, I think of you as a devoted scientist, wife, mother, and professor and somehow it all seems fine. Your ability to have a plan, build on it, and discover new opportunities will no doubt keep VT rich in future grants. You have been instrumental in helping me as a student and person. I am forever thankful for that.

Table of Contents

Attributions

This dissertation represents an original body of work by Thomas R. Brickler. The roles of co-authors and collaborators in this research are described below.

Chapter 2 is based on a manuscript co-authored with Amanda Hazy, Xia Wang, Stefanie Robel, and Michelle H. Theus: "An Age-dependent Role of the Angiopoeitin-Tie2 Axis in Endothelial Cells Following Traumatic Brain Injury," in preparation for submission.

Amanda Hazy is a graduate student in biomedical and veterinary sciences at Virginia Tech University in the lab of Michelle Theus. She assisted in data collection, specifically helping with behavioral experiments, tail vein injections, and experimental design/ data collection for qPCR.

Xia Wang is the laboratory technician of Michelle Theus' lab at Virginia Tech University. She has helped with data collection and helping with mouse work.

Stefanie Robel, Ph.D. is an Assistant Professor at the School of Neuroscience at Virginia Tech University. She helped with data collection, specifically imaging $GFAP^+$ brain slides and helping with data interpretation.

Michelle H. Theus, Ph.D. is an Assistant Professor in the department of Biomedical Sciences and Pathobiology at Virginia Tech University. She participated in study design, data acquisition and analysis, data interpretation, critical review and revision of the manuscript.

Chapter 3 is based on a manuscript co-authored with Kisha Gresham, Alexander Winemiller, Stefanie Robel, and Michelle H. Theus: "Model and Strain-Dependent Effects on Adult Cerebral Pial Collateral Remodeling Following Traumatic Brain Injury," in preparation for submission.

Kisha Gresham is a graduate student in translational biology, medicine and health program at Virginia Tech University in the lab of Michelle Theus. She assisted in data collection, specifically helping with imaging and data analysis of astrocyte reactivity.

Alexander Winemiller was an undergraduate student at Virginia Tech University and worked in the lab of Stefanie Robel at the time of data collection. He assisted in data acquisition specifically helping with the weight drop model.

Stefanie Robel, Ph.D. is an Assistant Professor at the School of Neuroscience at Virginia Tech University. She helped with study design, helping with the weight drop model, and data interpretation.

Michelle H. Theus, Ph.D. is an Assistant Professor in the department of Biomedical Sciences and Pathobiology at Virginia Tech University. She participated in study design, data acquisition and analysis, data interpretation, critical review, and revision of the manuscript.

Chapter 4 is based on a manuscript co-authored with Kisha Gresham, Irving C. Allen, Armand Meza, Sheryl Coutermarsh-Ott, Tere M. Williams, Daniel E. Rothschild and Michelle H. Theus: "Non-essential role for the NLRP1 Inflammasome Complex Following Traumatic Brain Injury," published in Mediators of Inflammation.

Kisha Gresham is a graduate student in translational biology, medicine and health program at Virginia Tech University in the lab of Michelle Theus. She assisted in data collection.

Irving C. Allen, Ph.D. is an Assistant Professor in the department of Biomedical Sciences and Pathobiology at Virginia Tech University. He participated in study design, data acquisition and analysis, data interpretation, critical review, and revision of the manuscript.

Armand Meza was an undergraduate student at Virginia Tech University and worked in the lab of Irving C. Allen at the time of data collection. He assisted in data acquisition.

Sheryl Coutermarsh-Ott, DVM, DACVP is a graduate student in biomedical and veterinary sciences at Virginia Tech University in the lab of Irving C. Allen. She assisted in data collection and interpretation.

Tere M. Williams was a graduate student in biomedical and veterinary sciences at Virginia Tech University in the lab of Irving C. Allen. She assisted in data collection and interpretation.

Daniel E. Rothschild is a graduate student in biomedical and veterinary sciences at Virginia Tech University in the lab of Irving C. Allen. He assisted in data collection and interpretation.

Michelle H. Theus, Ph.D. is an Assistant Professor in the department of Biomedical Sciences and Pathobiology at Virginia Tech University. She participated in study design, data acquisition and analysis, data interpretation, critical review and revision of the manuscript.

Overview of Dissertation

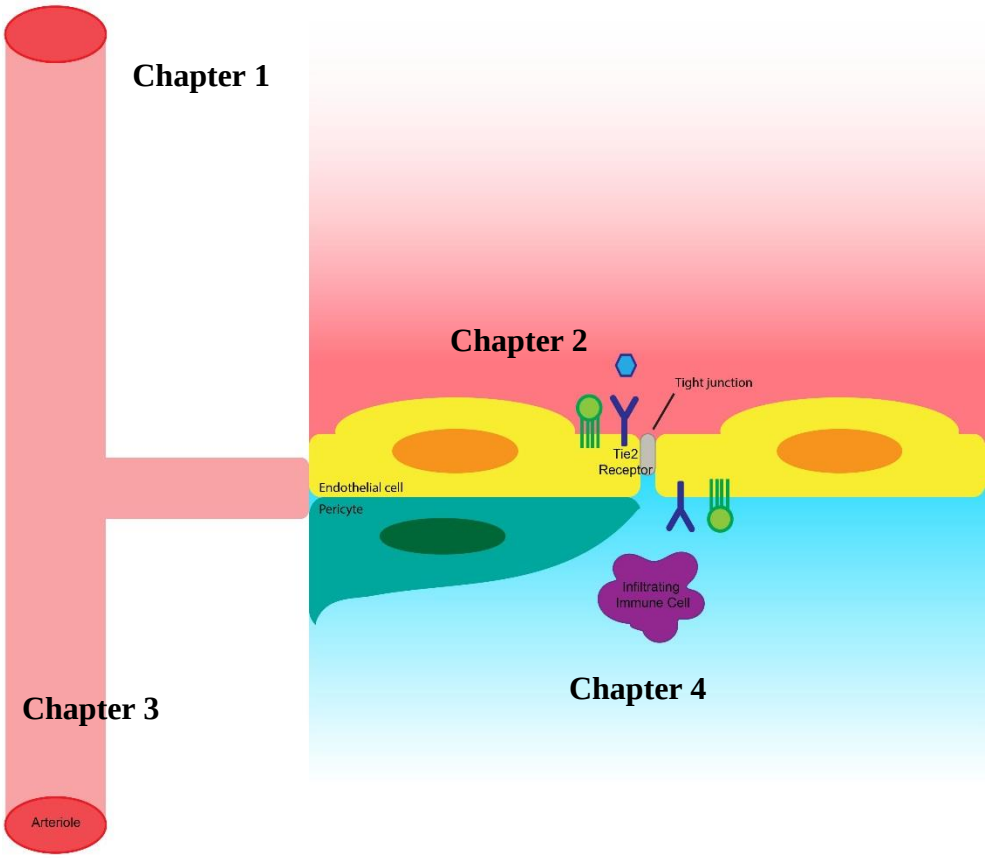

Figure 1. Schematic of the brain's arteriole vessels down to the microvasculature represented by individual endothelial cells (ECs) that are surrounded by pericytes. ECs express the Tie2 receptor and tight junction proteins, which help regulate EC survival and blood brain barrier (BBB) integrity, respectively. After traumatic brain injury (TBI), immune cells can enter brain tissue and a prolonged inflammatory response interferes with repair mechanisms complicating the recovery process. This dissertation explores the role of an age-dependent response of the vasculature following cortical controlled impact (CCI) injury, the vasculature's response following different severities of TBI, and the role of the innate immune system after CCI injury. **Chapter 1** will serve as an overview of the vascular system, particularly focusing in on the arteriole network and what happens to the neural vascular unit (NVU) after different models of

TBI. **Chapter 2** focuses on an age-specific response of the vasculature following cortical controlled impact (CCI) injury. We show that juvenile postnatal day 21 mice have significantly less cortical tissue loss compared to adult mice 4 days after CCI injury. To begin to elucidate the acute repair mechanisms that may play a role in tissue protection in the juvenile brain, we began to investigate the vascular response. We found acute restoration of cerebral blood flow (CBF) to the area of injury in juvenile mice. To determine next what may be contributing to this increase in CBF we assessed the diameter and density of the arteriole collateral network and the microvasculature (MV). We found an increase in diameter of surface pial collateral vessels and a greater density of the MV in juvenile CCI-injured mice compared to adult CCI-injured mice. We also observed that the microvessels in juvenile CCI-injured mice appeared healthier and more intact compared to adult CCI-injured mice, which prompted us to investigate infiltrating immune cells within the peri-lesion and BBB permeability. We found that adult CCI-injured mice had an increase in $CD11b^+$ immune cells within the peri-lesion and greater BBB permeability assessed by Evan's Blue extravasation compared to juvenile CCI-injured mice. Gene expression analysis using qPCR shows an increase in Angiopoietin- 1 (Ang-1) expression in juvenile CCI-injured mice. Interfering with the Ang/Tie2 signaling cascade using Tie2-Fc soluble proteins attenuated the neuroprotection seen in juvenile mice suggesting a direct role of the endothelial cell Angiopoietin-Tie2 axis in tissue protection. While we observed pial arteriole collateral remodeling following CCI-injury in the juvenile brain (Chapter 2), **Chapter 3** begins to investigate the role of arteriole vessels in two different strains of adult mice, CD1 and C57BL/6, by assessing the collateral response following either CCI-injury or the mild repetitive injury using the weight drop model. We found that CCI-injury resulted in impaired collateral remodeling in both strains that correlated with no changes in CBF or tissue protection. In

contrast, the mild repetitive injury resulted in collateral remodeling in the C57BL/6 strain, but not in the CD1 strain suggesting a strain- dependent and model- dependent response of the collateral network. **Chapter 4** focuses on inflammation of the brain by specifically looking at the role of the innate immune response after CCI-injury. This study was prompted by the findings of chapter 2, which showed an increase in infiltrating immune cells after CCI-injury in adult mice, which may contribute to BBB permeability and tissue loss. Recently, the NLR inflammasome has been shown to become activated after TBI causing the release of IL-Iβ. To test whether the inflammasome contributes to acute TBI neuronal tissue loss we assessed IL-1β, IL-18, and IL-6 expression in Nlrp1 Knockout, ASC knockout and wild type mice. Although we see attenuation of IL-1β in both our knockout mice, there is no difference in lesion volume compared to wild type mice suggesting that the inflammasome does not significantly contribute to acute neural injury.

Chapter 1: Literature Review

Traumatic Brain Injury

Traumatic brain injury (TBI) is a debilitating neurological condition associated with long-term consequences that affect 1.7 million people annually in the United States with a cost of care estimated around 76 billion dollars and rising (*1-5*). While the general population is at risk for injury, gender and age increase the risk potential for sustaining a TBI (*3, 6, 7*). Males have a threefold higher mortality rate from head trauma compared to females and the incidence of TBI is disproportionately high in the juvenile population (*6-8*). While there is a vast spectrum of neuropathologies associated with TBI, 80% of all TBIs reported in the clinic are categorized as mild or concussive injuries (*9-12*). An initial external mechanical force (blast waves, direct impact, or penetration) to the brain, initiates a complex cascade of pathophysiological responses including axonal and cellular damage, disruption of blood flow leading to hypoxia and ischemia, inflammation, release of excitatory amino acids and intracellular stores of calcium, as well as the generation of oxygen free radicals (*13-18*). These responses result in chronic neuronal damage and dysfunction (*19, 20*). While the severity of the initial trauma is linked to disability and mortality rate, most mild TBI (mTBI) patients suffer long-term disabilities (*21-25*). Cognitive dysfunction that persists for months to years after the initial insult is one of the many devastating consequences of TBI (*21-25*). Over time, subtle neurobehavioral deficits in memory and attention can decline, while most motor functions improve (*26-28*). Recently, there have been several studies that have established TBI as a risk factor for sustaining another head injury and new evidence suggests successive head injuries (repetitive mild traumatic brain injury (rmTBI)) have been linked to neurodegenerative diseases such as Alzheimer's Disease (AD) (*9, 15, 21, 29-32*).

Clinicians rely heavily on computed tomography (CT) angiography scans to help better diagnose the severity of head trauma by observing changes in cerebral blood flow (CBF). A significant number of patients that immediately (up to six hours post-injury) come into the clinic after having sustained a head injury have depressed levels of CBF, dropping dangerously to levels almost half of non-injured brains (*4, 33, 34*). While continued depressed levels of CBF can lead to a poor prognosis, restoration of CBF can be linked to improvements in neurological recovery (*35, 36*). Another pathological hallmark of TBI that also has an impact on neurological recovery is the extent of edema (*37-39*). Edema can be caused by cellular swelling, which is initiated by water accumulation in the cell (*40, 41*). Normally in neurons, astrocytes, and endothelial cells, sodium (Na^+) enters in and out of the cell by passive transport through the sodium potassium pump (*42-45*). To prevent an influx of Na^+ and water, the cause of cell swelling, energy dependent (ATP) elimination of Na^+ is required (*49, 52*). After TBI, there is an abundance of Na^+ ions that can enter cells, increasing their water content (*49-50*). The underlying ischemia depletes the energy-dependent function of the pump and the build-up of Na^+ ions causes the cells to swell (*49-52*). Another cause of edema can be directly linked to the breakdown of the blood brain barrier (BBB) (*45-47*). The precise mechanisms of BBB breakdown will be discussed later; however, in short, impairment of the BBB after TBI causes an uncontrolled influx of albumin and other plasma proteins that usually cannot cross the barrier to enter the brain. As cellular space is limited in the brain, these plasma proteins increase the net volume of the brain, which causes the brain to swell (*48, 49*).

TBI is a heterogeneous injury, which makes it difficult to treat. There have been multiple phase III clinical trials to help prevent or reduce secondary injury (excitotoxicity, inflammation, apoptosis); however, there is still no effective treatment for TBI (*50-53*). While there are

multifarious factors as to why no one clinical trial has produced a cure, the failures of these clinical trials has put a large emphasis and skepticism on relevant animal models of TBI. For example, while progesterone administration after TBI was seen to reduce edema and tissue damage in rats, these same findings were not observed in clinical trials of the hormone (*54, 55*). In addition, while animal models have been instrumental in elucidating particular pathways involved during the process of secondary injuries, such as interfering with the aquaporin-4 receptor to limit cerebral edema, pharmacological development is lacking (*39, 56*). The vast spectrum of pathologies seen in the clinic with human TBI also highlight challenges of creating clinically relevant animal models that help replicate the complexity of the disease, proving multiple models need to be utilized. The focus of this review is to evaluate three established TBI models, weight drop, cortical controlled impact (CCI), and repetitive mild TBI (rmTBI) and how these models influence cerebrovascular injury and recovery (Figure, 1).

The Cerebrovascular Network

In humans, the brain receives blood from two sources: the internal carotid arteries and the vertebral arteries (*57-60*). The vertebral arteries from the two hemispheres connect to form the basilar artery on the ventral surface of the brain while the internal carotid artery branches to form two major cerebral arteries, the anterior cerebral artery (ACA) and the middle cerebral artery (MCA) (*60-62*). The internal carotid artery and the basilar artery join in an arterial ring to form the circle of Willis, which further supplies blood to the brain (*63-66*). The structure of the circle of Willis is advantageous and important for the brain to continue to receive blood flow if a major artery becomes blocked (*63, 64*). The blood vessels in the brain are further broken down into two main categories of vessels: the large feeding arteries such as the MCA, ACA, and large penetrating arteries that enter the brain parenchyma within Virchow-Robin space and are classified as

extraparenchymal vessels (*67, 68*). The blood vessels that start where the Virchow-Robin space end are called intraparenchymal vessels (*68-70*). As the arterioles move deeper into the brain, the vessels become progressively smaller and are termed cerebral capillaries (*71-73*). These capillaries are lined by endothelial cells (ECs) and allow for an interface of communication to the neighboring neurons (*71-73*). Approximately 30-40% of the blood's oxygen passes into the brain parenchyma from small arteries, arterioles, and capillaries to fuel cerebral metabolism (*69*).

Unlike other cell types in the body like myoblasts that can store carbohydrates for later energy consumption, neurons do not have the capacity to internally store sugars, thus they are dependent on a continuous blood supply (*74*). The constant source of energy (oxidative phosphorylation of glucose) derived from blood is used by neurons through the hydrolysis of adenosine triphosphate (ATP) to maintain resting potentials, facilitate action potentials, and help restore ionic concentrations after synaptic transmission *(69)*. Thus, there is a tight association between neural activity and CBF; any fluctuations in CBF can cause an immediate energy shortage for neurons and cease functioning of ATP that may lead to irreversible damage to the neuron *(69)*.

The Blood Brain Barrier

In contrast to other organs, the brain's vascular network is lined with endothelial cells (ECs) that are tightly coupled together to provide a physical barrier from the circulatory system called the blood brain barrier (BBB) *(101-105)*. The belief that the BBB is a static structure in charge of protecting the brain from the rest of the body is partly false as the BBB acts as a dynamic interface between blood and neuronal tissue (*75-78*). As part of this physical barrier, numerous transmembrane and membrane-associated cytoplasmic proteins called tight junctions (TJ), assemble multimolecular complexes between adjacent ECs which regulate transport from the

blood to the brain. TJs comprise a number of proteins, including occludins, claudins, and junctional adhesions molecules (JAMs) that help regulate BBB permeability based on their structural organization (*79-83*). TJ proteins are expressed early in brain development, as early as 14 weeks of gestation in human brain capillaries, helping form the integrity of the BBB to be fully formed by birth (*84*). In the mouse, TJ proteins can be identified as early as embryonic day 14-17 and deletion or disruption of TJ protein, claudin-5, in mouse studies results in a leaky BBB (*84, 85*). Transcellular transport of molecules is also regulated by mural cells that ensheathe and stabilize ECs and help regulate blood flow in the brain. These mural cells act as a second barrier behind ECs and help guide astrocyte endfeet onto blood vessels (*45, 86-88*).

Astrocytic endfeet contact mural cells and are closely apposed to the outer endothelium *(119)*. These special astrocyte processes help regulate electrolyte/water balance and protein transport through the expression of aquaporin-4 and glucose transporter-1 (Glut-1), respectively through the BBB (*89-92*). As cues for vasodilation and vasoconstriction (calcium and nitric oxide) are released by astrocytes onto blood vessels, astrocytes are highly synchronized within the NVU and communicate with one another and the perivascular cells through gap junction proteins (connexin (Cx) 30 and 43) (*93-97*). In addition to controlling hemodynamic changes at the capillary level, astrocytes also regulate the function of the BBB. Important growth factors such a basic fibroblast growth factor (bFGF) and angiopoietin-1 (Ang-1) are constitutively secreted by astrocytes to help maintain BBB integrity by promoting EC survival and promoting TJ function (*98-101*). Physical disruption of astrocytes in cases of gliomas or targeted deletion/interference of gap junction proteins leads to BBB permeability (*102*). There are many dyes, such as Evan's Blue that bind to plasma proteins and immunohistochemical techniques such as IgG staining that bind to albumin, that can be used to quantitate the extent of BBB permeability (*103, 104*). Normally

plasma proteins and albumin cannot cross the BBB, so presence of these factors through the visualization of dyes and staining can help quantitate the extent of BBB damage (*103, 104*).

In an inflammatory state, the TJs between ECs may be opened to allow entrance of mononuclear cells (*105*). Microglia, the resident immune cells of the brain, play an important role in innate immune activation in the brain (*106*). The role of microglia in maintaining or interfering with BBB integrity in ischemia is not fully understood, but recent studies have shown that blocking microglial activation helps to keep the BBB from further breaking down (*106*).

The unifying structural component to all of all these vessel types is a monolayer of cells called endothelial cells (ECs). ECs are not passive barriers but are highly dynamic cells that can sense and respond to changes in the brain microenvironment (*107*). As blood pulsates through vessels, ECs experience mechanical forces such as fluid shear stress (FSS) and hemodynamic forces that cause ECs to release factors which aid in constriction or dilation (*108*). Mechanical forces such as FSS can influence EC gene expression patterns on the transcriptional level, changing EC phenotype to reorient their axis according to the direction of flow (*107, 108*).

The Arteriole Collateral Network

The circle of Willis is the largest collateral pathway and an important adaptation in the brain to prevent cerebral ischemia as the structure can help re-route blood flow following obstruction (*61, 66, 109-111*). Collateral vessels are arteriole- to- arteriole anastomoses that interconnect major arterial trees and are critical in maintaining regional CBF upon reduction of cerebral perfusion (*57, 111-113*). Under physiological conditions, collateral-specific ECs experience zero net flow across the vessel surface because of equal pressure gradients on each side of the vessel (*113, 114*). However, narrowing or occlusion of the feeding vessels increases

FSS and this increase in blood pressure within the vessel causes ECs to proliferate to adjust to the change in pressure (*107*). The process of EC proliferation that causes an overall remodeling of the collateral vessel is called arteriogenesis. (*113-115*).

Understanding the adaptive process of arteriogenesis, the growth of pre-existing collaterals is crucial in treating a host of vascular occlusive diseases as evidence shows that the status of collateral vessels is linked to better recovery in ischemic stroke (*113, 115-117*). Improvements in arteriogenesis correlate with early tissue protection as the remodeled arterioles are able to supply blood from outside the area of occlusion to surrounding tissue. Arteriole vessels also carry ten times more blood volume compared to capillaries (*57, 118*). While evidence of arteriogenesis exists in models of stroke (*61, 113, 116, 117*) and hind-limb ischemia (*113, 114, 119, 120*), limited knowledge exists regarding collateral remodeling after brain trauma.

Smooth Muscle Cells

In order for large arteriole blood vessels to mature and function properly, smooth muscle cells (SMCs) are an essential component to the vessel wall. Large arterioles ranging from 10-30µm contain one to three layers of SMCs that can be visualized with alpha smooth muscle actin (*121-124*). SMCs play a critical role in controlling vascular tone by altering lumen diameter through contraction and relaxation; thus, they can regulate vessel diameter acutely from cues given by the endothelial cell (EC) (*125-127*). For example, increases in shear stress sensed by the ECs causes the ECs to release nitric oxide (NO) which diffuses onto SMCs to cause relaxation (*128*). Conversely, a decrease in shear stress sensed by the ECs causes a release of endothelin and angiotensin II to cause the SMC to constrict (*129*). For long-term vessel stabilization, SMCs can

also regulate blood vessel maturation by secreting extracellular matrix molecules like collagen to surround ECs and provide the vessel with an extra layer of protection (*130-134*). SMCs also constitutively release angiopoietin 1 (Ang1) that binds to the specific EC receptor Tie2 (*135, 136*). Binding of Ang1 onto Tie2 promotes vessel stability (*101, 137, 138*). Studies that have deleted either Ang1 or Tie2 have shown a deregulated association of SMCs to ECs, which contributes to vessel leakiness (*99, 138*).

Differentiated SMCs proliferate at low rates and express contractile proteins (*139*). Interestingly, vessels contain different ratios of mature contractile SMCs and highly proliferative synthetic SMCs, which is highlighted by heterogeneous staining intensities of adjacent SMCs on the same vessel, suggesting differences in gene expression that confer these differences in phenotype (*129, 140, 141*). Further evidence has shown that four SMC phenotypes with distinct gene expression profiles have been isolated from the same artery of the rat by sorting different contractile and synthetic proteins (*142, 143*). While contractile SMCs are the majority phenotype observed on a vessel, synthetic SMCs can aid in vessel remodeling (*144-146*). Variation in SMC phenotypes are attributed to differences in embryological origin and seem to be genetically programmed (*140, 141*). However, environmental stimuli, such as factors released after vascular injury have been shown to shift the ratio from contractile to synthetic (*124, 126, 129, 131, 134*). These precise environmental cues that signal a “de-differentiation” from contractile to synthetic SMC are compounded by the genetic programming of the SMC (*124, 126, 129, 131, 134*). Due to their ability to have an acute impact on EC lumen diameter and ability to stabilize a blood vessel, SMCs are an important cell type involved in vessel remodeling. It would be very interesting to profile the phenotypes (contractile versus synthetic) on collateral vessels as these vessels have an acute remodeling response after vascular occlusion (*113, 124*).

Animal Models of TBI

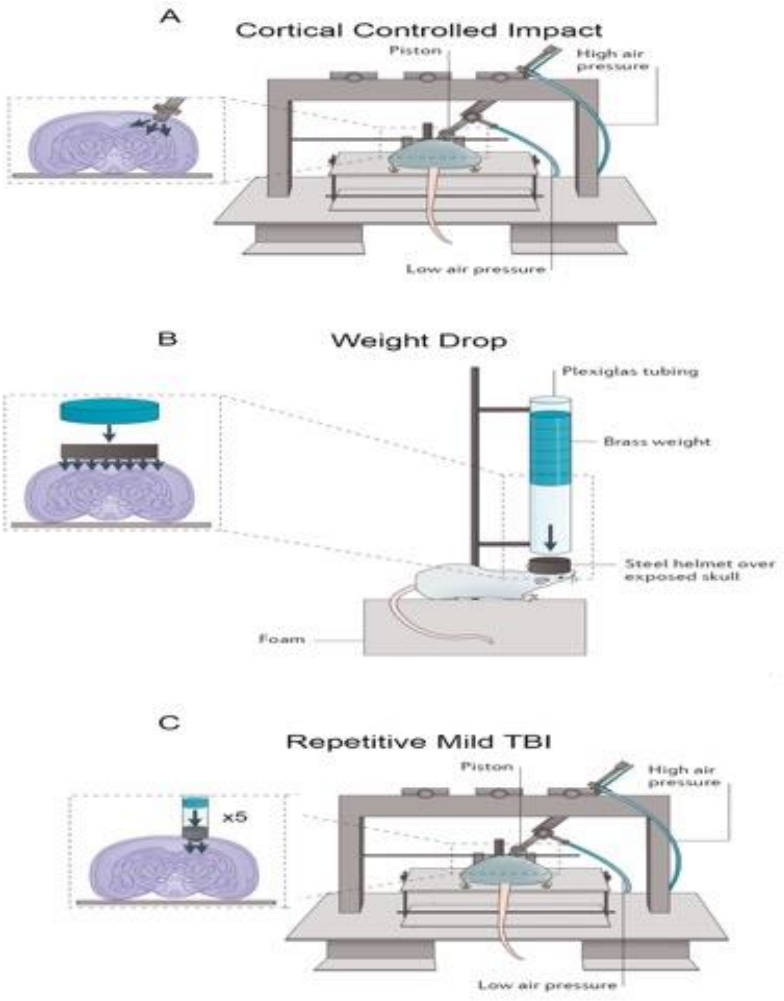

Figure 1. Experimental set up for three mouse models of TBI. (A) The controlled cortical impact (CCI) injury model uses an electromagnetically driven piston to penetrate the brain at a controllable distance and velocity onto the intact dura. (B) In the weight drop model a free falling weight, guided through a tube, strikes the exposed skull. (C) The repetitive TBI model uses the set distance and velocity from the CCI model to strike the exposed skull a total of five times, spaced every 48 hours. This figure is modified, with permission, from REF (*147*) © (2013) Nature Publishing Group.

Weight Drop Model

Diffuse axonal injury (DAI) is one of the most common pathological features of mTBI (*148-151*). In humans, diffuse axonal injury (DAI) is typically caused by sports concussions and diagnosed in the clinic with an immediate loss of consciousness and cognitive dysfunction (*152-154*). Closed head injury models with free head rotation have been developed to model sport concussions and one of these models is the weight drop model. The weight drop model set-up consists of a free falling weight that is guided through a tube and strikes an exposed skull (*155, 156*) (Figure 1B). No craniotomy is needed, and a stainless steel disk is placed on the midline of the brain, between bregma and lambda to prevent skull fracture (*37*). The height and mass of the weight can be adjusted to change injury severity. The weight drop model produces DAI with widespread damage to neurons, axons, and the microvasculature and closely mimics these pathologies seen in the clinical population (*11, 153, 157, 158*). Single mTBIs are shown to cause subtle and transient immunohistochemical abnormalities and minor changes in behavior with no neuronal tissue loss (*11, 159, 160*). A drawback of this model is the high mortality rate seen in mice due to respiratory depression (*161, 162*); however, the model is inexpensive, fast between surgeries, and easy to use.

Cortical Controlled Impact

In the laboratory setting, focal TBIs represent pathologies resulting from a blow to the head with a focal injury site and subtle widespread injury (*163-166*). The CCI model uses a pneumatic or electromagnetic impact device to put a piston onto the exposed dura to mimic cortical tissue loss (*147, 165-167*) (Figure 1A). The velocity and depth can be controlled prior to the impact to cause reproducible hits to the underlying tissue, which is the hallmark pathological feature of this model (*165, 166, 168*). There is a progressive decline of CBF associated with the trauma that leads

to neuronal tissue loss (*169, 170*). The contusion itself is hemorrhagic, necrotic, and will undergo cavitation over time (*169*). In addition, the BBB is highly disrupted with reactive astrocytes and activated microglia which can cause further damage (*164*). Functional and cognitive impairments correlate with histopathological findings and these behavioral deficits can last up to a year post-injury (*171-174*). Although most CCI devices are expensive, the high reproducible control over the impact and injury make this device attractive for TBI modeling.

Repetitive Mild TBI

More recently, different groups have applied the CCI model onto the closed skull to help understand the underlying pathologies associated with repetitive mild injuries to the brain (*10, 159, 175, 176*) (Figure 1C). Unlike the pathologies associated with a single mTBI (*11, 153, 157, 158*), due to the brain's window of vulnerability (*11, 177*), successive injuries exacerbate the histological findings seen after a single mTBI with increases in BBB permeability, reactive astrocytes, and greater diffuse axonal damage with no signs of neuronal loss (*94, 99-101*). In addition, while there are transient deficits in behavior seen after a single mTBI (*11, 159, 160*), rmTBI causes greater lasting cognitive impairments seen in motor deficits, memory tasks, and state of consciousness (*159, 178, 179*). Although the use of the CCI device causes reproducibility of the injuries, the thin nature of the mouse skull can fracture over time with each successive hit (*162*).

Vascular Changes in Different Models of TBI

CBF Changes after TBI

One of the most notable and primary changes after TBI is in the cerebral vasculature with fluctuations that occur in CBF, depending on injury severity (*14, 146, 180, 181*). Impairment of

the vasculature is seen in moderate and severe TBI cases; however, fluctuations in CBF after mTBI or rmTBI are less known (*4, 182, 183*). In the CCI model, within minutes after impact, there is a loss of perfusion at the impact site and this reduction of CBF reaches ischemic conditions (*4, 183-185*). Further depressed levels of CBF throughout the brain can be monitored for at least 4 hours post- injury and this reduction of CBF can reach as low as 50% of the normal perfusion (*183, 186*). There are confounding studies regarding CBF changes that occur in mTBI such as in the weight drop model (*146, 187-189*). Studies have shown that these concussive injuries can cause mild reductions of blood flow or even increases of blood flow after injury (*190-192*). Despite these unknown CBF fluctuations after mTBI, what can be agreed upon is that an injured brain is highly vulnerable to ischemic conditions (*190*). CBF changes after rmTBI are one of the least understood phenomenon in the neurotrauma community (*189, 193*). Recent studies have shown that repetitive injuries induce long-lasting decreases in CBF, which is absent after a single hit, and the reduction of CBF is dependent on the number of hits the brain receives and the amount of time between each hit (*193, 194*). While cerebrovascular responses after rmTBI are currently under investigation, studies show reductions of CBF after rmTBI may be linked to vascular dysfunction and other findings have correlated impaired cognitive behavior with cerebrovascular dysfunction (*195, 196*). A decrease in blood supply to the brain and subsequent reduction in metabolism mediates tissue damage and leads to functional deficits regardless of the type of head injury (*197, 198*).

Endothelial Cell-specific Changes in the Vascular Network after TBI

The endothelial cell (EC) response and activation to trauma is important for promoting brain homeostasis after injury; however, how individual ECs respond to trauma are unknown (*199, 200*). Studies that focus on the EC response to hypertension, an increase in blood flow, can be

applied to the early stages of CCI injury where surrounding vessels see an increase in blood flow, due to the mechanical forces attributed to this injury. For example, studies that looked at high flow rates of blood through the carotid arteries in a rabbit model of hypertension found an increase of EC proliferation, evidenced by $Brdu^+$ ECs, to highlight how ECs accommodate the increase in shear stress across the cell wall (*201*). Furthermore, arterial remodeling due to EC-dependent mechanisms related to blood flow and wall shear stress have been shown to occur in distinct phases to promote overall vessel remodeling (*107, 200*). Once an increase of shear stress forces is sensed by mechanoreceptors found on the surface of ECs, EC proliferation is stimulated (*107*). This proliferation is followed by basement membrane and internal elastic lamina degradation and then followed by SMC proliferation (*107, 202*). EC proliferation contributes to vessel enlargement and a vessel that does not receive proper blood flow is found to regress (*203*).

Microvascular injury has been reported in CCI models in rodents (*202, 204, 205*). For example, studies in rats have shown a decrease in microvascular density on the ipsilateral side of injury while the density on the contralateral side and sham-injured animals remained similar (*205*). Structural changes to the ECs of the injured microvascular were also observed; these changes included large cytoplasmic vacuoles within ECs, discontinuous vessels, regression of vessels, focal EC swelling, and widening of intercellular junctions (*205*).

Blood Brain Barrier Permeability

Controlled Cortical Impact:

The mechanical forces associated with CCI injury that cause a focal impact to the brain has been shown to result in the breakdown of the BBB in animal studies (*48, 206-210*). After CCI injury, the BBB is highly permeable, within 30 minutes after impact (*4, 20, 202, 210, 211*). In

these early phases, BBB leakage is attributed to disruption of TJ proteins, displacement and activation of astrocytes and astrocyte endfeet, compression of the vasculature, and reduction of vascular lumens (*20, 202, 212-215*). Monitoring BBB permeability dynamics after injury through Evan's blue or anti-IgG, which binds to albumin have coincided with either increases or decrease in TJ expression (*146, 215*). For example, in a rat CCI model, an increase of IgG staining intensity correlated with an inverse staining expression of claudin-5 and the relative gene expression measured by qPCR (*215*). The leakiness of the BBB and the dysfunction of the associated cell types perpetuate brain injury because plasma proteins that were once prevented from entering the brain can now cross the BBB and further cause edema and swelling of the brain (*44*). Thus, neuroprotective strategies that target this acute breakdown and promote quicker repair could prove beneficial preventing further tissue loss.

Weight Drop and rmTBI:

Mounting evidence now shows that even mTBIs can cause transient BBB leakage. Unlike in the CCI model, the weight drop model causes an acute transient opening of the BBB (*48, 210*). However, in cases, such as in rmTBI where there is accumulated diffuse axonal injury, this can lead to metabolic disturbances which can cause a focal point of ischemia (*20, 216, 217*). The dynamic role of the BBB in rmTBI is still unknown; however, pathological evidence of an increase in microglia activation and reactive astrogliosis, correlates with BBB leakage. The transient disturbance of CBF causes astrocytes to swell allowing for the passage of plasma proteins to cross the BBB and cause mild brain swelling (*195, 196*).

Conclusion

Animal models in TBI have been an important tool for the development of potentially translatable techniques and helping to elucidate the mechanisms underlying brain injury. TBI is a

heterogeneous injury in the human population (*1, 217*). The patient population differs with respect to the degree of severity, location, and type (contusion vs concussion or both) of injury. This sets the course that there is no one true gold standard animal model that fully recapitulates the entirety of the human condition and emphasizes the need to understand the nuances of each individual injury. Therefore, the development and examination of multiple TBI models will aid investigations into the pathophysiological underpinnings of the complex disorder. Importantly, the success of any TBI animal model is reproducibility of the injury so that each model has some degree of standardization. While the weight drop model and the CCI model have been well studied in the field, new models that recapitulate what happens after repetitive injuries are gaining momentum. Animal models also remain necessary in testing therapeutic agents and upholding the safety of clinical trials. One area of TBI research that has been understudied is the vascular response and repair to injury and whether these changes play a major role in tissue damage and functional decline. Although these studies are few, recent findings demonstrate that prolonged BBB permeability can dictate injury severity because of secondary injuries associated with TBI and the increase of edema. Therefore, further strategies aimed at limiting this response may provide functional benefits and improve tissue recovery. In addition, understanding the cellular and molecular mechanisms regulating BBB breakdown across multiple models may aid in knowing the therapeutic window for drug delivery in each form of TBI and whether severity, location, and cause should be considered. In addition, the role of larger arteriole collateral vessels in redistributing blood flow to enable proper biomechanical stimuli across the luminal surface of microvessels and maintain survival signals is unclear. The current work focuses on these responses across several models of TBI and directly investigates the endothelial cell-specific role in the CCI model following juvenile and adult injury.

References

1. V. G. Coronado *et al.*, Trends in Traumatic Brain Injury in the U.S. and the public health response: 1995-2009. *J Safety Res* **43**, 299-307 (2012).
2. D. Fife, J. Jagger, The contribution of brain injury to the overall injury severity of brain-injured patients. *J Neurosurg* **60**, 697-699 (1984).
3. J. R. Marin, M. D. Weaver, D. M. Yealy, R. C. Mannix, Trends in visits for traumatic brain injury to emergency departments in the United States. *JAMA* **311**, 1917-1919 (2014).
4. D. S. DeWitt, D. S. Prough, Traumatic cerebral vascular injury: the effects of concussive brain injury on the cerebral vasculature. *J Neurotrauma* **20**, 795-825 (2003).
5. D. J. Thurman, C. Alverson, K. A. Dunn, J. Guerrero, J. E. Sniezek, Traumatic brain injury in the United States: A public health perspective. *J Head Trauma Rehabil* **14**, 602-615 (1999).
6. D. J. Thurman, The Epidemiology of Traumatic Brain Injury in Children and Youths: A Review of Research Since 1990. *J Child Neurol* **31**, 20-27 (2016).
7. C. C. Giza, M. L. Prins, Is being plastic fantastic? Mechanisms of altered plasticity after developmental traumatic brain injury. *Dev Neurosci* **28**, 364-379 (2006).
8. A. J. Schneier, B. J. Shields, S. G. Hostetler, H. Xiang, G. A. Smith, Incidence of pediatric traumatic brain injury and associated hospital resource utilization in the United States. *Pediatrics* **118**, 483-492 (2006).
9. H. Zetterberg, S. Gandy, Repetitive concussions--How dangerous are they? *Mol Cell Neurosci* **66**, 73-74 (2015).
10. J. A. Creed, A. M. DiLeonardi, D. P. Fox, A. R. Tessler, R. Raghupathi, Concussive brain trauma in the mouse results in acute cognitive deficits and sustained impairment of axonal function. *J Neurotrauma* **28**, 547-563 (2011).
11. H. L. Laurer *et al.*, Mild head injury increasing the brain's vulnerability to a second concussive impact. *J Neurosurg* **95**, 859-870 (2001).
12. J. F. Malec *et al.*, The mayo classification system for traumatic brain injury severity. *J Neurotrauma* **24**, 1417-1424 (2007).
13. A. I. Maas, N. Stocchetti, R. Bullock, Moderate and severe traumatic brain injury in adults. *Lancet Neurol* **7**, 728-741 (2008).
14. M. Fujita, E. P. Wei, J. T. Povlishock, Intensity- and interval-specific repetitive traumatic brain injury can evoke both axonal and microvascular damage. *J Neurotrauma* **29**, 2172-2180 (2012).
15. M. Franzblau *et al.*, Vascular damage: a persisting pathology common to Alzheimer's disease and traumatic brain injury. *Med Hypotheses* **81**, 842-845 (2013).
16. T. Brickler *et al.*, Nonessential Role for the NLRP1 Inflammasome Complex in a Murine Model of Traumatic Brain Injury. *Mediators Inflamm* **2016**, 6373506 (2016).
17. Z. S. Bailey *et al.*, Cerium Oxide Nanoparticles Improve Outcome After In Vitro and In Vivo Mild Traumatic Brain Injury. *J Neurotrauma*, (2016).
18. J. R. Kulbe, R. L. Hill, I. N. Singh, J. A. Wang, E. D. Hall, Synaptic Mitochondria Sustain More Damage than Non-Synaptic Mitochondria after Traumatic Brain Injury and Are Protected by Cyclosporine A. *J Neurotrauma*, (2016).
19. A. Yarlagadda, S. Kaushik, A. H. Clayton, Blood brain barrier: the role of calcium homeostasis. *Psychiatry (Edgmont)* **4**, 55-59 (2007).

20. R. Prakash, S. T. Carmichael, Blood-brain barrier breakdown and neovascularization processes after stroke and traumatic brain injury. *Curr Opin Neurol* **28**, 556-564 (2015).
21. K. Dams-O'Connor *et al.*, Risk for late-life re-injury, dementia and death among individuals with traumatic brain injury: a population-based study. *J Neurol Neurosurg Psychiatry* **84**, 177-182 (2013).
22. S. L. Wald, S. R. Shackford, J. Fenwick, The effect of secondary insults on mortality and long-term disability after severe head injury in a rural region without a trauma system. *J Trauma* **34**, 377-381; discussion 381-372 (1993).
23. K. D. Cicerone, L. N. Tanenbaum, Disturbance of social cognition after traumatic orbitofrontal brain injury. *Arch Clin Neuropsychol* **12**, 173-188 (1997).
24. M. A. Grealy, D. A. Johnson, S. K. Rushton, Improving cognitive function after brain injury: the use of exercise and virtual reality. *Arch Phys Med Rehabil* **80**, 661-667 (1999).
25. H. S. Levin, H. M. Eisenberg, N. R. Wigg, K. Kobayashi, Memory and intellectual ability after head injury in children and adolescents. *Neurosurgery* **11**, 668-673 (1982).
26. M. Lippert-Gruner, J. Kuchta, M. Hellmich, N. Klug, Neurobehavioural deficits after severe traumatic brain injury (TBI). *Brain Inj* **20**, 569-574 (2006).
27. C. Fraser *et al.*, Driving plasticity in human adult motor cortex is associated with improved motor function after brain injury. *Neuron* **34**, 831-840 (2002).
28. J. Biernaskie, D. Corbett, Enriched rehabilitative training promotes improved forelimb motor function and enhanced dendritic growth after focal ischemic injury. *J Neurosci* **21**, 5272-5280 (2001).
29. K. M. Guskiewicz *et al.*, Association between recurrent concussion and late-life cognitive impairment in retired professional football players. *Neurosurgery* **57**, 719-726; discussion 719-726 (2005).
30. O. Kokiko-Cochran *et al.*, Altered Neuroinflammation and Behavior after Traumatic Brain Injury in a Mouse Model of Alzheimer's Disease. *J Neurotrauma* **33**, 625-640 (2016).
31. T. M. Sivanandam, M. K. Thakur, Traumatic brain injury: a risk factor for Alzheimer's disease. *Neurosci Biobehav Rev* **36**, 1376-1381 (2012).
32. J. T. Weber, Experimental models of repetitive brain injuries. *Prog Brain Res* **161**, 253-261 (2007).
33. G. J. Bouma *et al.*, Ultra-early evaluation of regional cerebral blood flow in severely head-injured patients using xenon-enhanced computerized tomography. *J Neurosurg* **77**, 360-368 (1992).
34. A. Jullienne *et al.*, Chronic cerebrovascular dysfunction after traumatic brain injury. *J Neurosci Res* **94**, 609-622 (2016).
35. Y. Inoue *et al.*, Changes in cerebral blood flow from the acute to the chronic phase of severe head injury. *J Neurotrauma* **22**, 1411-1418 (2005).
36. T. W. Langfitt, W. D. Obrist, T. A. Gennarelli, M. J. O'Connor, C. A. Weeme, Correlation of cerebral blood flow with outcome in head injured patients. *Ann Surg* **186**, 411-414 (1977).
37. D. M. Morales *et al.*, Experimental models of traumatic brain injury: do we really need to build a better mousetrap? *Neuroscience* **136**, 971-989 (2005).
38. S. Margulies *et al.*, Combination Therapies for Traumatic Brain Injury: Retrospective Considerations. *J Neurotrauma* **33**, 101-112 (2016).

39. T. Higashida *et al.*, The role of hypoxia-inducible factor-1alpha, aquaporin-4, and matrix metalloproteinase-9 in blood-brain barrier disruption and brain edema after traumatic brain injury. *J Neurosurg* **114**, 92-101 (2011).
40. R. J. Sevick *et al.*, Cytotoxic brain edema: assessment with diffusion-weighted MR imaging. *Radiology* **185**, 687-690 (1992).
41. J. Q. Chen, C. C. Zhang, S. N. Jiang, H. Lu, W. Wang, Effects of Aquaporin 4 Knockdown on Brain Edema of the Uninjured Side After Traumatic Brain Injury in Rats. *Med Sci Monit* **22**, 4809-4819 (2016).
42. A. W. Unterberg, J. Stover, B. Kress, K. L. Kiening, Edema and brain trauma. *Neuroscience* **129**, 1021-1029 (2004).
43. A. L. Betz, S. R. Ennis, G. P. Schielke, J. T. Hoff, Blood-to-brain sodium transport in ischemic brain edema. *Adv Neurol* **52**, 73-80 (1990).
44. A. L. Betz, F. Iannotti, J. T. Hoff, Brain edema: a classification based on blood-brain barrier integrity. *Cerebrovasc Brain Metab Rev* **1**, 133-154 (1989).
45. N. J. Abbott, Astrocyte-endothelial interactions and blood-brain barrier permeability. *J Anat* **200**, 629-638 (2002).
46. M. Wahl, A. Unterberg, A. Baethmann, L. Schilling, Mediators of blood-brain barrier dysfunction and formation of vasogenic brain edema. *J Cereb Blood Flow Metab* **8**, 621-634 (1988).
47. O. Gotoh, T. Asano, T. Koide, K. Takakura, Ischemic brain edema following occlusion of the middle cerebral artery in the rat. I: The time courses of the brain water, sodium and potassium contents and blood-brain barrier permeability to 125I-albumin. *Stroke* **16**, 101-109 (1985).
48. P. Barzo, A. Marmarou, P. Fatouros, F. Corwin, J. Dunbar, Magnetic resonance imaging-monitored acute blood-brain barrier changes in experimental traumatic brain injury. *J Neurosurg* **85**, 1113-1121 (1996).
49. M. C. Papadopoulos, S. Krishna, A. S. Verkman, Aquaporin water channels and brain edema. *Mt Sinai J Med* **69**, 242-248 (2002).
50. H. Sun, H. F. Lingsma, E. W. Steyerberg, A. I. Maas, External Validation of the International Mission for Prognosis and Analysis of Clinical Trials in Traumatic Brain Injury: Prognostic Models for Traumatic Brain Injury on the Study of the Neuroprotective Activity of Progesterone in Severe Traumatic Brain Injuries Trial. *J Neurotrauma* **33**, 1535-1543 (2016).
51. D. Stein, I. Sayeed, C. Espinosa-Garcia, F. Atif, E. G. Sergeeva, Goldstein et al.'s secondary analysis of progesterone clinical trial for TBI can only reflect the same trial design flaws: A response to "Very Early Administration of Progesterone Does Not Improve Neuropsychological Outcomes in Subjects with Moderate to Severe Traumatic Brain Injury". *J Neurotrauma*, (2017).
52. C. S. Robertson *et al.*, Effect of erythropoietin and transfusion threshold on neurological recovery after traumatic brain injury: a randomized clinical trial. *JAMA* **312**, 36-47 (2014).
53. P. D. Adelson *et al.*, Comparison of hypothermia and normothermia after severe traumatic brain injury in children (Cool Kids): a phase 3, randomised controlled trial. *Lancet Neurol* **12**, 546-553 (2013).
54. D. W. Wright *et al.*, ProTECT: a randomized clinical trial of progesterone for acute traumatic brain injury. *Ann Emerg Med* **49**, 391-402, 402 e391-392 (2007).

55. R. L. Roof, R. Duvdevani, D. G. Stein, Progesterone treatment attenuates brain edema following contusion injury in male and female rats. *Restor Neurol Neurosci* **4**, 425-427 (1992).
56. D. Shlosberg, M. Benifla, D. Kaufer, A. Friedman, Blood-brain barrier breakdown as a therapeutic target in traumatic brain injury. *Nat Rev Neurol* **6**, 393-403 (2010).
57. D. S. Liebeskind, Collateral circulation. *Stroke* **34**, 2279-2284 (2003).
58. O. Y. Bang, M. Goyal, D. S. Liebeskind, Collateral Circulation in Ischemic Stroke: Assessment Tools and Therapeutic Strategies. *Stroke* **46**, 3302-3309 (2015).
59. A. Krishnaswamy, J. P. Klein, S. R. Kapadia, Clinical cerebrovascular anatomy. *Catheter Cardiovasc Interv* **75**, 530-539 (2010).
60. P. L. Silbert, B. Mokri, W. I. Schievink, Headache and neck pain in spontaneous internal carotid and vertebral artery dissections. *Neurology* **45**, 1517-1522 (1995).
61. M. Brozici, A. van der Zwan, B. Hillen, Anatomy and functionality of leptomeningeal anastomoses: a review. *Stroke* **34**, 2750-2762 (2003).
62. H. C. Alves, F. T. Pacheco, A. J. Rocha, Collateral blood vessels in acute ischemic stroke: a physiological window to predict future outcomes. *Arq Neuropsiquiatr* **74**, 662-670 (2016).
63. N. Saeki, A. L. Rhoton, Jr., Microsurgical anatomy of the upper basilar artery and the posterior circle of Willis. *J Neurosurg* **46**, 563-578 (1977).
64. B. J. Alpers, R. G. Berry, R. M. Paddison, Anatomical studies of the circle of Willis in normal brain. *AMA Arch Neurol Psychiatry* **81**, 409-418 (1959).
65. H. E. Riggs, C. Rupp, Variation in form of circle of Willis. The relation of the variations to collateral circulation: anatomic analysis. *Arch Neurol* **8**, 8-14 (1963).
66. J. Liu *et al.*, Vascular remodeling after ischemic stroke: mechanisms and therapeutic potentials. *Prog Neurobiol* **115**, 138-156 (2014).
67. E. Hamel, Perivascular nerves and the regulation of cerebrovascular tone. *J Appl Physiol (1985)* **100**, 1059-1064 (2006).
68. B. Cauli, E. Hamel, Revisiting the role of neurons in neurovascular coupling. *Front Neuroenergetics* **2**, 9 (2010).
69. L. Ostergaard *et al.*, Cerebral small vessel disease: Capillary pathways to stroke and cognitive decline. *J Cereb Blood Flow Metab* **36**, 302-325 (2016).
70. A. G. Hudetz, Blood flow in the cerebral capillary network: a review emphasizing observations with intravital microscopy. *Microcirculation* **4**, 233-252 (1997).
71. J. S. Goldberg, K. K. Hirschi, Diverse roles of the vasculature within the neural stem cell niche. *Regen Med* **4**, 879-897 (2009).
72. W. C. Aird, Phenotypic heterogeneity of the endothelium: II. Representative vascular beds. *Circ Res* **100**, 174-190 (2007).
73. H. Girouard, C. Iadecola, Neurovascular coupling in the normal brain and in hypertension, stroke, and Alzheimer disease. *J Appl Physiol (1985)* **100**, 328-335 (2006).
74. G. C. Petzold, D. F. Albeanu, T. F. Sato, V. N. Murthy, Coupling of neural activity to blood flow in olfactory glomeruli is mediated by astrocytic pathways. *Neuron* **58**, 897-910 (2008).
75. E. A. Neuwelt *et al.*, Engaging neuroscience to advance translational research in brain barrier biology. *Nat Rev Neurosci* **12**, 169-182 (2011).

76. E. A. Pozhilenkova, O. L. Lopatina, Y. K. Komleva, V. V. Salmin, A. B. Salmina, Blood-brain barrier-supported neurogenesis in healthy and diseased brain. *Rev Neurosci*, (2017).
77. R. C. Janzer, M. C. Raff, Astrocytes induce blood-brain barrier properties in endothelial cells. *Nature* **325**, 253-257 (1987).
78. R. C. Brown *et al.*, Protection against hypoxia-induced increase in blood-brain barrier permeability: role of tight junction proteins and NFkappaB. *J Cell Sci* **116**, 693-700 (2003).
79. I. Cooper, K. Cohen-Kashi-Malina, V. I. Teichberg, Claudin-5 expression in in vitro models of the blood-brain barrier. *Methods Mol Biol* **762**, 347-354 (2011).
80. S. M. Stamatovic, A. M. Johnson, R. F. Keep, A. V. Andjelkovic, Junctional proteins of the blood-brain barrier: New insights into function and dysfunction. *Tissue Barriers* **4**, e1154641 (2016).
81. H. Wolburg, A. Lippoldt, Tight junctions of the blood-brain barrier: development, composition and regulation. *Vascul Pharmacol* **38**, 323-337 (2002).
82. J. D. Huber, R. D. Egleton, T. P. Davis, Molecular physiology and pathophysiology of tight junctions in the blood-brain barrier. *Trends Neurosci* **24**, 719-725 (2001).
83. U. Kniesel, H. Wolburg, Tight junctions of the blood-brain barrier. *Cell Mol Neurobiol* **20**, 57-76 (2000).
84. N. J. Abbott, Blood-brain barrier structure and function and the challenges for CNS drug delivery. *J Inherit Metab Dis* **36**, 437-449 (2013).
85. T. Soma *et al.*, Thr(207) of claudin-5 is involved in size-selective loosening of the endothelial barrier by cyclic AMP. *Exp Cell Res* **300**, 202-212 (2004).
86. L. He *et al.*, Analysis of the brain mural cell transcriptome. *Sci Rep* **6**, 35108 (2016).
87. A. Armulik *et al.*, Pericytes regulate the blood-brain barrier. *Nature* **468**, 557-561 (2010).
88. S. Dohgu, F. Takata, Y. Kataoka, Brain pericytes regulate the blood-brain barrier function. *Nihon Yakurigaku Zasshi* **146**, 63-65 (2015).
89. R. Cabezas *et al.*, Astrocytic modulation of blood brain barrier: perspectives on Parkinson's disease. *Front Cell Neurosci* **8**, 211 (2014).
90. G. P. Nicchia *et al.*, The role of aquaporin-4 in the blood-brain barrier development and integrity: studies in animal and cell culture models. *Neuroscience* **129**, 935-945 (2004).
91. G. T. Manley *et al.*, Aquaporin-4 deletion in mice reduces brain edema after acute water intoxication and ischemic stroke. *Nat Med* **6**, 159-163 (2000).
92. J. Zhou *et al.*, Altered blood-brain barrier integrity in adult aquaporin-4 knockout mice. *Neuroreport* **19**, 1-5 (2008).
93. M. V. Bennett *et al.*, Connexin and pannexin hemichannels in inflammatory responses of glia and neurons. *Brain Res* **1487**, 3-15 (2012).
94. J. E. Contreras *et al.*, Metabolic inhibition induces opening of unapposed connexin 43 gap junction hemichannels and reduces gap junctional communication in cortical astrocytes in culture. *Proc Natl Acad Sci U S A* **99**, 495-500 (2002).
95. N. Karpuk, M. Burkovetskaya, T. Fritz, A. Angle, T. Kielian, Neuroinflammation leads to region-dependent alterations in astrocyte gap junction communication and hemichannel activity. *J Neurosci* **31**, 414-425 (2011).
96. N. M. Kumar, N. B. Gilula, The gap junction communication channel. *Cell* **84**, 381-388 (1996).

97. M. V. Bennett, J. E. Contreras, F. F. Bukauskas, J. C. Saez, New roles for astrocytes: gap junction hemichannels have something to communicate. *Trends Neurosci* **26**, 610-617 (2003).
98. J. I. Alvarez, T. Katayama, A. Prat, Glial influence on the blood brain barrier. *Glia* **61**, 1939-1958 (2013).
99. Z. G. Zhang *et al.*, Correlation of VEGF and angiopoietin expression with disruption of blood-brain barrier and angiogenesis after focal cerebral ischemia. *J Cereb Blood Flow Metab* **22**, 379-392 (2002).
100. N. Nourhaghighi, K. Teichert-Kuliszewska, J. Davis, D. J. Stewart, S. Nag, Altered expression of angiopoietins during blood-brain barrier breakdown and angiogenesis. *Lab Invest* **83**, 1211-1222 (2003).
101. L. Eklund, P. Saharinen, Angiopoietin signaling in the vasculature. *Exp Cell Res* **319**, 1271-1280 (2013).
102. P. Ezan *et al.*, Deletion of astroglial connexins weakens the blood-brain barrier. *J Cereb Blood Flow Metab* **32**, 1457-1467 (2012).
103. N. R. Saunders, K. M. Dziegielewska, K. Mollgard, M. D. Habgood, Markers for blood-brain barrier integrity: how appropriate is Evans blue in the twenty-first century and what are the alternatives? *Front Neurosci* **9**, 385 (2015).
104. N. R. Saunders *et al.*, The rights and wrongs of blood-brain barrier permeability studies: a walk through 100 years of history. *Front Neurosci* **8**, 404 (2014).
105. A. Varatharaj, I. Galea, The blood-brain barrier in systemic inflammation. *Brain Behav Immun* **60**, 1-12 (2017).
106. M. A. Yenari, L. Xu, X. N. Tang, Y. Qiao, R. G. Giffard, Microglia potentiate damage to blood-brain barrier constituents: improvement by minocycline in vivo and in vitro. *Stroke* **37**, 1087-1093 (2006).
107. E. Sho *et al.*, High flow drives vascular endothelial cell proliferation during flow-induced arterial remodeling associated with the expression of vascular endothelial growth factor. *Exp Mol Pathol* **75**, 1-11 (2003).
108. B. P. Chen *et al.*, DNA microarray analysis of gene expression in endothelial cells in response to 24-h shear stress. *Physiol Genomics* **7**, 55-63 (2001).
109. A. W. Hoksbergen, B. Fulesdi, D. A. Legemate, L. Csiba, Collateral configuration of the circle of Willis: transcranial color-coded duplex ultrasonography and comparison with postmortem anatomy. *Stroke* **31**, 1346-1351 (2000).
110. K. Devault *et al.*, Blood Flow in the Circle of Willis: Modeling and Calibration. *Multiscale Model Simul* **7**, 888-909 (2008).
111. B. Okyere *et al.*, Endothelial-Specific EphA4 Negatively Regulates Native Pial Collateral Formation and Re-Perfusion following Hindlimb Ischemia. *PLoS One* **11**, e0159930 (2016).
112. J. E. Faber, W. M. Chilian, E. Deindl, N. van Royen, M. Simons, A brief etymology of the collateral circulation. *Arterioscler Thromb Vasc Biol* **34**, 1854-1859 (2014).
113. D. Chalothorn, J. A. Clayton, H. Zhang, D. Pomp, J. E. Faber, Collateral density, remodeling, and VEGF-A expression differ widely between mouse strains. *Physiol Genomics* **30**, 179-191 (2007).
114. F. Pipp *et al.*, Elevated fluid shear stress enhances postocclusive collateral artery growth and gene expression in the pig hind limb. *Arterioscler Thromb Vasc Biol* **24**, 1664-1668 (2004).

115. A. Helisch, W. Schaper, Arteriogenesis: the development and growth of collateral arteries. *Microcirculation* **10**, 83-97 (2003).
116. P. Meier *et al.*, Beneficial effect of recruitable collaterals: a 10-year follow-up study in patients with stable coronary artery disease undergoing quantitative collateral measurements. *Circulation* **116**, 975-983 (2007).
117. B. K. Menon *et al.*, Regional leptomeningeal score on CT angiography predicts clinical and imaging outcomes in patients with acute anterior circulation occlusions. *AJNR Am J Neuroradiol* **32**, 1640-1645 (2011).
118. M. Heil *et al.*, Blood monocyte concentration is critical for enhancement of collateral artery growth. *Am J Physiol Heart Circ Physiol* **283**, H2411-2419 (2002).
119. D. Scholz *et al.*, Ultrastructure and molecular histology of rabbit hind-limb collateral artery growth (arteriogenesis). *Virchows Arch* **436**, 257-270 (2000).
120. M. Arras *et al.*, Monocyte activation in angiogenesis and collateral growth in the rabbit hindlimb. *J Clin Invest* **101**, 40-50 (1998).
121. A. C. Montezano, R. A. Lopes, K. B. Neves, F. Rios, R. M. Touyz, Isolation and Culture of Vascular Smooth Muscle Cells from Small and Large Vessels. *Methods Mol Biol* **1527**, 349-354 (2017).
122. E. Brogi, T. Wu, A. Namiki, J. M. Isner, Indirect angiogenic cytokines upregulate VEGF and bFGF gene expression in vascular smooth muscle cells, whereas hypoxia upregulates VEGF expression only. *Circulation* **90**, 649-652 (1994).
123. G. K. Owens, Regulation of differentiation of vascular smooth muscle cells. *Physiol Rev* **75**, 487-517 (1995).
124. G. K. Owens, M. S. Kumar, B. R. Wamhoff, Molecular regulation of vascular smooth muscle cell differentiation in development and disease. *Physiol Rev* **84**, 767-801 (2004).
125. A. Regent *et al.*, Proteomic analysis of vascular smooth muscle cells in physiological condition and in pulmonary arterial hypertension: Toward contractile versus synthetic phenotypes. *Proteomics* **16**, 2637-2649 (2016).
126. S. M. Schwartz, G. R. Campbell, J. H. Campbell, Replication of smooth muscle cells in vascular disease. *Circ Res* **58**, 427-444 (1986).
127. G. R. Gordon, H. B. Choi, R. L. Rungta, G. C. Ellis-Davies, B. A. MacVicar, Brain metabolism dictates the polarity of astrocyte control over arterioles. *Nature* **456**, 745-749 (2008).
128. M. S. Kannan, S. Guiang, D. E. Johnson, Nitric oxide: biological role and clinical uses. *Indian J Pediatr* **65**, 333-345 (1998).
129. S. S. Rensen, P. A. Doevendans, G. J. van Eys, Regulation and characteristics of vascular smooth muscle cell phenotypic diversity. *Neth Heart J* **15**, 100-108 (2007).
130. J. Tucka *et al.*, Akt1 regulates vascular smooth muscle cell apoptosis through FoxO3a and Apaf1 and protects against arterial remodeling and atherosclerosis. *Arterioscler Thromb Vasc Biol* **34**, 2421-2428 (2014).
131. M. J. Mulvany, O. K. Hansen, C. Aalkjaer, Direct evidence that the greater contractility of resistance vessels in spontaneously hypertensive rats is associated with a narrowed lumen, a thickened media, and an increased number of smooth muscle cell layers. *Circ Res* **43**, 854-864 (1978).
132. G. R. Grotendorst, H. E. Seppa, H. K. Kleinman, G. R. Martin, Attachment of smooth muscle cells to collagen and their migration toward platelet-derived growth factor. *Proc Natl Acad Sci U S A* **78**, 3669-3672 (1981).

133. E. P. Amento, N. Ehsani, H. Palmer, P. Libby, Cytokines and growth factors positively and negatively regulate interstitial collagen gene expression in human vascular smooth muscle cells. *Arterioscler Thromb* **11**, 1223-1230 (1991).
134. M. Yamamoto, K. Yamamoto, T. Noumura, Type I collagen promotes modulation of cultured rabbit arterial smooth muscle cells from a contractile to a synthetic phenotype. *Exp Cell Res* **204**, 121-129 (1993).
135. T. Acker, H. Beck, K. H. Plate, Cell type specific expression of vascular endothelial growth factor and angiopoietin-1 and -2 suggests an important role of astrocytes in cerebellar vascularization. *Mech Dev* **108**, 45-57 (2001).
136. H. Beck, T. Acker, C. Wiessner, P. R. Allegrini, K. H. Plate, Expression of angiopoietin-1, angiopoietin-2, and tie receptors after middle cerebral artery occlusion in the rat. *Am J Pathol* **157**, 1473-1483 (2000).
137. L. Eklund, B. R. Olsen, Tie receptors and their angiopoietin ligands are context-dependent regulators of vascular remodeling. *Exp Cell Res* **312**, 630-641 (2006).
138. Y. Zhao *et al.*, Angiopoietin 1 counteracts vascular endothelial growth factor-induced blood-brain barrier permeability and alleviates ischemic injury in the early stages of transient focal cerebral ischemia in rats. *Neurol Res* **32**, 748-755 (2010).
139. G. K. Owens, Role of mechanical strain in regulation of differentiation of vascular smooth muscle cells. *Circ Res* **79**, 1054-1055 (1996).
140. A. C. Gittenberger-de Groot, M. C. DeRuiter, M. Bergwerff, R. E. Poelmann, Smooth muscle cell origin and its relation to heterogeneity in development and disease. *Arterioscler Thromb Vasc Biol* **19**, 1589-1594 (1999).
141. E. R. Pfaltzgraff, D. M. Bader, Heterogeneity in vascular smooth muscle cell embryonic origin in relation to adult structure, physiology, and disease. *Dev Dyn* **244**, 410-416 (2015).
142. T. Christen *et al.*, Cultured porcine coronary artery smooth muscle cells. A new model with advanced differentiation. *Circ Res* **85**, 99-107 (1999).
143. M. G. Frid, E. P. Moiseeva, K. R. Stenmark, Multiple phenotypically distinct smooth muscle cell populations exist in the adult and developing bovine pulmonary arterial media in vivo. *Circ Res* **75**, 669-681 (1994).
144. G. K. Owens, G. Wise, Regulation of differentiation/maturation in vascular smooth muscle cells by hormones and growth factors. *Agents Actions Suppl* **48**, 3-24 (1997).
145. B. Poller, J. Drewe, S. Krahenbuhl, J. Huwyler, H. Gutmann, Regulation of BCRP (ABCG2) and P-glycoprotein (ABCB1) by cytokines in a model of the human blood-brain barrier. *Cell Mol Neurobiol* **30**, 63-70 (2010).
146. J. Badaut, G. J. Bix, Vascular neural network phenotypic transformation after traumatic injury: potential role in long-term sequelae. *Transl Stroke Res* **5**, 394-406 (2014).
147. Y. Xiong, A. Mahmood, M. Chopp, Animal models of traumatic brain injury. *Nature Reviews Neuroscience* **14**, 128-142 (2013).
148. V. E. Johnson, W. Stewart, D. H. Smith, Axonal pathology in traumatic brain injury. *Exp Neurol* **246**, 35-43 (2013).
149. D. I. Graham, J. H. Adams, J. A. Nicoll, W. L. Maxwell, T. A. Gennarelli, The nature, distribution and causes of traumatic brain injury. *Brain Pathol* **5**, 397-406 (1995).
150. J. H. Adams, D. I. Graham, T. A. Gennarelli, W. L. Maxwell, Diffuse Axonal Injury in Nonmissile Head-Injury. *J Neurol Neurosur Ps* **54**, 481-483 (1991).

151. J. H. Adams *et al.*, Diffuse axonal injury in head injury: definition, diagnosis and grading. *Histopathology* **15**, 49-59 (1989).
152. M. Inglese *et al.*, Diffuse axonal injury in mild traumatic brain injury: a diffusion tensor imaging study. *J Neurosurg* **103**, 298-303 (2005).
153. D. H. Smith, D. F. Meaney, W. H. Shull, Diffuse axonal injury in head trauma. *J Head Trauma Rehabil* **18**, 307-316 (2003).
154. B. E. Leininger, S. E. Gramling, A. D. Farrell, J. S. Kreutzer, E. A. Peck, 3rd, Neuropsychological deficits in symptomatic minor head injury patients after concussion and mild concussion. *J Neurol Neurosurg Psychiatry* **53**, 293-296 (1990).
155. A. Marmarou *et al.*, A new model of diffuse brain injury in rats. Part I: Pathophysiology and biomechanics. *J Neurosurg* **80**, 291-300 (1994).
156. M. A. Foda, A. Marmarou, A new model of diffuse brain injury in rats. Part II: Morphological characterization. *J Neurosurg* **80**, 301-313 (1994).
157. S. M. DeFord *et al.*, Repeated mild brain injuries result in cognitive impairment in B6C3F1 mice. *J Neurotrauma* **19**, 427-438 (2002).
158. Y. Yoshiyama *et al.*, Enhanced neurofibrillary tangle formation, cerebral atrophy, and cognitive deficits induced by repetitive mild brain injury in a transgenic tauopathy mouse model. *J Neurotrauma* **22**, 1134-1141 (2005).
159. B. Mouzon *et al.*, Repetitive mild traumatic brain injury in a mouse model produces learning and memory deficits accompanied by histological changes. *J Neurotrauma* **29**, 2761-2773 (2012).
160. M. J. Kane *et al.*, A mouse model of human repetitive mild traumatic brain injury. *J Neurosci Methods* **203**, 41-49 (2012).
161. I. Khalin *et al.*, A mouse model of weight-drop closed head injury: emphasis on cognitive and neurological deficiency. *Neural Regen Res* **11**, 630-635 (2016).
162. V. E. Johnson, D. F. Meaney, D. K. Cullen, D. H. Smith, Animal models of traumatic brain injury. *Handb Clin Neurol* **127**, 115-128 (2015).
163. D. I. Shreiber *et al.*, Experimental investigation of cerebral contusion: histopathological and immunohistochemical evaluation of dynamic cortical deformation. *J Neuropathol Exp Neurol* **58**, 153-164 (1999).
164. D. I. Shreiber, D. H. Smith, D. F. Meaney, Immediate in vivo response of the cortex and the blood-brain barrier following dynamic cortical deformation in the rat. *Neurosci Lett* **259**, 5-8 (1999).
165. J. W. Lighthall, Controlled cortical impact: a new experimental brain injury model. *J Neurotrauma* **5**, 1-15 (1988).
166. C. E. Dixon, G. L. Clifton, J. W. Lighthall, A. A. Yaghmai, R. L. Hayes, A controlled cortical impact model of traumatic brain injury in the rat. *J Neurosci Methods* **39**, 253-262 (1991).
167. S. C. Cortez, T. K. McIntosh, L. J. Noble, Experimental fluid percussion brain injury: vascular disruption and neuronal and glial alterations. *Brain Res* **482**, 271-282 (1989).
168. D. H. Smith *et al.*, A Model of Parasagittal Controlled Cortical Impact in the Mouse - Cognitive and Histopathologic Effects. *J Neurotraum* **12**, 169-178 (1995).
169. J. C. Goodman, L. Cherian, R. M. Bryan, Jr., C. S. Robertson, Lateral cortical impact injury in rats: pathologic effects of varying cortical compression and impact velocity. *J Neurotrauma* **11**, 587-597 (1994).

170. P. M. Kochanek *et al.*, Cerebral blood flow at one year after controlled cortical impact in rats: assessment by magnetic resonance imaging. *J Neurotrauma* **19**, 1029-1037 (2002).
171. P. M. Washington *et al.*, The effect of injury severity on behavior: a phenotypic study of cognitive and emotional deficits after mild, moderate, and severe controlled cortical impact injury in mice. *J Neurotrauma* **29**, 2283-2296 (2012).
172. G. B. Fox, L. Fan, R. A. Levasseur, A. I. Faden, Sustained sensory/motor and cognitive deficits with neuronal apoptosis following controlled cortical impact brain injury in the mouse. *J Neurotraum* **15**, 599-614 (1998).
173. N. Marklund, L. Hillered, Animal modelling of traumatic brain injury in preclinical drug development: where do we go from here? *Br J Pharmacol* **164**, 1207-1229 (2011).
174. C. E. Dixon *et al.*, One-year study of spatial memory performance, brain morphology, and cholinergic markers after moderate controlled cortical impact in rats. *J Neurotrauma* **16**, 109-122 (1999).
175. R. E. Bennett, C. L. Mac Donald, D. L. Brody, Diffusion tensor imaging detects axonal injury in a mouse model of repetitive closed-skull traumatic brain injury. *Neurosci Lett* **513**, 160-165 (2012).
176. M. J. Hylin *et al.*, Repeated mild closed head injury impairs short-term visuospatial memory and complex learning. *J Neurotrauma* **30**, 716-726 (2013).
177. S. L. Andersen, Trajectories of brain development: point of vulnerability or window of opportunity? *Neurosci Biobehav Rev* **27**, 3-18 (2003).
178. G. Kanayama *et al.*, The effects of repetitive mild brain injury on cytoskeletal protein and behavior. *Methods Find Exp Clin Pharmacol* **18**, 105-115 (1996).
179. Y. Olsson, Studies on vascular permeability in peripheral nerves. 3. Permeability changes of vasa nervorum and exudation of serum albumin in INH-induced neuropathy of the rat. *Acta Neuropathol* **11**, 103-112 (1968).
180. V. Pop, J. Badaut, A neurovascular perspective for long-term changes after brain trauma. *Transl Stroke Res* **2**, 533-545 (2011).
181. C. Werner, K. Engelhard, Pathophysiology of traumatic brain injury. *Br J Anaesth* **99**, 4-9 (2007).
182. K. L. Davis, L. W. Jenkins, D. S. DeWitt, D. S. Prough, Mild traumatic brain injury does not modify the cerebral blood flow profile of secondary forebrain ischemia in Wistar rats. *J Neurotrauma* **15**, 615-625 (1998).
183. D. S. DeWitt, D. S. Prough, C. L. Taylor, J. M. Whitley, Reduced cerebral blood flow, oxygen delivery, and electroencephalographic activity after traumatic brain injury and mild hemorrhage in cats. *J Neurosurg* **76**, 812-821 (1992).
184. D. C. Engel *et al.*, Changes of cerebral blood flow during the secondary expansion of a cortical contusion assessed by 14C-iodoantipyrine autoradiography in mice using a non-invasive protocol. *J Neurotrauma* **25**, 739-753 (2008).
185. K. Zweckberger *et al.*, Effect of early and delayed decompressive craniectomy on secondary brain damage after controlled cortical impact in mice. *J Neurotrauma* **23**, 1083-1093 (2006).
186. L. Cherian, C. S. Robertson, C. F. Contant, Jr., R. M. Bryan, Jr., Lateral cortical impact injury in rats: cerebrovascular effects of varying depth of cortical deformation and impact velocity. *J Neurotrauma* **11**, 573-585 (1994).
187. H. Nawashiro, K. Shima, H. Chigasaki, Immediate cerebrovascular responses to closed head injury in the rat. *J Neurotrauma* **12**, 189-197 (1995).

188. B. T. Kalish, M. J. Whalen, Weight Drop Models in Traumatic Brain Injury. *Methods Mol Biol* **1462**, 193-209 (2016).
189. T. K. Len, J. P. Neary, Cerebrovascular pathophysiology following mild traumatic brain injury. *Clin Physiol Funct Imaging* **31**, 85-93 (2011).
190. E. C. Junger *et al.*, Cerebral autoregulation following minor head injury. *J Neurosurg* **86**, 425-432 (1997).
191. S. Strebel, A. M. Lam, B. F. Matta, D. W. Newell, Impaired cerebral autoregulation after mild brain injury. *Surg Neurol* **47**, 128-131 (1997).
192. J. Becelewski, K. Pierzchala, [Cerebrovascular reactivity in patients with mild head injury]. *Neurol Neurochir Pol* **37**, 339-350 (2003).
193. J. Thompson, W. Sebastianelli, S. Slobounov, EEG and postural correlates of mild traumatic brain injury in athletes. *Neurosci Lett* **377**, 158-163 (2005).
194. E. M. Buckley *et al.*, Decreased microvascular cerebral blood flow assessed by diffuse correlation spectroscopy after repetitive concussions in mice. *J Cereb Blood Flow Metab* **35**, 1995-2000 (2015).
195. J. O. Ojo *et al.*, Chronic Repetitive Mild Traumatic Brain Injury Results in Reduced Cerebral Blood Flow, Axonal Injury, Gliosis, and Increased T-Tau and Tau Oligomers. *J Neuropathol Exp Neurol* **75**, 636-655 (2016).
196. C. E. Lynch *et al.*, Chronic cerebrovascular abnormalities in a mouse model of repetitive mild traumatic brain injury. *Brain Inj* **30**, 1414-1427 (2016).
197. P. A. Casey, M. C. McKenna, G. Fiskum, M. Saraswati, C. L. Robertson, Early and sustained alterations in cerebral metabolism after traumatic brain injury in immature rats. *J Neurotrauma* **25**, 603-614 (2008).
198. S. Ashwal *et al.*, Proton MR spectroscopy detected glutamate/glutamine is increased in children with traumatic brain injury. *J Neurotrauma* **21**, 1539-1552 (2004).
199. K. A. Stanness *et al.*, Morphological and functional characterization of an in vitro blood-brain barrier model. *Brain Res* **771**, 329-342 (1997).
200. M. Takahashi, K. Shimada, B. C. Berk, [Fluid shear stress-mediated signal transduction in endothelial cells: temporal signaling events]. *Rinsho Ketsueki* **39**, 124-125 (1998).
201. H. A. Baba, A. Takeda, C. Schmid, M. Nagano, Early proliferative changes in hearts of hypertensive Goldblatt rats: an immunohistochemical and flow-cytometrical study. *Basic Res Cardiol* **91**, 275-282 (1996).
202. S. Sangiorgi *et al.*, Early-stage microvascular alterations of a new model of controlled cortical traumatic brain injury: 3D morphological analysis using scanning electron microscopy and corrosion casting. *J Neurosurg* **118**, 763-774 (2013).
203. P. J. Lindsberg, A. L. Siren, J. M. Hallenbeck, Microvascular perfusion during focal vasogenic brain edema: a scanning laser fluorescence microscopy study. *Microvasc Res* **53**, 92-103 (1997).
204. O. Y. Glushakova, D. Johnson, R. L. Hayes, Delayed increases in microvascular pathology after experimental traumatic brain injury are associated with prolonged inflammation, blood-brain barrier disruption, and progressive white matter damage. *J Neurotrauma* **31**, 1180-1193 (2014).
205. A. F. Logsdon *et al.*, Role of Microvascular Disruption in Brain Damage from Traumatic Brain Injury. *Compr Physiol* **5**, 1147-1160 (2015).

206. P. D. Adelson, M. J. Whalen, P. M. Kochanek, P. Robichaud, T. M. Carlos, Blood brain barrier permeability and acute inflammation in two models of traumatic brain injury in the immature rat: a preliminary report. *Acta Neurochir Suppl* **71**, 104-106 (1998).
207. W. Li *et al.*, A quantitative MRI method for imaging blood-brain barrier leakage in experimental traumatic brain injury. *PLoS One* **9**, e114173 (2014).
208. N. Marchi *et al.*, Consequences of repeated blood-brain barrier disruption in football players. *PLoS One* **8**, e56805 (2013).
209. W. P. Meehan, 3rd, J. Zhang, R. Mannix, M. J. Whalen, Increasing recovery time between injuries improves cognitive outcome after repetitive mild concussive brain injuries in mice. *Neurosurgery* **71**, 885-891 (2012).
210. M. K. Baskaya, A. M. Rao, A. Dogan, D. Donaldson, R. J. Dempsey, The biphasic opening of the blood-brain barrier in the cortex and hippocampus after traumatic brain injury in rats. *Neurosci Lett* **226**, 33-36 (1997).
211. F. L. Cardoso, D. Brites, M. A. Brito, Looking at the blood-brain barrier: molecular anatomy and possible investigation approaches. *Brain Res Rev* **64**, 328-363 (2010).
212. A. Rodriguez-Baeza, F. Reina-de la Torre, A. Poca, M. Marti, A. Garnacho, Morphological features in human cortical brain microvessels after head injury: a three-dimensional and immunocytochemical study. *Anat Rec A Discov Mol Cell Evol Biol* **273**, 583-593 (2003).
213. A. C. McKee *et al.*, Chronic traumatic encephalopathy in athletes: progressive tauopathy after repetitive head injury. *J Neuropathol Exp Neurol* **68**, 709-735 (2009).
214. J. L. Lin, Y. H. Huang, Y. C. Shen, H. C. Huang, P. H. Liu, Ascorbic acid prevents blood-brain barrier disruption and sensory deficit caused by sustained compression of primary somatosensory cortex. *J Cereb Blood Flow Metab* **30**, 1121-1136 (2010).
215. S. Nag, R. Venugopalan, D. J. Stewart, Increased caveolin-1 expression precedes decreased expression of occludin and claudin-5 during blood-brain barrier breakdown. *Acta Neuropathol* **114**, 459-469 (2007).
216. H. L. Tian *et al.*, Risk factors for posttraumatic cerebral infarction in patients with moderate or severe head trauma. *Neurosurg Rev* **31**, 431-436; discussion 436-437 (2008).
217. J. Ghajar, Traumatic brain injury. *Lancet* **356**, 923-929 (2000).

Chapter 2:

An Age-dependent Role of the Angiopoeitin-Tie2 Axis Following Traumatic Brain Injury

Thomas R. Brickler[1], Amanda Hazy[1], Xia Wang[1], Stefanie Robel[2], and Michelle H Theus[1]

[1]The Department of Biomedical Sciences and Pathobiology, Virginia-Maryland Regional College of Veterinary Medicine, 215 Duck Pond Drive, Blacksburg, VA, 24061 USA

[2]Virgnia Tech Carillion Research Institute, College of Medicine, 2 Riverside Circle, Roanoke, VA 24016 USA

Abstract

While there are many studies that have focused on how the pediatric and immature brain responds after traumatic brain injury (TBI), there are a limited amount of studies that address how the adolescent brain recovers after TBI. It has been shown that children have worse clinical outcome after TBI; however, the mechanisms that underlie enhanced recovery may actually occur through age-specific processes. The objective of this study was to investigate the adolescent response to TBI using moderate cortical controlled impact (CCI) injury in adult and postnatal day 21 juvenile/adolescent mice. Here we show that 4 days post-CCI injury, juvenile mice have significantly less cortical tissue loss compared to adult mice. Furthermore, juvenile mice display a significant increase in blood flow restoration to the area of injury as early as 2 days post-CCI injury and an increase in expression of tight junction proteins, claudin-5 and occludin-1, that prevents BBB permeability to Evan's Blue (EB) dye that was not observed in adult mice. The vascular environment is better preserved and protected in juvenile mice after CCI-injury as juvenile mice have larger diameter collateral vessels, more $CD31^+$ vessels within the peri-lesion, and less infiltrating $CD11b^+$ cells compared to adult mice. We have also observed an age-dependent behavioral difference to injury between juvenile and adult mice as juvenile mice were resistant to

motor and memory deficits using the rotarod and novel object recognition behavioral tests, respectively. Gene expression analysis using qPCR on purified endothelial cells (ECs) reveals expression differences between juvenile and adult mice in the angiopoietin (Ang)- Tie2 signaling cascade. Preventing Tie2 signaling attenuated the neuroprotection seen in P21 mice. Thus, our findings demonstrate an age-dependent response of the Ang-Tie2 axis in playing a direct role in preventing tissue damage following CCI-injury. Targeting Tie2 signaling may, therefore, be a potential therapeutic target for tissue protection against head injury.

Introduction

Traumatic brain injury (TBI) is the leading cause of death and morbidity in children and adolescents (*1-6*). Clinical studies that measure cognitive and behavioral disturbances conclude that children who suffer TBI have a worse clinical outcome compared to adults (*1, 2*). However, our understanding of how the adolescent brain responds to trauma is significantly understudied. Clinical reports that have focused on the adolescent population have shown adolescent TBI patients have experienced the greatest magnitude of functional improvement compared to adult TBI patients (*3*). These findings that measured the outcome of adolescent TBI patients utilized the Disability Rating Scale (DRS) and the Glasgow Coma Scale (GCS) and found adolescents showed better improvements in cognitive and motor tasks, however, the mechanisms of these age-specific neurological improvements after injury remain unknown (*3*). Experimental animal studies that induce trauma to the developing brain have advanced our mechanistic understanding of injury response and recovery, but the numbers of these studies within the adolescent/juvenile brain are limited (*4, 5*). In similar pursuit of the clinical research, the majority of these experimental studies focus on the rodent neonatal/immature brain, which has also been shown to be highly vulnerable to TBI (*6-9*). Interestingly, work within the stroke field have highlighted an age-specific resistance to blood brain barrier (BBB) damage after cerebral ischemia (*4*). The brain's vasculature is lined with tightly associated endothelial cells (ECs), pericytes, and astrocytes that make up the BBB (*10, 11*). Oxidative stress caused by ischemia can induce damage to the BBB by disassociating ECs, pericytes, and astrocytes (*11, 12*). In the study performed by Muramatsu *et al,* adolescent postnatal day 21 (P21) rats and immature P7 and P14 rats were subject to cerebral hypoxic-ischemia and stained for IgG, which binds to albumin and is a marker for BBB permeability (*13*). After the injury, P7 and P14 brains had robust staining for IgG, while P21brains had little to no IgG leakage

within the brain parenchyma (*4*). These studies demonstrate that there are mechanistic differences in age response of the BBB to cerebral ischemia.

While TBI is unique in the sense that there is a force applied to the brain, the multifaceted pathological process shares a similar disease characteristic, cerebral ischemia, to that of stroke (*14*). Studies that have measured cerebral blood flow (CBF) after fluid percussion injury (FPI) in rats have shown CBF is depressed about 44% compared to non-injured shams (*15*). Pioneering studies that compared the response of CBF after FPI between newborn and juvenile pigs found CBF levels to remain depressed in newborn pigs while CBF restoration occurred faster in juvenile pigs. Differences in CBF between newborn and juvenile pigs after FPI was further supported by differences in the size of the pial arterioles (*16*). The authors found that the increase in CBF after FPI in juvenile pigs was due to the large diameter size of the pial arterioles that was not observed in the newborn pigs (*16*). These studies further exemplify that the vascular function within the juvenile brain does not share a pattern of vulnerability with respect to age after TBI (*5*). Other studies suggest the preservation of key vascular responses such as acute hemodynamics (*31-35*) microvascular density (*36-39*), and BBB integrity (*11, 40-42*) may prevent calcium perturbations, mitigating the secondary phases of cellular injury induced by cell stress, inflammation, and apoptosis (*17, 18*). Mechanisms underlying blood vessel maintenance and function show intact blood vessels after trauma are important to provide proper vascularization of the tissue while injured/leaky blood vessels have an opposite effect. Injured vessels contribute to the progressive nature of tissue loss by impeding endogenous tissue repair and leaving the underlying tissue void of vascularization (*35, 43-46*). Interestingly, many vascular factors that either promote vessel stability or destabilization are expressed after TBI (*19, 20*). The angiopoietins (Ang-1 and Ang-2) and the Tie2 receptor tyrosine kinases form a major signaling pathway that is exclusively EC-

specific (*21, 22*). Ang-1 is expressed by mural cells that surround mature blood vessels while Ang-2 is expressed by ECs (*23*). Although both Ang-1 and Ang-2 bind to the Tie2 receptor, they mediate different effects when bound and the presence of other vascular factors like vascular endothelial growth factor (VEGF) can change the cellular response to Ang binding making this system context dependent (*24*). Ang-2 expression is elevated in times of hypoxia and can elicit sprouting of blood vessels (*25*). In contrast, Ang-1 has a higher affinity for the Tie2 receptor compared to Ang-2 and plays a necessary role in vessel stability (*24, 26*). Given the experimental evidence that there is an age-dependent vascular response in juveniles to TBI, there may also be an age-dependent mechanism within the ECs that promote this response (*27, 28*). Therefore, understanding the mechanism(s) of the EC-specific Angiopoetin-Tie2 signaling cascade within the adolescent brain, which has demonstrated resistance to ischemic injury could prove beneficial for understanding how these blood vessels are able to respond robustly after TBI and applying these mechanism(s) for therapy to other age groups.

The current study assesses the injury-induced cellular and acute vascular changes in the brains of both adult and juvenile mice following cortical controlled impact (CCI) injury. Given that the mouse cortex reaches approximately 100% of its adult weight by P21 and key brain maturation events have been established, this is an appropriate age to model the human adolescent brain (*184)*. These maturation events include the development of the BBB with the establishment of tight junction proteins and astrocyte end feet coverage and the maturation of the vasculature with associated mural cells (*29-36*). Differences between the adult and juvenile brain arise in synaptic proliferation and pruning events to be ongoing in the adolescent brain and glial maturation does not terminate well into adulthood (*29-36*). We have chosen the CCI model given the clinical relevance of the injury pathologies it produces such as contusion, ischemia, and subdural

hematoma as these pathological features have also been observed in the clinic (*37-40*). Specifically, we tested the hypothesis that differences in acute vascular changes exist between juvenile and adult mice and the EC-specific Angiopoietin-Tie2 axis in juvenile mice confers tissue protection. We further tested the role of Tie2 signaling by blocking angiopoietin binding onto Tie2 using the Tie2-FC soluble receptor protein and found neuroprotection to be attenuated in juvenile mice. These findings highlight differences between the juvenile and adult brain response to CCI-injury and further provide support for an age-dependent defense of the vasculature to TBI.

Materials and Methods

CCI Injury. Animals were prepared for CCI as previously described (*41*). Male CD1 mice at postnatal day 21 and 2-4 months were anesthetized with ketamine and xylazine intraperitoneal (i.p.) injection and positioned in a stereotaxic frame. Body temperature was monitored with a rectal probe and maintained at 37°C with a controlled heating pad set. A 5mm craniotomy was made using a portable drill over the right parietal-temporal cortex (−2.5 mm A/P and 2.0 mm lateral from bregma). Injury was induced by moderate CCI using the *e*CCI- 6.3 device (Custom Design & Fabrication; 3mm impounder) at a velocity of 3.5 m/s, depth of 1.0 mm, and 150 ms impact duration (*42, 43*). Sham controls received anesthesia, skin incisions and sutures only. Following injury, the incision was closed using Vetbond tissue adhesive (3M, St. Paul, MN, USA) and the animals were placed into a heated cage until fully recovered from anesthesia. All experiments were conducted in accordance with the NIH Guide for the Care and Use of Laboratory Animals and were conducted under the approval of the Virginia Tech Institutional Animal Care and Use Committee (IACUC; #12-081/15-063) and the Virginia Maryland Regional College of Veterinary Medicine.

Blood Flow Analysis. Cerebral blood flow measurement was conducted using Moor Laser Doppler Imager (Moor LDI 5061 and Moor Software Version 5.3, from Moor Instruments) as previously described (*44*). Mice were anesthetized and kept at 37.0 $\pm$ 0.5ºC body temperature. The measurements were performed pre-CCI, post-CCI, and then under 1.5-2% isoflurane 3 h post-CCI and for a consecutive 4 d post-CCI. Tissue perfusion is quantified with a region of interest (ROI) defined around the area of injury. Corresponding areas in contralateral hemispheres and sham were similarly surveyed. Shams acted as internal controls and the valid pixel (VP) and mean pixel (MP) of ROIs of each hemisphere of sham animals was averaged. The ratio of injured animal's corresponding hemispheres to sham hemispheres was used to plot the time-course.

Behavioral Evaluations. A battery of behavioral tests were performed on juvenile (P21) and adult (2-4 months) sham and CCI-injured mice 4, 7, and 14 days post-CCI injury by an observer unaware of experimental groups. For training and testing days, animals were habituated into the training room for one hour prior to testing and all assessments took place roughly at the same time each testing day. The order of behavioral tests was as follows: novel object recognition, inverted screen, beam balance, and Rotarod.

Novel Object Recognition. Hippocampal learning and memory were evaluated using novel object recognition (NOR) testing. Twenty-four hours before testing days, mice were familiarized with two identical objects and allowed to explore for five minutes in an open field plane. Mice were placed in the center of the testing area, facing away from the objects. On testing days, a novel object replaced one of the familiar objects and the mice were video recorded for five minutes. The objects and testing area were cleaned in between trials to eliminate odor preference.

Evaluation of hippocampal learning and memory is displayed as a preference index: the ratio of time exploring the novel object to the total time exploring both objects. The mouse is perceived as exploring an object when the animal's nose comes within 2 cm of the object. A preference index of greater than 50% indicates novel object preference.

Inverted Screen Test. Muscle strength was evaluated using Kondziela's inverted screen test. In short, mice are placed in the center of a wire mesh screen and a stop clock is started. The screen is a 43 cm square of wire mesh that is 12 mm squares of 1mm diameter wire and encased by 4 cm of wood. Over two seconds, the screen is rotated to an inverted position with the animal's head declining first. The screen is held 50 cm above a padded surface. The test is complete when the mouse falls off the screen or if the mouse has been inverted for 60 s. Muscle strength is displayed as the time to fall (seconds).

Beam Balance. Motor coordination and balance were evaluated using a beam balance test as previously described. The apparatus consists of a flat 1-meter beam of 6mm thickness resting 50 cm above a padded surface. At the finish point of the beam, a black box where nesting material from home cages is placed to attract mice to this finish point. The time it takes mice to travel a total of 80 cm is recorded. Mice are placed at the start point of the beam and a stop clock is started when the animal's nose crosses the start of 80 cm distance and the clock is stopped when the animal's nose crosses the end of 80 cm. Animals were pre-trained 24 h prior to CCI injury with 4 trials each on the 6 mm beam (1 minutes resting in between trails) each day. Animals were also observed for any hindlimb slips when walking across the beam and this was also recorded. Evaluation of balance beam after the injury was averaged per animal trials on the testing day.

Rotarod Assessment. Sensorimotor function was evaluated using Rotarod testing, as previously described (*41*) . Assessment was performed on the Economex (Columbus Instruments, Columbus, OH) at the aforementioned time points. The starting velocity was set at 10 rpm and accelerated to 0.1 rpm/sec. Animals were pre-trained for 4 consecutive days prior to CCI injury with 4 trials (2 minutes resting in between trails) each day. A baseline was collected on the fourth day of training. During testing days, each of the four trials ended when the animal fell off the Rotarod (fall latency) and the time (seconds) was recorded. Evaluation of motor function after injury was based on averaged individual scores relative to each animal's baseline latencies and represented as percentages of baseline.

Vessel Painting. Vessel painting on post-natal and CCI-injured mice was modified from previous studies (*45*). Briefly, mice were injected s.c. with heparin (2,000 units/kg), and sodium nitroprusside (SNP, 0.75 mg/kg) five minutes prior to euthanization using an overdose of isoflurane. When breathing stopped, the chest cavity was opened and then cardiac perfused using a Gilson MiniPuls3 peristaltic perfusion pump (Gilson Scientific, Bedfordshire, UK). Using a continuous infusion, 6-10 ml of 1x phosphate buffered saline (PBS) containing 20 units/ml heparin was perfused to flush blood from the cerebrovascular system, then 10 ml DiI (0.01µg/ml, Invitrogen)– 4% sucrose–PBS-heparin mixture was perfused to label the vasculature (0.7 ml/min for P1, 1.0 ml/min P7 and 2ml/min for P21 and adult flow rate), and finally, 4% cold paraformaldehyde (PFA) was perfused to fix the tissue. All reagents were filter sterilized and debris free. After perfusion, brains were carefully removed from the skull and placed in PFA overnight. Fixed brains were imaged at multiple image planes at 4x magnification on an upright fluorescence microscope (BX-51, Olympus America), using mosaic tile imaging from

StereoInvestigator software (MBF, Williston, VT). After imaging brains were transferred to 20% sucrose overnight, then embedded in OCT on dry ice.

Quantification of collateral number and diameter. Collateral number and diameter was obtained from vessel painted brains at 10x magnification and analyzed in StereoInvestigator software (MBF, Williston, VT). The number of collaterals between the MCA, ACA, and PCA trees and the number of anastomoses within these trees was counted to give the total collateral number. Once collaterals were identified, diameters were measured using the quick measure line. Two measurements were taken for each collateral and averaged to give the relative size of the vessel.

Immunostaining. For immunostaining, whole mount, perfused-fixed tissue sections were blocked in 2% FISH gel with 0.1% Triton for 5 hours and incubated with primary antibody overnight in block at 4°C (mouse anti-Smooth Muscle Actin (SMA): 1/200 (Santa Cruz Biotechnology SC-53142); NISSL 1/200 (Invitrogen N21480). Whole mount fresh tissue sections were blocked in 2% FISH gel with 0.1% Triton for 5 hours and incubated with primary antibody overnight in block at 4°C (goat-anti- CD31: 1/200 (BD AF-3628); mouse anti- CD11b: 1/200 (R&D MAB1124) or rabbit anti-Glial Fibrillary Acidic Protein (GFAP): 1/200 (Cell Signaling 12389S). Sections were washed 4 times with 1X PBS and incubated with anti-rabbit, mouse, goat Alexa Fluor 488-conjugated secondary antibodies or anti- mouse Alex Flour 594- conjugated secondary antibodies (Molecular Probes, Carlsbad, CA) for 1h at RT. Whole mounts were counterstained with DAPI (1 µg/ml, Molecular probes, Carlsbad, CA) and mounted in Pro-Long anti-fade mounting solution (Molecular probes, Carlsbad, CA). To visualize Brdu, sections were fixed in 10% buffered formalin and incubated in 2N HCl as previously described (24).

Stereological Analysis:

Evaluation of Lesion volume. Lesion volume was assessed by a blinded investigator using Caveleri Estimator from StereoInvestigator (MicroBrightField, Williston, VT, USA) and an Olympus BX51TRF motorized microscope (Olympus America, Center Valley, PA, USA). Lesion volume (mm^3) was determined as previously described (*41, 46*). Briefly, volume analysis was performed by estimating the area of tissue loss in the ipsilateral cortical hemisphere for five coronal serial sections at or around the epicenter (−1.1 to -2.6 mm posterior from bregma) of injury. Nissl stained serial sections were viewed under fluorescent illumination (GFP) at a magnification of 4x. A random sampling scheme was used that estimates every 10th section from rostral to caudal, yielding five total sections to be analyzed. A randomly placed grid with 100 µm spaced points was placed over the ipsilateral hemisphere and the area of the lesion was marked within each grid. Lesion boundaries were identified by loss of NISSL staining, pyknotic neurons, and tissue hemorrhage. The marketed areas, using grid spacing, was then used to estimate total tissue volume based on section thickness, section interval, and total number of sections within the Caveleri program, StereoInvestigator. Data is represented as the volume of tissue loss or lesion volume (mm^3) for juvenile and adult mice.

Smooth Muscle Cell Diameter, CD31 density, and CD11b counts. Briefly, diameter, density, and counts were performed in the ipsilateral cortical hemisphere for five coronal serial sections at or around the epicenter (−1.1 to -2.6 mm posterior from bregma) of injury. Smooth muscle cell (SMA) stained serial sections were viewed under fluorescent illumination (GFP) at a magnification of 20x and an exhaustive count was performed to obtain the diameter of SMA^+/DI^+ vessels that were found on the surface, hippocampus, and interstitial tissue, using a different probe to demarcate where the vessel was found. SMA diameter (µm) was assessed using the Nucleator

method from StereoInvestigator (MicroBrightField, Williston, VT, USA) and an Olympus BX51TRF motorized microscope (Olympus America, Center Valley, PA, USA). The diameter was determined by identifying cross-sectional SMA^+ vessels and placing a probe that shoots out four random rays in the center of each cross section. The points where the rays intersect the SMA^+ vessel is marked and a radius is calculated. For CD31 density, dapi stained serial sections were viewed under fluorescent illumination (UV) at a magnification of 4x to draw a contour 1mm from the top of the cortex around the area of injury. The optical fractionator method was used and a counting frame set to randomly sample spaces covering the entire region of interest. $CD31^+$ were counted within each counting frame under fluorescent illumination (GFP) at a magnification of 20x to obtain appropriate coefficients of error. Density is estimated from taking into account section thickness and number of probes place within each counting frame. CD11b counts were performed under fluorescent illumination (RFP), six random 20x images were taken around the area of injury and CD11b cells were counted to give an estimate of infiltrating cells.

Isolation of $CD31^+$ cells: Adult or P21 mice were sacrificed by decapitation under anesthesia and injured cortex were extracted from 4d post-CCI and sham mice using neural dissociation kit (Miltenyi Biotec, Auburn, CA). Six to seven mice were used per group for each isolation. Single-cell suspension from freshly dissociated brain tissue was subjected to $CD31^+$ magnetic beads and column separation, as per manufacturer instructions to separate $CD31^+$ fraction from the rest of the flow through (MACS; Miltenyi Biotec, Auburn, CA).

Quantitative real-time PCR: Total RNA of $CD31^+$ cells and flow through was isolated according to the manufactures instructions using Trizol extraction (Invitrogen). RNA quantification

was carried out by measuring absorbance with spectrophotometer ND-1000 (NanoDrop). RNA was reverse transcribed into cDNA with Im-Prom II Reverse Transcription System (Promega, Madison, WI). RNA samples were treated with DNase I (ThermoFisher, Waltham, MA) before reverse transcription. Each DNase reaction (1 μg RNA, 1 μL 10X DNase I buffer, 1 μL DNase I, 0.5 μL RNase inhibitor, up to 10 μL with water) was incubated at 37 ℃ for 60 minutes before inactivation by the addition of 1 μL 50 mM EDTA and incubation at 65 ℃ for 10 min. The DNase-treated RNA samples were incubated with oligo (dT) 15 primer at 70 for 5 min. (250 ng RNA, 1 μL oligo (dT) 15, up to 5 μL with water) and chilled on ice for 5 minutes to allow annealing before reverse transcription. To prepare the cDNA samples, 15 μL reverse transcription mix (3.7 μL water, 4 μL 5X ImProm-II buffer, 4.8 μL 25 mM $MgCl_2$, 1 μL 10 mM dNTPs, 0.5 μL RNase inhibitor, 1 μL ImProm-II reverse transcriptase) were added per 5 μL RNA sample and reverse transcription was performed using the following PCR scheme: 25 ℃ for 5 min.; 42 ℃ for 1 hour; 70 ℃ for 15 min. For qRTPCR analysis, 7 ng cDNA per reaction were amplified using SYBR Green PCR Master Mix (Applied Biosystems, Foster City, CA). Gene primer sequences are shown in Table 1. Expression changes were calculated using ΔΔCq values with reference to Gapdh internal control gene then calculated as relative expression compared to appropriate sham samples. To test the purity of the $CD31^+$ fraction, relative expression was compared to appropriate flow through samples.

Table 1: Forward and Reverse mRNA primer sequences used for qPCR of $CD31^+$ cells and flow through (non-$CD31^+$ fraction).

Gene: mRNA Forward Sequence	**Gene:** mRNA Reverse Sequence
Mcp1: TCACCTGCTGCTACTCATTCACCA	**Mcp1:** TACAGCTTCTTTGGGACACCTGCT
Enos: ATGAGTTCAGAGATTGGCATGA	**Enos**: CTTGTCTTTCCACAGGGATGAG
Casp 12: AATGGAGGTAAATGCTGGATTG	**Casp 12:** ACGTGGACAAAGCTTCAGTGTA
Bcl2: CCTGTGGATGACTGAGTACCTG	**Bcl2:** AGCCAGGAGAAATCAAACAGAG
Ang 1: CGAAAGCTGACAGATGTTGAGA	**Ang 1:** TTTGTCTGTTGGAGAAGTTGCT
Ang 2: GGAAAAGCAGATTTTGGATCAG	**Ang 2:** TTCTGCTCCTTCATGGACTGTA
Vegf: GAAGTCCCATGAAGTGATCCAG	**Vegf:** TCACCGCCTTGGCTTGTCA
Flk1: GGGACCTGGACTGGCTTTG	**Flk1:** CCGCATTCAGTCACCAATACC
Flt1: TTCGGAAGACAGAAGTTCTCGTT	**Flt1:** GACCTCGTAGTCACTGAGGTTTTG
Neun: CACTCTCTTGTCCGTTTGCTTC	**Neun:** CTGCTGGCTGAGCATATCTGTA
GFAP:ACCAGTAACATGCAAGAGACAGAG	**GFAP:** GATAGTCGTTAGCTTCGTGCTTG
PdgfrB: GGTACGTGTGAAGGTGTCAGAA	**PdgfrB:** ACTCTCACTCAGCTCCAGCAC
Tie2: AAATGACCCTAGTGAAGCCAGA	**Tie2:** GTCAGGAGGTAAGACTCGGTTG
Cldn5: ATGCAGTGCAAGGTGTATGAAT	**Cldn5:** CCGGTCAAGGTAACAAAGAGTG
Ocln1: TGGATCGGTATGATAAGTCCAA	**Ocln1:** CATAGTCAGATGGGGGTGGAG
mGAPDH: ATTGTGTCCGTCGTGGATCTGA	**mGAPDH:** AGATGCCTGCTTCACCACCTTCTT

Blood Brain Barrier: A 0.5% sterile Evans blue (EB, Sigma E2129) solution was prepared in PBS and passed through a 0.2µm filter to remove powder that has not dissolved. Mice having undergone either sham or CCI surgery were injected with 200µl Evans Blue intraperitoneally. 3h after EB injection, brains were removed from the ipsilateral and contralateral hemispheres cortexes and incubated separately in 500µl Formamide (Invitrogen, 15515-026) for 24 h at 55º C. Samples were centrifuged to pellet the tissue and absorbance was measured at 610 nm using a NanoDrop 1000 Spectrophotometer (Thermo Scientific, Wilmington, DE.) Formamide was used to blank the instrument. EB absorbance for each injured animals was normalized to sham.

Tie2-Fc Infusion Studies: Juvenile mice at P21 were prepared for CCI injury as previously mentioned. Immediately after injury, juvenile mice received a 100 µL injection of either Fc control (Sino Biological Inc. S016080615) soluble protein diluted in 3 mL sterile saline or Tie2-Fc soluble protein (Sino Biological Inc. 51087-M0ZH) diluted in 3 mL sterile saline to give a final

concentration of 100 mg/ml. The animals received twice daily tail vein injections of 100 μL of either Fc or Tie2-Fc for a total of two days. After the two days, juvenile mice were sacrificed and lesion analysis was performed on fresh frozen tissue sections.

Statistical analysis. Data was graphed using GraphPad Prism, version 4 (GraphPad Software, Inc., San Diego, CA). Student's two-tailed t-test was used for comparison of two experimental groups. For three or more groups, multiple comparisons were done using one-way and two-way ANOVA where appropriate followed by Tukey or Bonferroni test for multiple pairwise examinations. Changes were identified as significant if P was less than 0.05. Mean values were reported together with the standard error of the mean (SEM).

Results

Juvenile Mice Have Reduced Lesion Volume

Clinical evidence suggests that the juvenile TBI patient population has a better clinical outcome following injury, though our understanding of the mechanisms involved is limited (*3*). To begin examining experimentally how the juvenile brain responds to TBI we sought to analyze the acute and sub-acute neural tissue damage between adult and juvenile mice. Specifically, we evaluated injury outcome in adult and juvenile mice, using the cortical controlled impact (CCI) model (*42, 43, 46*), at 4 and 14 days post- injury. Serial sections were subjected to NISSL staining and lesion boundaries were demarcated by the loss of NISSL stain, pyknotic neurons and tissue hemorrhage (Figure 1). Using the Caveleri estimator, we found juvenile mice ($1.5\pm0.13mm^3$; n=8) (Figure 1B) have a significant reduction in lesion volume (F=16.63, P=0.16) compared to adult mice ($2.5\pm0.08mm^3$; n=6) (Figure 1A) at 4 days post-CCI injury (Figure 1E). Sub-acute neural protection was also seen at 14 days post-CCI injury where juvenile mice ($1.2\pm0.10mm^3$; n=6)

(Figure 1D) had reduced lesion volume compared to adult (2.15±0.20mm^3; n=7) (Figure 1C) mice. These results indicate that juvenile mice have better tissue protection in the cortex following acute TBI compared to adult mice and this tissue protection is also persevered at a more sub-acute time point.

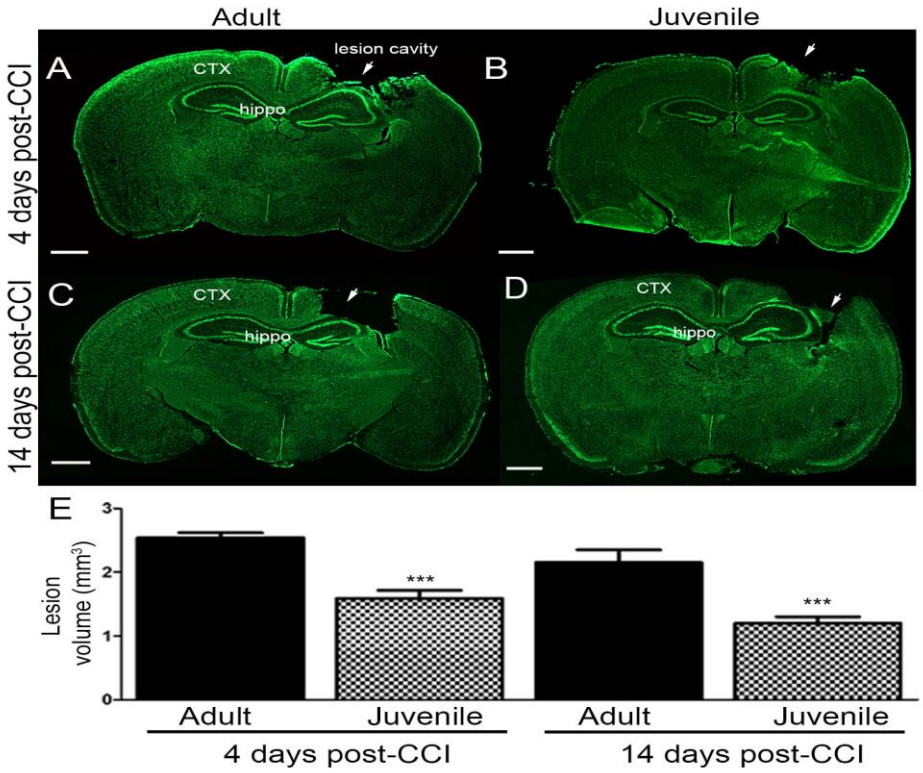

Figure 1. Comparison of Lesion Volume at 4 and 14 days post-CCI. Nissl stained sections collected at 4 and 14 days post-CCI from adult (A-C; respectively) and juvenile (B-D; respectively) brains show juvenile mice have less tissue loss. Quantified analysis (E) of lesion volume using Caveleri Estimator. Bar graph displays significant smaller lesion volume (mm^3) at 4 and 14 days in juvenile compared to adult. Dataset represented as mean +/- SEM. ***P<0.0001. CTX- cortex; hippo- hippocampus. (Adult n= 6-7 per group); (juvenile n= 6-8 per group). Scale bar 1mm.

Age-dependent Difference in Cerebral Blood Flow Recovery after TBI

As we found that juvenile mice exhibited acute tissue protection following CCI injury, we were interested to see if this overt neuroprotection was due to differences in CBF between juvenile and adult mice. To test this, juvenile and adult mice were subjected to non-invasive high-resolution infrared laser Doppler imaging to measure perfusion in the brain before and after CCI injury (Figure 2). The region of interest (ROI) was defined as an oval over the area of focally induced injury and outlined in Figure 2B-F. Relative blood flow using the defined ROI for each CCI-injured mouse gave a perfusion for unit (pfu) value based on color intensity (blood flow) and was compared to the average pfu values of sham-injured aged matched controls using the same ROI. Prior to injury, adult (Figure 2A) and juvenile (Figure 2D) mice display no differences in perfusion. There was a similar drop in perfusion in the area of injury immediately after CCI injury in both juvenile (0.345±0.03pfu; n=10) (Figure 2E) and adult (0.462±0.04pfu; n=7) mice (Figure 2B). This drop in perfusion was sustained at 3 hours to 1 days post-injury between adult (0.297±0.03pfu; 0.53±0.06pfu) and juvenile (0.36±0.02pfu; 0.56±0.06pfu) mice (Figure 2G). However, 2 days post-injury, juvenile mice (0.58±0.04pfu) had better perfusion to the area of injury compared to adult (0.413±0.06pfu) mice (Figure 2G). This increase in perfusion was significant in juvenile (0.67±0.05pfu; 0.62± 0.05pfu) mice from 3 to 4-days (Figure 2F) post-CCI injury compared to adult (0.38±0.06pfu; 0.44± 0.03pfu) mice (Figure 2C and 2G). In addition, we measured the blood perfusion on the contralateral side of injury and found juvenile (1.03±0.12pfu) mice have a significant increase in perfusion 3 hours post-CCI injury compared to adult (0.70±0.06pfu) mice and this increase in perfusion trended higher throughout the time course compared to adult mice (Figure 2H). These results indicate that there is an acute restoration of CBF to the area of injury in juvenile mice after CCI injury that is not observed in adult mice.

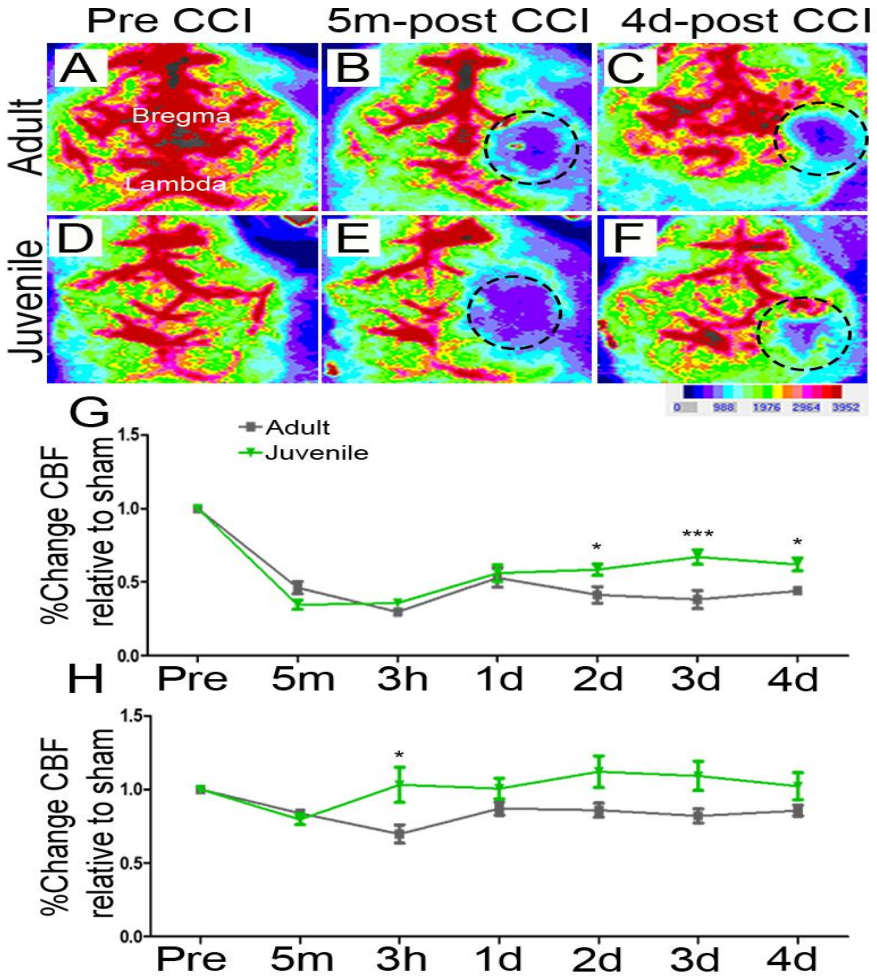

Figure 2. Cerebral Blood Flow in Adult and Juvenile mice following CCI injury. Relative intensity of blood flow analysis using the Laser Doppler Imager shows adult (A-C) and juvenile (D-F) mice have loss of blood flow after 5-minutes post-CCI injury denoted by dotted circle, which represents the region of interest (ROI) (B and E; respectively), compared to pre- injury (A and D; respectively). 4 days post-CCI injury, juvenile mice (F) have increase in blood flow perfusion around area of injury, compared to pre (D) and post (E) scans and to adult mice (C). Quantitative (G) analysis using relative intensity around ROI displays juvenile mice have a significant increase in blood flow to the area of injury starting at 2 days post-CCI and continuing onto 4 days compared

to adult. Juvenile mice have a significant increase in perfusion on the contralateral side (H) 3 hours following CCI injury and a trend toward an increase in perfusion with time. Dataset represented as mean +/- SEM relative to age-matched sham-injured mice. $^{***}P<0.0001$; $^{*}P<0.05$. Bregma and lambda points noted on images. (Adult and Juvenile CCI n= 7 and n=10 per group) (Adult and juvenile sham n=8 and n=11 per group).

Juvenile Mice Have Larger Pial Collaterals 4 Days Post-CCI injury

Pial arteriole vessels in juvenile pigs have been found to expand in diameter and contribute to the increase in CBF following FPI injury (*5*). In addition, experimental and clinical studies in the stroke field have demonstrated that the number and extent of pial arteriole collateral vessel remodeling correlate with early tissue protection (*47-49*). As our juvenile CCI model has demonstrated both neuroprotection and an early restoration of CBF, here we sought to analyze the effects of pial collateral vessel remodeling between adult and juvenile mice following CCI injury (Figure 3). At 4 days post-injury, adult and juvenile mice were analyzed for the density and diameter of pial collaterals using vessel painting on the ipsilateral (F=9.5; P=0.41) and contralateral (F=3.25; P=0.17) cortex (Figure 3A). Vessel painting selectively labels the arteriole network using a fluorescent lipophilic cationic dye (DiI) that is administered into the left ventricle during cardiac perfusion (*45*). Using this method, we observed that there was no difference in the number of collaterals between adult (9.40$\pm$1.67; n=10) and juvenile (13$\pm$1.42; n=10) sham-injured animals on both the contralateral and ipsilateral surface (Figure 3A and 3B). Not surprisingly, both adult (4.18$\pm$0.50; n=11) and juvenile (8.7$\pm$0.83; n=14) CCI-injured mice saw a significant reduction in the number of collaterals on the ipsilateral side of injury compared to non-injured age-matched sham animals (Figure 3A and 3B). Yet, juvenile CCI-injured mice had a significantly

smaller reduction in the ipsilateral number of collaterals compared to adult CCI-injured mice (Figure 3A).

We then measured the overall diameter of these collateral vessels on the ipsilateral (F=7.06; P=0.0004) and contralateral (F=6.23; P=0.0031) sides 4 days post-CCI injury. Collateral diameters were comparable between age-matched sham-injured mice (Figure 3C and 3D). We saw no change in diameter between adult sham-injured (17.99±0.47µm; n=5) and adult CCI-injured (16.38±0.69µm) collateral vessels on the ipsilateral and contralateral sides, 4 days post-CCI injury (Figure 3C and 3D). Interestingly, juvenile CCI-injured (25.43±0.27µm; n=6) mice had a significant increase in diameter on the ipsilateral side of injury compared to juvenile sham-injured (18.99 ±0.71µm; n=7) mice (Figure 3C). This overall increase in collateral diameter seen in juvenile CCI-injured mice was significantly larger than the diameter of collateral vessels in adult CCI-injured mice (Figure 3C).

As we observed an overall increase in collateral diameter in juvenile CCI-injured mice, we next wanted to analyze the number of collaterals with specific diameters that ranged from 0-20 µm, 21-25 µm, 26-30 µm, 31-39 µm, and 40 µm on both the ipsilateral and contralateral surface to get a better understanding of how density and diameter of collateral vessels may contribute to early tissue protection (Figure 3E and 3F). We found the number of remaining ipsilateral pial collateral vessels at 0-20 µm was reduced in juvenile CCI-injured (1.17±0.48; n=6) mice compared to adult CCI-injured (4.20±0.74; n=5) mice (Figure 3E). No difference was observed between adult sham-injured (5.67±0.49; n=6) and juvenile sham-injured (5.0±0.66; n=7) animals (Figure 3E and 3F). However, when we looked at larger diameter vessels within the 26-30 µm and 31-39 µm range, juvenile CCI-injured (1.8±0.80) mice trended to have more collaterals that fell within these ranges compared to adult CCI-injured (0.4±0.25) and juvenile sham-injured (1.17±0.47) animals

(Figure 3E). Interestingly, this trend of the number of collaterals that fall in the 26-30 µm and 31-39 µm was also seen on the contralateral side of injury (Figure 3F). We also observed a significant decrease in the number of collaterals within the 0-20 µm in juvenile CCI-injured (1.67±1.11; n=6) mice compared to adult CCI-injured (5.6±0.25; n-5) and juvenile sham-injured (4.74±0.18; n=7) mice on the contralateral side of injury (Figure 3F).

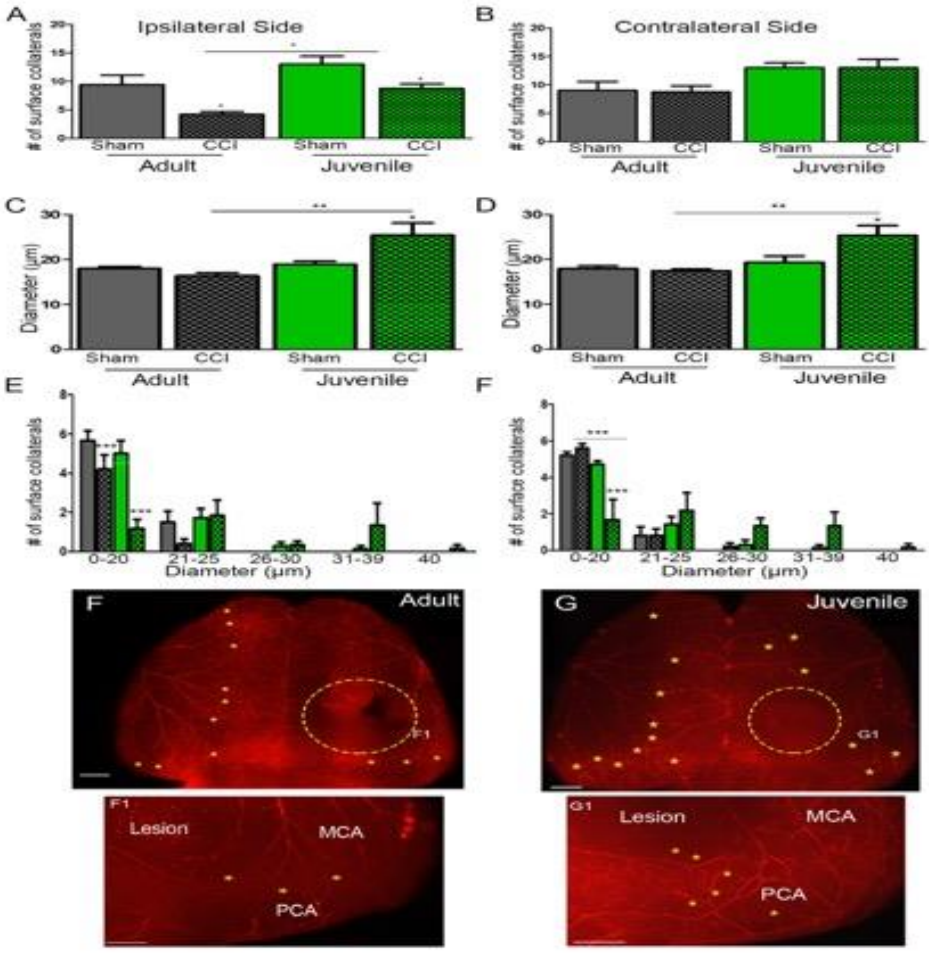

Figure 3. Comparison of collateral density and diameter at 4 days following CCI injury. Bar graph (A) shows a significant quantitative reduction in collateral numbers on the ipsilateral side of injury in both adult and juvenile CCI-injured mice compared to age-matched sham-injured mice. Injured juvenile mice lose fewer collaterals compared to adult injured mice. Bar graph (B) shows

that there is no change in the density of collaterals on the contralateral side of injury between adult and juvenile CCI-injured mice. Quantitative data (C) of the diameter of collateral vessels gets significantly larger in juvenile CCI-injured mice compared to juvenile sham-injured mice. Juvenile CCI-injured mice have larger diameter collateral vessels compared to adult CCI-injured mice. There is no change in collateral diameter between adult sham-injured and adult CCI-injured mice. On the contralateral side of injury, bar graph (D) shows juvenile CCI-injured mice have a significantly larger diameter of collateral vessels compared to juvenile sham-injured mice. Juvenile CCI-injured mice have a greater diameter in collaterals compared to adult CCI-injured mice. There is no change in diameter between adult CCI-injured and adult sham-injured mice. Bar graph (E) of the breakdown of collateral vessel diameters show juvenile CCI-injured mice have fewer diameter collaterals in the 0-20 µm range compared to juvenile sham-injured mice. Juvenile CCI-injured mice have fewer collaterals in the 0-20 µm range compared to adult CCI-injured mice. Vessel painted whole brain images from adult (F) and juvenile (G) CCI-injured mice. Near the area of injury, collateral vessels appear to be smaller in diameter in adult (G^1) compared to juvenile (F^1) mice. Dataset represented as mean +/- SEM. $^{***}P<0.001$; $^{**}P<0.01$ $^{*}P<0.05$. The dotted yellow circle marks focal CCI-injury and loss of vasculature in vessel painted images. Asterisks mark collateral vessels. Middle Cerebral Artery (MCA), Posterior Cerebral Artery (PCA), and lesion noted on images (Adult and Juvenile CCI n= 5 and n=6 per group) (Adult and juvenile sham n= 5 and n=7 per group). Scale bar 1mm.

While conducting the number and diameter analysis of collateral vessels on our vessel painted images of adult CCI-injured (Figure 3F) and juvenile CCI-injured (Figure 3G) brains, we began to notice that collateral territories (middle cerebral artery (MCA-ACA); MCA-posterior

cerebral artery (PCA); and MCA-MCA) closer to the area of injury had larger diameter collateral vessels compared to collateral territories further away from the area of injury. While this was evident in juvenile CCI-injured mice (Figure 3G[1]) we did not see the same effect in adult CCI-injured (Figure 3F[1]) mice. Thus, we decided to quantitate our observation (Figure 4). Further examination of the number and the location-territory of collateral vessels that are lost after CCI-injury revealed collaterals between the MCA and anterior cerebral artery (ACA) branches are most affected (Figure 4A). Not surprisingly, adult CCI-injured (2.05±0.33) and juvenile CCI-injured (2.5±0.53) mice had significantly fewer collaterals within the MCA-ACA compared to adult sham-injured (3.5± 0.93) and juvenile sham-injured (4.49±1.53) mice (Figure 4A). No other territories saw a significant change in number between our CCI-injured and sham-injured groups (Figure 4A). Interestingly, the contralateral MCA-ACA territory in juvenile CCI-injured (3.94± 1.5) mice had more collateral vessels compared to adult CCI-injured (2.61± 1.16) mice, while there were no other territories on the contralateral side that saw a change in number among our CCI-injured and sham-injured groups (Figure 4D). Consistent with our observations, diameter analysis among territories adjacent to the area of injury revealed that the MCA-PCA branches and intra MCA-MCA branches were significantly larger in juvenile CCI-injured (25.92±0.53 µm) mice compared to adult CCI-injured (17.85±2.09 µm) and juvenile sham-injured (17.22±0.14 µm) mice. Examination of collateral vessels on the contralateral side to injury revealed that among all collateral territories (MCA-ACA; MCA-PCA; and MCA-MCA) juvenile CCI-injured mice (24.27 ±1.07 µm) had significantly larger diameter collaterals compared to juvenile sham-injured (18.01 ±0.22 µm) mice. In the MCA-ACA and MCA-PCA territory, this increase in the size of the collateral vessels was also significantly larger between juvenile CCI-injured and adult CCI-injured (18.11 ±1.22 µm) mice. There was no change in collateral diameter between adult CCI-injured

mice and adult sham-injured (19.0 ±1.15 µm) mice. These findings suggest that while CCI-injury disrupts collateral vessels in both adult CCI-injured and juvenile CCI-injured mice, the remaining collateral vessels found in the juvenile CCI-injured brain expand in diameter, while this is not observed in adult CCI-injured mice. Further examination revealed that collateral vessels found near the area of injury in juvenile CCI-injured mice were the vessels that expanded most in size.

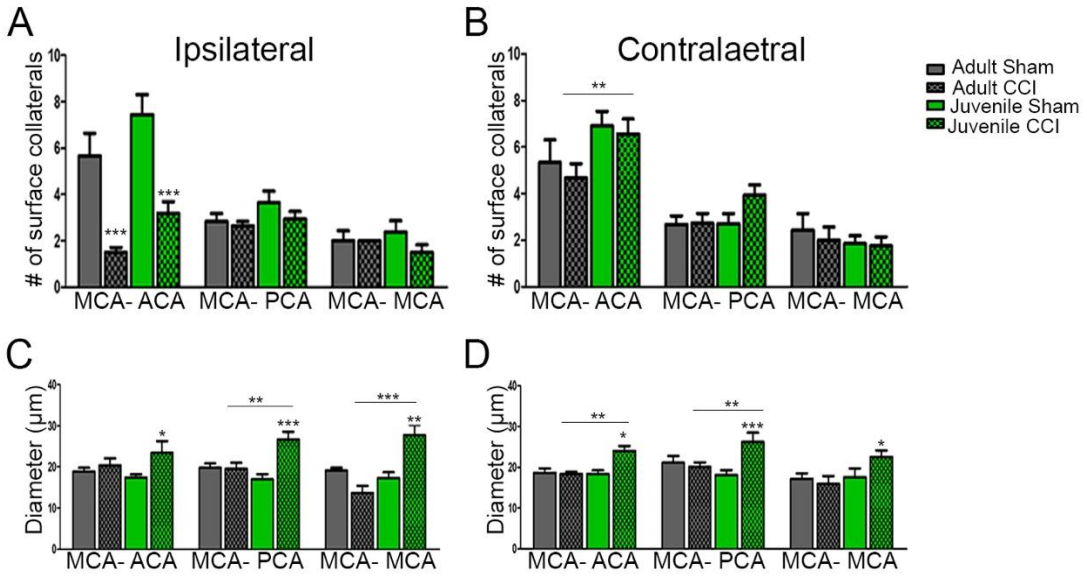

Figure 4. Comparison of collateral density and diameter at 4 days following CCI injury among collateral territories. Bar graph (A-B) represent the number of collaterals that are found in the different collateral territories between adult and juvenile mice. Bar graph (A) shows on the ipsilateral side in all groups, the number of collaterals between adult and juvenile sham-injured mice are similar. After CCI injury, there is a significant decrease in the number of collaterals that fall within the MCA- ACA territory between adult and juvenile CCI-injured mice compared to age-matched sham-injured mice. Bar graph (B) shows on the contralateral side of injury the density

of collaterals between adult and juvenile sham-injured mice is similar. After CCI injury, juvenile mice have significantly more collaterals between the MCA- ACA territory compared to adult CCI-injured mice. Bar graphs (C-D) represents the diameter of collaterals that fall within each collateral territory between adult and juvenile mice. Bar graph (C) shows on the ipsilateral side of injury there is no change in collateral diameter among the territories between adult CCI-injured and adult sham-injured mice. Juvenile CCI-injured mice have a significant increase in diameter in all collateral territories compared to juvenile sham-injured mice. Juvenile CCI-injured mice have a significant increase in collateral diameter within the MCA-PCA and MCA- MCA branches compared to adult CCI-injured mice. Bar graph (D) on the contralateral side of injury shows adult CCI-injured mice and adult sham-injured mice see no change in diameter size in all collateral territories. Juvenile CCI-injured mice have significantly larger diameter collateral vessels in all territories compared to juvenile sham-injured mice. Juvenile CCI-injured mice have significantly larger collaterals within the MCA-ACA and MCA-PCA branches compared to adult CCI-injured mice. Dataset represented as mean +/- SEM. $^{***}P<0.001$; $^{**}P<0.01$ $^{*}P<0.05$. (Adult and Juvenile CCI n= 5 and n=6 per group) (Adult and juvenile sham n= 5 and n=7 per group)

Juvenile Mice Have Larger Pial Collaterals 14 Days Post CCI-injury

While we analyzed the diameters of collateral vessels at an acute time point, we wanted to ensure these changes in diameter are due to vessel remodeling and not due to spontaneous vessel enlargement as a consequence of CCI-injury (*50, 51*). Thus, we repeated the 4-day post-CCI collateral analysis at 14 days post-CCI (Figure 5). Spontaneous vessel spasms are shown to resolve 11 days post-injury in children and in experimental blast injuries in rodents, thus we were interested in looking at vessel diameters at this sub-acute time point (*51, 52*). We found that

numbers of surface collaterals in the ipsilateral (F=5.86; P=0.0037) and the contralateral (F=1.79; P=0.90) sides among the groups had similar trends to the 4-day data. Thus, we found adult CCI-injured (5.38±0.53; n=8) and juvenile CCI-injured (8.23±0.64; n=13) mice lost similar numbers of collaterals on the ipsilateral side of injury compared to adult sham-injured (10.20±1.50; n=10) and juvenile sham-injured (12.56±1.70; n=8) animals (Figure 5A). Similar to the 4-day data, analysis on the contralateral side of injury revealed no change in collateral numbers among the animal groups at the 14-day time point (Figure 5B).

Interestingly, similar to the 4-day diameter data, the collateral diameters on the ipsilateral (F=5.04; P=0.0004) hemisphere of the juvenile CCI-injured mice (22.03µm±1.22; n=7) remained significantly larger compared to adult CCI-injured (17.35µm±1.34; n=6) and juvenile sham-injured (17.76µm±0.11; n=6) mice at the more sub-acute time point (Figure 5C). The collateral diameters on the contralateral (F=12.10; P=0.1796) hemisphere were also significantly larger in juvenile CCI-injured (24.01µm±0.62; n=7) mice compared to juvenile sham-injured (18.82µm±0.68; n=6) and adult CCI-injured (17.61µm±0.61; n=6) mice 14 days post-CCI injury (Figure 5D).

We next wanted to determine if similar trends of density and diameter of collateral vessels held true to the 4-day data at the 14-day time point. Again, we analyzed the number of collaterals with specific diameters that ranged from 0-20 µm, 21-25 µm, 26-30 µm, 31-39 µm, and 40 µm on both the ipsilateral and contralateral surface (Figure 5E and 5F). On the ipsilateral surface we found that juvenile CCI-injured (1.86±0.55; n=7) mice had a significant loss of the number of collateral vessels in the 0-20 µm range compared to adult CCI-injured (3.00±0.45; n=6) and juvenile sham-injured (5.83±0.65; n=6) mice (Figure 5E). However, juvenile CCI-injured (1.29±0.52; n=7) mice showed a significant increase in the number of collaterals that fell in the

21-25 µm range compared to adult CCI-injured (0.50±0.34; n=6) and juvenile sham-injured (1.33±0.33; n=6) mice (Figure 5E). Juvenile CCI-injured mice also trended to have more vessels that fell in the large diameter ranges of 26-30 µm and 31-39 µm (Figure 5E). Analysis on the contralateral surface in both adult CCI-injured (5.83±0.87; n=6) and juvenile CCI-injured (2.0±0.58; n=7) mice revealed a significant reduction in the number of collaterals that fell in the 0-20 µm range compared to adult sham-injured (5.0±0.52; n=6) and juvenile sham-injured (6.17±0.87; n=6) mice, respectively (Figure 5F). Taken together this data demonstrates that the increase in diameter observed in juvenile CCI-injured mice at 4-days post-CCI injury was also evident at 14-days post-CCI injury, while changes in collateral diameter of adult CCI-injured mice were not observed.

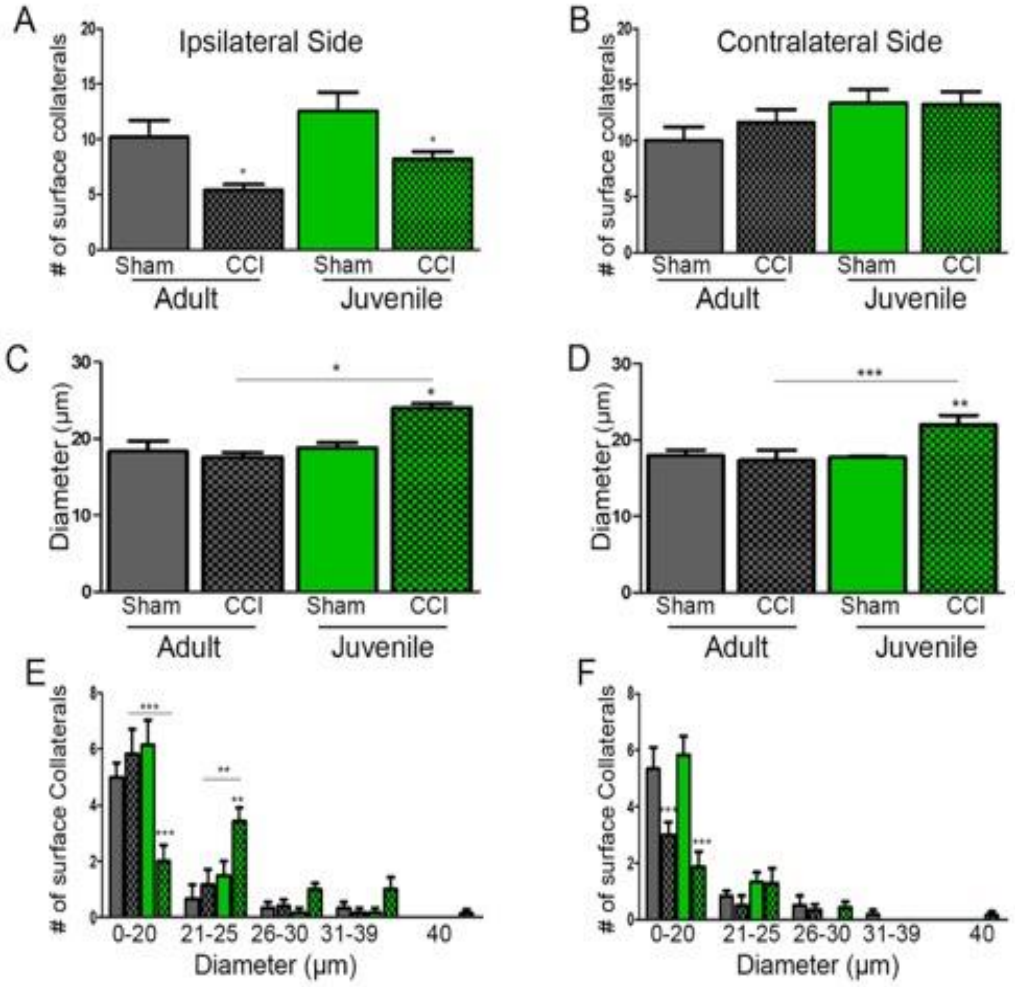

Figure 5. Comparison of collateral density and diameter at 14 days following CCI injury. Bar graph (A) shows a significant reduction in collateral numbers on the ipsilateral side of injury in both adult and juvenile CCI-injured mice compared to age match sham-injured controls. Bar graph (B) shows that there is no change in the density of collaterals on the contralateral side of injury between adult and juvenile mice. Quantitative data (C) of the diameter of collateral vessels show juvenile CCI-injured mice have significantly larger diameter collateral vessels compared to juvenile sham-injured and adult CCI-injured mice. There is no change in collateral diameter between adult CCI-injured and adult sham-injured mice. Bar graph (D) shows on the contralateral

side of injury, juvenile CCI-injured mice have significantly larger diameter collateral vessels compared to juvenile sham-injured and adult CCI-injured mice. There is no change in diameter between adult CCI-injured and adult sham-injured mice. Bar graph (E) represents the ipsilateral breakdown of collateral vessel diameters and shows juvenile CCI-injured mice have fewer diameter collaterals in the 0-20 µm range compared to juvenile sham-injured and adult CCI-injured mice. Juvenile CCI-injured mice have more collaterals in the 21-25 µm range compared to juvenile sham-injured and adult CCI-injured mice. Bar graph (F) represents the contralateral breakdown of collateral vessel diameters and shows adult and juvenile CCI-injured mice have significantly fewer collateral vessels in the 0-20 µm range compared to age- matched sham-injured controls. Dataset represented as mean +/- SEM. $^{***}P<0.001$; $^{**}P<0.01$ $^{*}P<0.05$. (Adult and Juvenile CCI n= 6 and n=7 per group) (Adult and juvenile sham n= 6 per group).

Juvenile Mice Have Larger Surface Diameter SMA^{+} Vessels 4 Days Post-CCI Injury

While we had observed the increase in diameter of surface collateral vessels in juvenile CCI-injured mice, we were next interested in quantifying surface diameter changes histologically as well as quantifying changes to the interstitial tissue and hippocampus (Figure 6). To do this, we stained serial coronal sections with smooth muscle actin (SMA) and measured the diameter of SMA^{+} vessels that co-labelled with DiI^{+} ECs from our vessel painting technique 4-days after CCI-injury. Analysis of SMA^{+}/DiI^{+} vessels ensured that we were quantifying the arteriole network and not veins that have also been found to be SMA^{+} (*53*). Diameter analysis was performed using the Nucleator Program on SMA^{+}/DiI^{+} vessels that were found on the surface (F=10.91; P=0.0796), within the interstitial cavity (F=2.20; P=0.124), and hippocampus (F=1.97; P=0.16) on the

ipsilateral side of injury (Figure 6A, 6B, 6C). First, we found that SMA^+/DiI^+ vessel diameters were similar in all brain regions (surface, interstitial, and hippocampus) of our analysis between adult sham-injured and juvenile sham-injured mice. When we quantified SMA^+/DiI^+ vessels found on the surface in adult CCI-injured (18.71µm$\pm$0.62; n=8) mice saw no change in surface diameter relative to adult sham-injured mice (20.84µm$\pm$0.85; n=10) (Figure 6A). Next, we found that juvenile CCI-injured (24.17µm$\pm$ 0.95; n=8) mice saw a significant increase in SMA^+/DiI^+ surface vessel diameter compared to juvenile sham-injured (20.34µm$\pm$0.33; n=7) mice (Figure 6A). The increase in surface diameter of SMA^+/DiI^+ vessels in juvenile CCI-injured mice was also significantly larger compared to adult CCI-injured animals (Figure 6A). We saw no change in SMA^+/DiI^+ vessel diameter in adult CCI-injured and juvenile CCI-injured mice compared to age-matched sham-injured controls within the interstitial tissue or hippocampus (Figure 6B and 6C). Here we demonstrate that SMA^+/DiI^+ vessels found on the ipsilateral surface of juvenile CCI-injured mice increase in diameter after CCI-injury while SMA^+/DiI^+ vessels found on the surface of adult CCI-injured mice do not change in size following CCI-injury. Furthermore, SMA^+/DiI^+ vessel diameter changes do not occur within the interstitial tissue or hippocampus following CCI-injury in adult and juvenile mice.

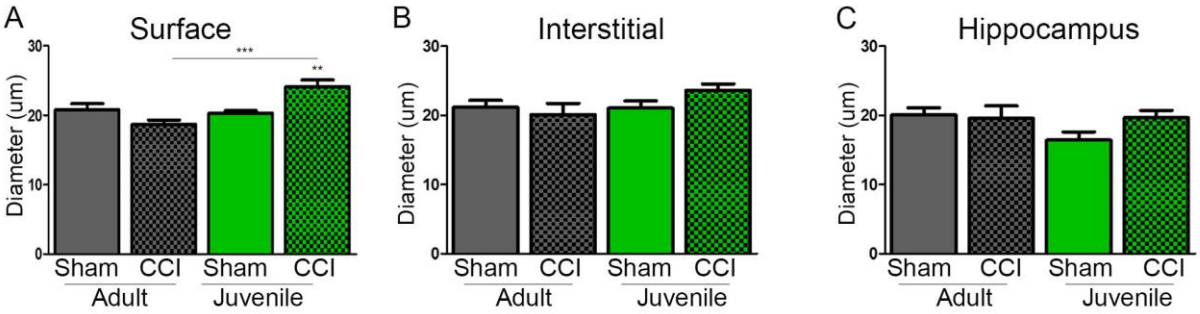

Figure 6. Comparison of SMA diameters 4 days post-CCI. Quantified analysis (A-C) of SMA^+/Di^+ vessels found on the surface, interstitial tissue, and hippocampus using Nucleator Program. Bar

graph (A) displays juvenile CCI-injured mice have significant larger diameter SMA^+ vessels found on the surface compared to juvenile sham-injured and adult CCI-injured mice. There is no change in diameter between adult CCI-injured and adult sham-injured animals. Bar graph (B) displays no change in diameter of SMA^+ vessels found in the interstitial tissue among the groups. Bar graph (C) displays no change in diameter of SMA^+ vessels found in the hippocampus among the groups. Data sets represented as mean +/- SEM. $^{***}P<0.0001$; $^{**}P<0.001$. (Adult and Juvenile CCI n= 3-8 and n=7-9 per group) (Adult and juvenile sham n=4-10 and n= 4-7 per group).

Juvenile Mice have more $CD31^+$ microvessels within the peri-lesion 4 Days Post-CCI injury

To expand upon our vascular findings, we were next interested in determining if we would observe microvascular differences in numbers between adult CCI-injured and juvenile CCI-injured mice within the peri-lesion (Figure 7). To do this, we stained coronal sections collected 4 days post-CCI injury, with CD31 (PECAM). Quantitative analysis was performed using the optical fractionator program, which allowed us to randomly sample sites throughout the peri-lesion and count for $CD31^+$ microvessels. Upon analysis, we noticed phenotypical differences of $CD31^+$ microvessels between adult CCI-injured and juvenile CCI-injured mice (Figure 7A and 7B). $CD31^+$ vessels found in the adult CCI-injured peri-lesion were observed to be fragmented, swollen, and unhealthy (Figure $7A^1$-$7A^3$). $CD31^+$ vessels found in the juvenile CCI-injured peri-lesion were observed to be intact, more abundant, and absent of cellular swelling (Figure $7B^1$-$7B^3$). We next quantified the number of $CD31^+$ microvessels within the peri-lesion between adult and juvenile mice (F=29.44; P=0.0001) (Figure 7C). First, we found that the density of $CD31^+$ vessels was similar between adult sham-injured (76403$\pm$7844; n=3) and juvenile sham-injured (80044$\pm$5477; n=3) mice (Figure 7C). Not surprisingly, following CCI-injury, both adult CCI-injured

(29951±2731; n-=5) and juvenile CCI-injured (47015±3104; n=6) mice saw a significant decrease in the number of $CD31^+$ microvessels in the peri-lesion compared to age-matched sham-injured controls (Figure 7C). Juvenile CCI-injured mice were found to have less of a reduction of $CD31^+$ vessels within the peri-lesion, leaving juvenile CCI-injured mice with significantly more $CD31^+$ vessels within the peri-lesion compared to the adult CCI-injured mice (Figure 7C).

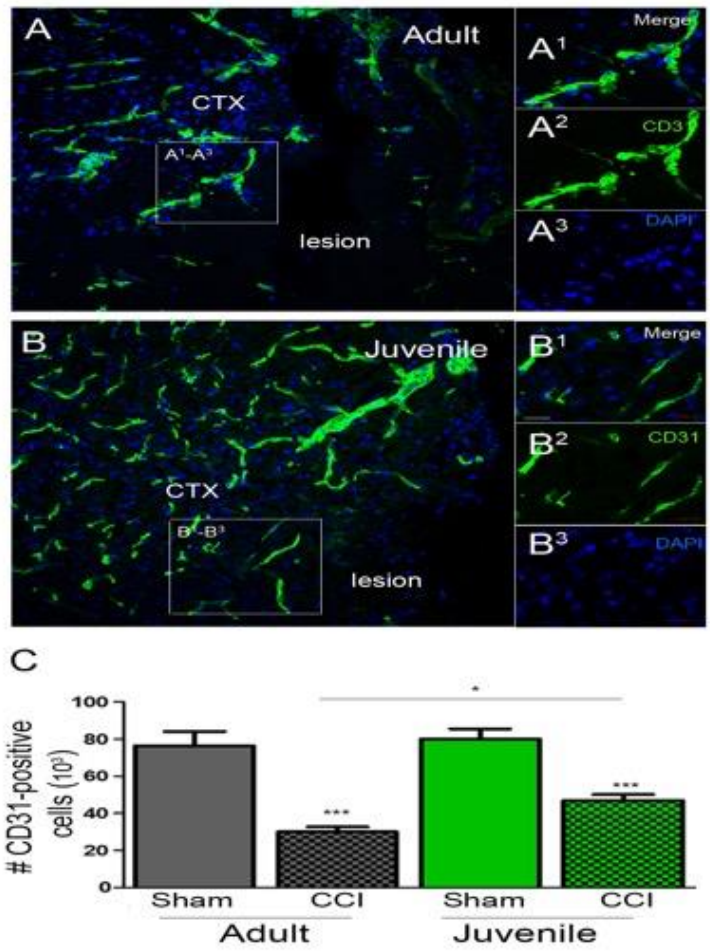

Figure 7. Comparison of $CD31^+$ density at 4 days post-CCI injury within the peri-lesion. Adult CCI-injured (A) and juvenile CCI-injured (B) brains show the density of $CD31^+$ vessels is less in adult CCI-injured mice compared to juvenile CCI-injured mice. The morphology of adult CCI-injured (A^1-A^3) $CD31^+$ vessels appear more fragmented compared to juvenile CCI-injured (B^1-

B[3]) CD31$^+$ vessels. Quantified analysis (C) of CD31$^+$ vessels using optical fractionator. Bar graph displays adult and juvenile sham-injured mice have similar densities of CD31$^+$ vessels. After CCI injury there is a significant loss of CD31$^+$ vessels within the peri-lesion of adult and juvenile CCI-injured mice compared to age-matched sham-injured controls. Juvenile CCI-injured mice lose significantly less CD31$^+$ vessels compared to adult CCI-injured mice. Data sets represented as mean +/- SEM. $^{***}P<0.0001$; $^{*}P<0.05$. (Adult and Juvenile CCI n= 5-6 per group) (Adult and juvenile sham n=3 per group). Scale bar 20µm.

Juvenile mice have less CD11b$^+$ cell infiltration and fewer observable hypertrophic GFAP$^+$ cells 4 Days Post-CCI Injury

Microglia are the resident immune cells of the brain and astrocytes provide a link to the vasculature, transporting glucose to fuel neural function (*54, 55*). Following CCI-injury in mice, both cells types become activated and contribute to neuronal tissue loss by secreting inflammatory cytokines that overtime impede the repair process (*56, 57*). We were interested to see if there were differences in infiltrating microglia cells within the peri-lesion and differences in astrocyte reactivity between adult and juvenile mice (Figure 8). For the microglia analysis, coronal tissue sections were collected 4 days after CCI-injury and stained for CD11b. Prior to quantification of infiltrating CD11b$^+$ cells, we noticed within the peri-lesion adult CCI-injured mice appeared to have more numbers of CD11b$^+$ cells compared to juvenile CCI-injured mice (Figure 8A-C and 8D-F, respectively). The rounded cell phenotype of the CD11b$^+$ cells was similar between adult CCI-injured and juvenile CCI-injured mice (Figure 8A-C and 8D-F). Quantification of infiltrating CD11b$^+$ cells consisted of counting the number of CD11b$^+$ cells in five coronal brain sections within six fields of view throughout the peri-lesion of adult and juvenile mice (F=13.08; P=0.002)

(Figure 8G). Not surprisingly, we found very few numbers of $CD11b^+$ cells within the corresponding regions in adult sham-injured (10.57±3.81; n=3) and juvenile sham-injured (9.73±0.71) mice (Figure 8G). Following CCI-injury the number of infiltrating $CD11b^+$ cells within the peri-lesion of both adult CCI-injured (111.1±21.42; n=5) and juvenile CCI-injured (53.34±3.98; n=7) mice increased relative to sham-injured controls. Similar to our initial observation, we found adult CCI-injured mice had significantly more $CD11b^+$ cells within the peri-lesion compared to juvenile CCI-injured mice (Figure 8G).

We next wanted to determine if there were differences in astrocyte reactivity between adult and juvenile mice. 4 days post-CCI injury coronal sections were stained for GFAP (Figure 8H-K). $GFAP^+$ cells were observed throughout the ipsilateral cortex and hippocampus in adult and juvenile sham-injured mice and adult and juvenile CCI-injured mice (Figure 8H-I and Figure 8J-K, respectively). We did not observe differences in numbers of $GFAP^+$ cells among our groups. While we observed $GFAP^+$ cells to be hypertrophic in both adult CCI-injured and juvenile CCI-injured brains the prevalence of $GFAP^+$ hypertrophic cells appeared to be more pronounced in adult CCI-injured brains compared to juvenile CCI-injured brains (Figure 8J and 8K, respectively). Taken together, we observed greater infiltration of $CD11b^+$ cells and more pronounced $GFAP^+$ cells in adult CCI-injured mice compared to juvenile CCI-injured mice.

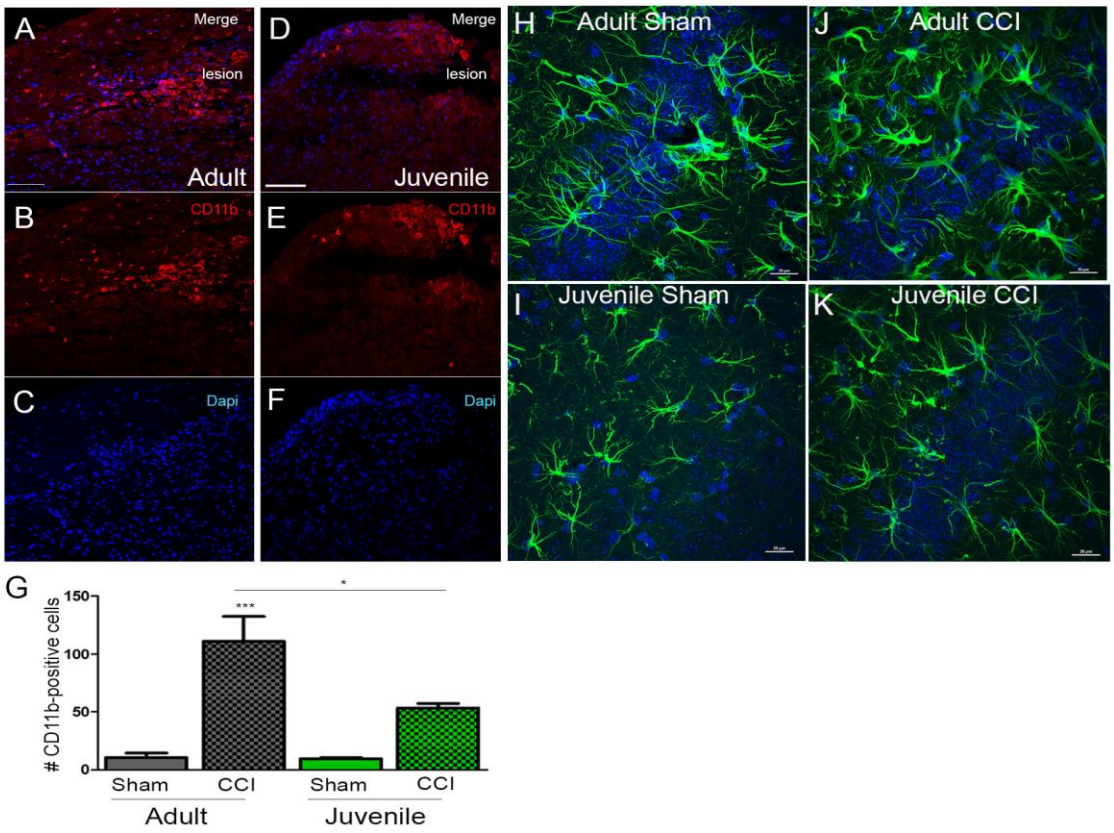

Figure 8. Comparison of the number of CD11b$^+$ infiltrating cells and GFAP reactivity at 4 days post-CCI injury. Adult CCI-injured (A-C) and juvenile CCI-injured (D-F) brains show adult CCI-injured mice appear to have more infiltrating CD11b$^+$ cells compared to juvenile CCI-injured mice. Quantified (G) analysis of CD11b$^+$ cells using random plains of view counts within the peri-lesion. Bar graph displays adult and juvenile sham-injured mice have similar densities of CD11b$^+$ cells. After CCI injury there is a significant increase of CD11b$^+$ cells within the peri-lesion of adult CCI-injured mice compared to adult sham-injured mice. Juvenile CCI-injured mice trend to have an increase of CD11b$^+$ cells compared to juvenile sham-injured mice. Adult CCI-injured mice have significantly more CD11b$^+$ cells within the peri-lesion compared to juvenile CCI-injured mice. No observable differences were seen in GFAP numbers between adult sham-injured (H) and adult CCI-injured (J) mice and between juvenile sham-injured (I) and juvenile CCI-injured (K) mice.

Adult CCI-injured mice appear to have more swollen, hypertrophic $GFAP^+$ cells compared to juvenile CCI-injured mice. Data sets represented as mean +/- SEM. $^{***}P<0.0001$; $^{*}P<0.05$. (Adult and Juvenile CCI n= 5-7 per group) (Adult and juvenile sham n=3 per group). Scale bar 20µm.

Juvenile Mice Have Less BBB Permeability 4 days Post-CCI injury

Blood Brain Barrier (BBB) damage has been shown to be a pathological hallmark of CCI-injury and the extent of BBB permeability can be contributed to further tissue loss as the homeostatic environment of the brain is disrupted (*10, 58, 59*). To examine whether adult and juvenile mice have differences in BBB integrity in our CCI model, we employed an Evans blue (EB) brain tissue extravasation assay following CCI-injury (Figure 9). CCI-injured mice and sham-injured controls were injected with EB at 4 days post-CCI injury and the amount of EB extravasation into the tissue was quantified using a spectrophotometer. We did not observe EB extravasation in the tissue of adult sham-injured or juvenile sham-injured mice and these animals acted as our age-matched relative controls to CCI-injured mice for our spectrophotometer readings (data not shown). CCI injury resulted in an increase in EB extravasation into adult CCI-injured and juvenile CCI-injured brains (Figure 9A and 9B). Quantitative assessment of EB extravasation from the injured cortex between adult CCI-injured (3.63 ± 0.37; n=6) and juvenile CCI-injured (0.33 ± 0.05; n=9) mice relative to age-matched sham-injured controls revealed juvenile mice have a significant reduction in EB absorbance compared to adult CCI-injured mice (Figure 9C).

To further investigate our findings from the EB extravasation assay we sought to compare tight junction (TJ) relative expression of claudin-5 and occludin-1 between adult CCI-injured and juvenile CCI-injured mice relative to age-matched sham-injured controls through qPCR (Figure 9D and 9E). To do this, 4 days post-CCI injury, adult CCI and sham – injured and juvenile CCI

and sham-injured endothelial cells (ECs) were magnetically separated using a CD31 antibody and RNA was isolated, per- group, from this $CD31^{+}$ population. While relative expression levels of claudin-5 and occludin-1 were low in both juvenile and adult CCI-injured mice relative to sham, for both claudin-5 and occludin-1, juvenile CCI-injured ECs trended to have higher relative expression (Figure 9D and 9E). Together the data from the EB extravasation and tight junction expression studies reveal juvenile CCI-injured mice have less BBB permeability following CCI-injury compared to adult CCI-injured mice.

Figure 9. Comparison of BBB integrity in adult and juvenile mice 4 days after CCI injury.

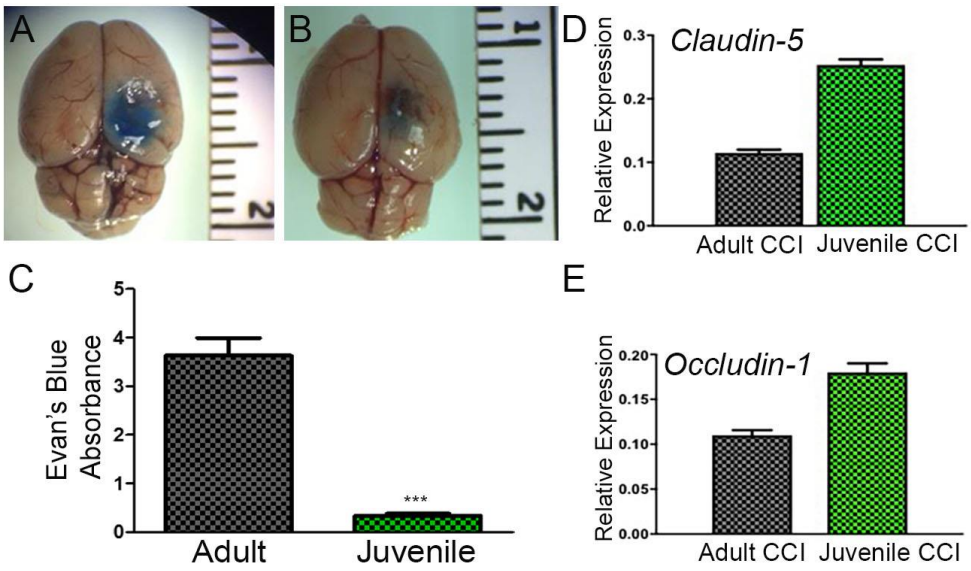

Representative images of adult CCI-injured (A) and juvenile CCI-injured (B) brains 3 hours following Evans Blue (EB) injections. Analysis (C) of EB extravasation assay using a spectrometer to read absorbance relative to age-matched sham-injured controls. Bar graph displays adult CCI-injured mice have a significant increase in EB absorption compared to juvenile CCI-injured mice. qPCR data of relative mRNA expression of isolated endothelial cells to age-matched sham-injured controls (D- E). Bar graph (D) shows juvenile CCI-injured mice trended to have up-regulation of

relative expression of claudin-5 compared to adult CCI-injured mice. Bar graph (E) shows juvenile CCI-injured mice trended to have up-regulation of relative expression of occludin-1 compared to adult CCI-injured mice. Data sets represented as mean +/- SEM. (Adult and Juvenile CCI n= 6 and n=9 per group) (Adult and juvenile sham n=5 per group).

EC Gene Expression Profile Difference Are Age-Dependent following CCI Injury

The finding of TJ expression differences between the ECs of juvenile CCI-injured and adult CCI-injured mice prompted us to investigate if there were differences in expression of other EC-associated factors between adult and juvenile mice following CCI-injury that may contribute to the vascular differences we observed. 4 days post-CCI or sham-injury, $CD31^+$ ECs were extracted from adult and juvenile brains through magnetic separation using a CD31 antibody and analyzed by qPCR. The $CD31^-$ fraction which contains a mixture of brain cell types was also analyzed by qPCR. Flt-1 (vascular endothelial growth factor receptor 1), GFAP (glial fibrillary acidic protein), NeuN, and Pdgfr8 (platelet-derived growth factor receptor) expression levels were analyzed between the $CD31^+$ EC fraction and the $CD31^-$ fraction among the corresponding treatment groups to show the purity of our $CD31^+$ EC fraction. Our findings demonstrate the relative expression of EC-specific Flt-1 receptor was greater in both adult CCI-injured (12.80$\pm$ 1.01) and juvenile CCI-injured (4.22$\pm$0.66) $CD31^+$ EC fraction compared to the $CD31^-$ fraction (Adult CCI Flt-1 0.01$\pm$ 0.00; Juvenile CCI Flt-1 0.62$\pm$0.09) (Figure 10A). Relative expression of astrocytic marker GFAP was found to be low in adult CCI-injured (0.04$\pm$ 0.01) and juvenile CCI-injured (0.04$\pm$ 0.01) $CD31^+$ EC fraction compared to the high expression found in the $CD31^-$ fraction (Adult CCI GFAP 108.9$\pm$ 4.05; Juvenile CCI GFAP 42.5$\pm$ 13.51) (Figure 10B). Relative expression of neuronal marker NeuN was found to be low in adult CCI-injured (0.00$\pm$ 0) and juvenile CCI-injured (0.13$\pm$ 0.01) $CD31^+$ EC and $CD31^-$ fractions (Adult CCI NeuN 0.11$\pm$ 0.01;

Juvenile CCI NeuN 0.13± 0.01) (Figure 10C). Relative expression of mural cell marker Pdgfr was found to be lower in adult CCI-injured (1.79± 0.26) and juvenile CCI-injured (0.01± 0.01) $CD31^+$ EC fraction compared to the $CD31^-$ fraction (Adult CCI Pdgfr 1.79± 0.26; Juvenile CCI Pdgfr 0.04±0.01) (Figure 10D). Results from this study confirmed that our $CD31^+$ fraction consisted mostly of a pure population of ECs.

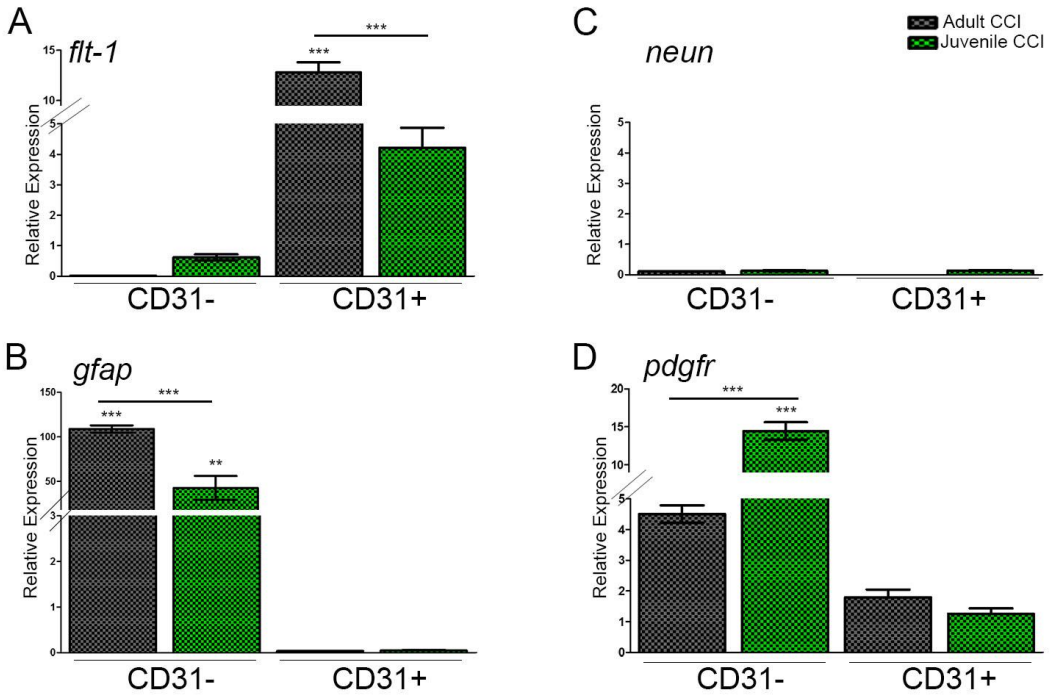

Figure 10. QPCR data to test the purity of isolated $C31^+$ EC fraction compared to $CD31^-$ fraction. mRNA from isolated $CD31^+$ ECs or $CD31^-$ from 7 animals per group at 4 days post-CCI or -sham injury and ran in triplicate with primers to test the purity of the samples. Gene abundances were normalized to Gapdh levels and relative expression to respective samples in the $CD31^-$ fraction. Bar graphs (A-D) represent relative mRNA expression between adult and juvenile isolated $CD31^+$ endothelial cell fraction and $CD31^-$ fraction. Data sets represented as

mean +/- SEM. $^{***}P<0.001$; $^{**}P<0.01$. (Adult and Juvenile CCI n= 7 per group) (Adult and juvenile sham n=7 per group).

Next we investigated the relative expression levels of MCP-1 (monocyte chemotactic protein 1); eNOS (endothelial cell nitric oxide synthase); caspase-12; BCL-2 (B-cell lymphoma 2); Ang-1 (angiopoeitin-1); Ang-2 (angiopoetin-2); VEGF (vascular endothelial growth factor); and Tie2 (TEK tyrosine kinase receptor) following CCI-injury in adult and juvenile mice using qPCR (Figure 11). Gene expression levels were made relative to age-matched sham-injured controls in both the $CD31^+$ EC fraction and $CD31^-$ EC fraction and sham-injured expression values are represented by the black line in Figure 11. Relative expression of monocyte marker, MCP-1, was found to be increased in adult and juvenile CCI-injured mice compared to adult and juvenile sham-injured mice in the $CD31^+$ EC fraction (Figure 11A). Juvenile CCI-injured mice had a significant up-regulation of MCP-1 relative to adult CCI-injured mice (Figure 11A). Within the $CD31^-$ EC fraction, juvenile CCI-injured had a significant up-regulation of MCP-1 expression compared to juvenile sham-injured and adult CCI-injured mice (Figure 11A). Relative expression of eNOS was significantly down-regulated in juvenile CCI-injured and adult CCI-injured mice relative to sham controls in the $CD31^+$ EC fraction (Figure 1B). Expression levels in the $CD31^-$ EC fraction show a down-regulation of eNOS in both adult and juvenile CCI-injured mice relative to sham controls, but a significant down-regulation in adult CCI-injured mice relative to sham (Figure 1B). Relative expression of inflammatory cytokine caspase-12 was down-regulated in the $CD31^+$ EC fraction of both juvenile CCI-injured and adult CCI-injured mice relative to sham controls (Figure 11C). Interestingly, the expression level of caspase- 12 within the $CD31^-$ EC fraction was significantly up-regulated in juvenile CCI-injured mice (Figure 11C). Relative

expression levels of anti-apoptotic marker, BCL-2 was significantly down-regulated in adult CCI-injured mice within the $CD31^+$ EC fraction (Figure 11D). It was down-regulated in juvenile CCI-injured mice within the $CD31^+$ EC fraction (Figure 11D). Interestingly, within the $CD31^-$ EC fraction, adult CCI-injured mice saw a significant down-regulation compared to adult sham-injured mice and this down-regulation was also significant compared to juvenile CCI-injured mice (Figure 11D). The relative expression levels for Ang-1, found to be released by astrocytes and mural cells to promote vessel stability, was found to be decreased in the $CD31^+$ EC fraction of both adult CCI-injured and juvenile CCI-injured mice relative to sham controls (Figure 11E). Surprisingly, juvenile CCI-injured mice had sustained Ang-1 expression in the $CD31^-$ EC fraction, which was found to be significantly up-regulated relative to adult CCI-injured mice (Figure 11E). Relative expression of Ang-2, found to be released by ECs during vessel remodeling, was significantly down-regulated in the $CD31^+$ EC fraction and the $CD31^-$ EC fraction relative to sham controls (Figure 11F). Adult CCI-injured mice saw a significant reduction of $CD31^+$ expression relative to adult sham-injured mice (Figure 11F). Relative expression of VEGF was found to be significantly up-regulated in adult CCI-injured mice within the $CD31^+$ EC fraction relative to adult sham-injured and juvenile CCI-injured mice (Figure 11G). While VEGF trended to be increased in both adult and juvenile CCI-injured mice in the $CD31^-$ EC fraction relative to sham-injured controls (Figure 1G). Relative expression levels of the Tie2 receptor was found to be down-regulated in adult and juvenile CCI-injured mice relative to sham controls in both the $CD31^+$ EC fraction and $CD31^-$ EC fraction (Figure 1H).

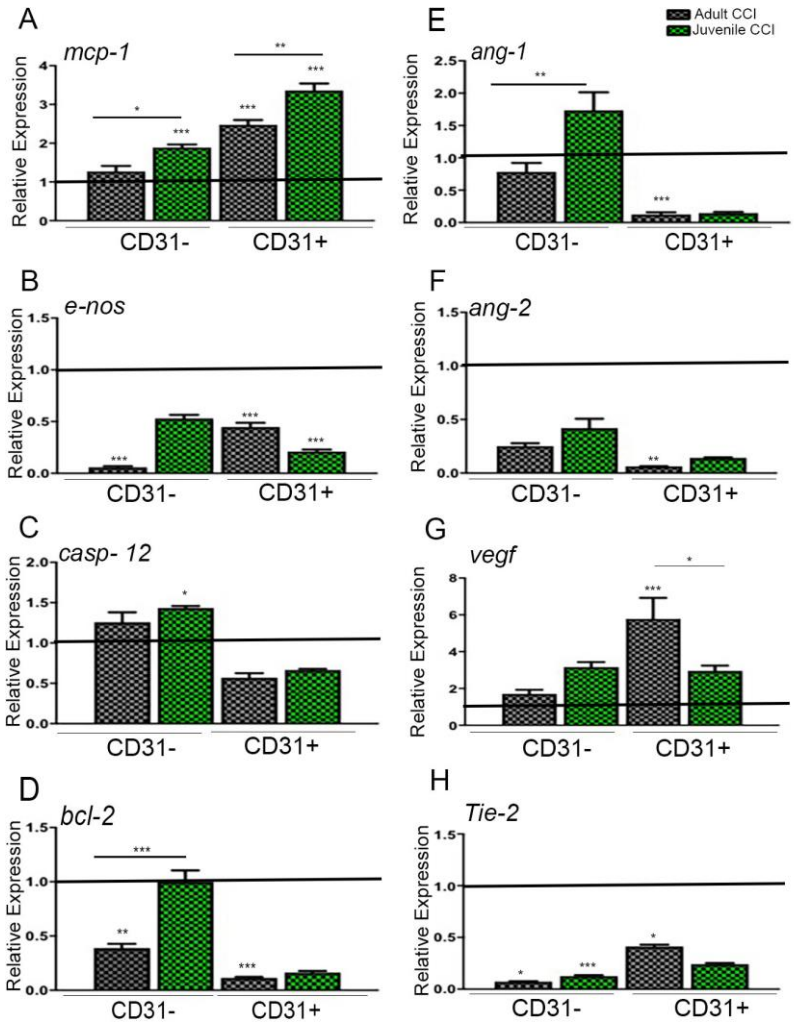

Figure 11. QPCR data to test different relative gene expression of isolated $CD31^+$ ECs and $CD31^-$ fraction between adult and juvenile mice. mRNA from isolated $CD31^+$ ECs or $CD31^-$ from 7 animals per group at 4 days post-CCI or -sham injury and ran in triplicate. Gene abundances were normalized to Gapdh levels and relative expression to sham-injured animals represented on the graphs with a black line (A-H). Bar graphs represent relative mRNA expression between adult and juvenile isolated $CD31^+$ endothelial cell fraction and $CD31^-$ fraction. Data sets represented as mean +/- SEM. $^{***}P<0.001$; $^{**}P<0.01$; $^{*}P<0.05$. (Adult and Juvenile CCI n= 7 per group) (Adult and juvenile sham n=7 per group).

Juvenile mice have a better functional outcome in behavior compared to adult mice after CCI injury

We also performed behavioral assessments to test whether motor deficit and recovery, memory, and balance/coordination were affected between adult and juvenile mice following CCI-injury (Figure 12). Mice were pre-trained on the Rotarod 4 days prior to CCI-injury then subjected to motor assessment at 4, 7 and 14 days post-sham or -CCI injury. Time to fall was recorded then normalized to the average baseline time for each mouse. No differences between groups were seen following sham-injury for each time points tested (Figure 12A). Motor deficits were observed following adult CCI-injury at all time point tested (4d- 60.2%± 3.52; 7d- 66.8%± 6.8; 14d- 74.18%±8.93: n=6) compared to baseline (Figure 12B). Interestingly, juvenile CCI-injured mice saw no motor deficits at all time points tested (4d- 116.4%± 5.30; 7d- 112.16%±5.75; 14d- 114.17± 5.21: n=13) compared to baseline (Figure 12B).

Adult and juvenile mice were subjected to Novel Object Recognition (NOR) testing at the before mentioned time points to observe if there were deficits in memory following CCI-injury. Specifically, we scored the amount of time exploring the novel object to the total time exploring both objects to give us our preference of object index score (preference index). At the 4 day time point tested, adult CCI-injured (51.91± 3.97) mice could not discern between the novel and familiar objects compared to adult sham-injured (65.17± 3.43) mice; however, this deficit in memory was not observed at the subsequent time points, 7 and 14 days, tested (Figure 12C). Interestingly, juvenile CCI-injured mice could discern between the novel and familiar objects compared to juvenile sham-injured mice at all time points tested (Figure 12D).

Mice were pre-trained on beam walk 4 days prior to CCI-injury then subjected to balance and coordination assessment at 4, 7 and 14 days post-sham or -CCI injury. Time to cross the beam

was recorded then normalized to the average baseline time for each mouse and the number of hind limb foot slips were noted then normalized to the average number of foot slips from baseline.

We found that it took juvenile CCI-injured (8.46s± 1.54) mice significantly more time to cross the beam compared to juvenile sham-injured (4.73s± 0.45) mice at 4 and 7 days post-CCI injury; however, this time deficit to cross the beam was not observed at 14 days post -CCI (Figure 12E). Interestingly, adult CCI-injured (3.63s± 0.47) mice did not show a time deficit to cross the beam compared to adult sham-injured (3.09s± 0.06) mice at all time points tested (Figure 12E).

Although adult CCI-injured mice crossed the beam faster compared to juvenile CCI-injured mice at 4 and 7 days post – CCI injury, at these time points, adult CCI-injured (0.96± 0.26) mice had significantly more left hind limb foot slips compared to adult sham-injured (0.17± 0.02) mice and juvenile CCI-injured (0.35± 0.02) mice (Figure 12F).

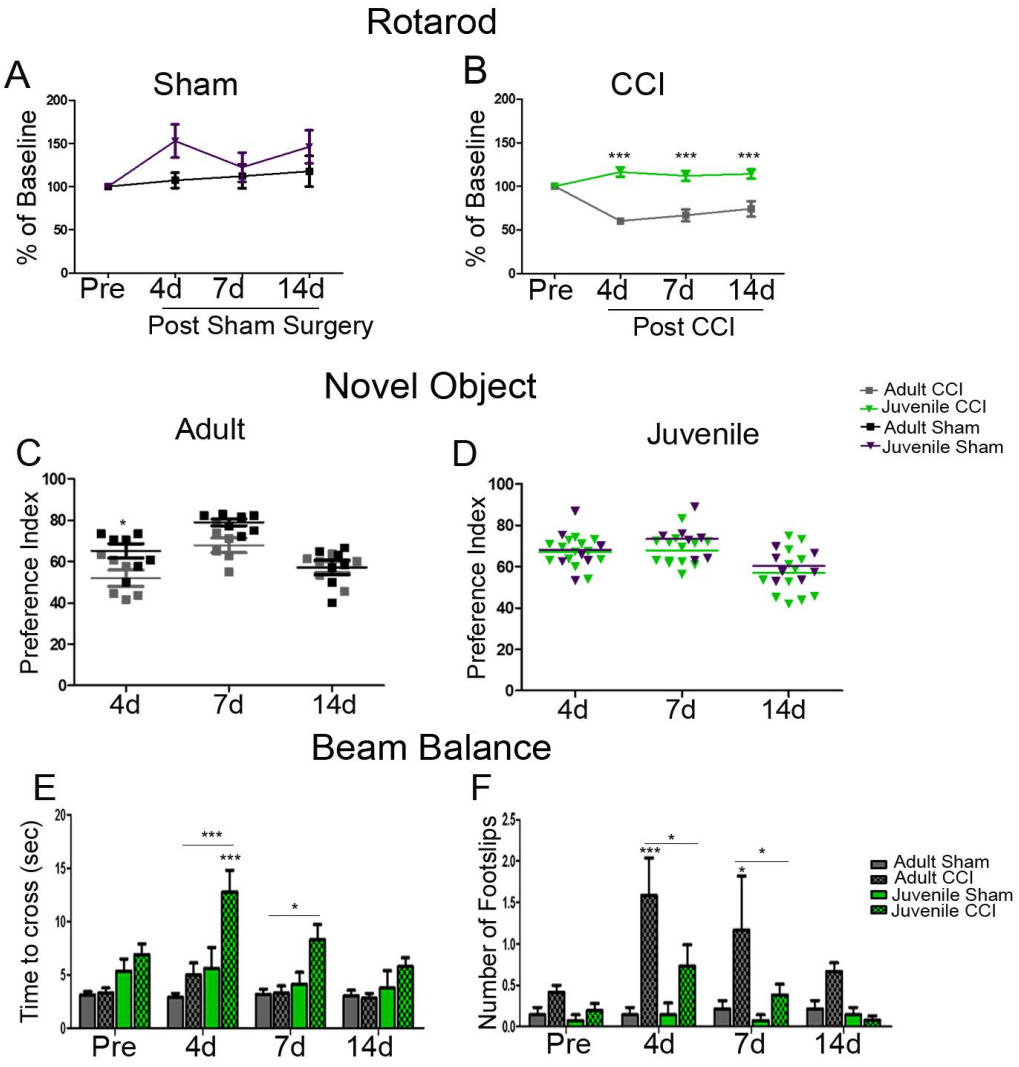

Figure 12. Behavioral testing in adult and juvenile mice following CCI injury. Rotarod (A-B) data presented as mean latency on rod compared to pre-injury. Graph (A) shows there is no significant difference between adult sham-injured and juvenile sham-injured mice. Graph (B) shows at 4, 7, and 14 days post-CCI injury, juvenile CCI-injured mice have significantly longer latency to fall compared to adult CCI-injured mice. Novel object recognition (C-D) data presented as the ratio of preference for the novel object to total time exploring objects. Graph (C) shows at 4 days post-CCI injury, adult CCI-injured mice spent significantly less time exploring

the novel object compared to adult sham-injured mice. Graph (D) shows juvenile CCI-injured and juvenile sham-injured mice show no significant difference in exploring the novel object at all time points. Beam balance (E-F) data presented as the time to cross the beam (E) and number of left hind limb foot slips (F). Graph (E) shows juvenile CCI-injured mice took significantly longer time to cross the beam compared to juvenile sham-injured at 4 and 7 days post-CCI. Juvenile CCI-injured mice took significantly longer time to cross the beam compared to and adult CCI-injured mice at 4 days- post CCI. Graph (F) shows adult CCI-injured mice had significantly more foot slips compared to adult sham-injured and juvenile CCI-injured mice at 4 and 7 days post-CCI. Data sets represented as mean +/- SEM. $^{***}P<0.001$; $^{*}P<0.05$. (Adult and Juvenile CCI n= 6 and n=13 per group) (Adult and juvenile sham n=7 per group).

Disruption of Ang-Tie2 Binding Causes Larger Lesion Volume in Juvenile Mice

From the relative vascular gene expression studies between adult CCI-injured and juvenile CCI-injured mice, we were particularly interested in determining if the Ang-Tie2 pathway had an age-dependent role in juvenile CCI-injury. To test this, P21 mice were subject to CCI injury and received twice daily tail vein injections of either control FC or Tie2-Fc soluble proteins for a total of two days. Specifically, we evaluated injury outcome between juvenile CCI-injured FC injections and juvenile CCI-injured Tie2-Fc injections, at 2 days post- injury (Figure, 13). Juvenile CCI-injured FC and juvenile CCI-injured Tie2-Fc serial sections were subjected to NISSL staining (Figure 13A and 13B). Using the Caveleri estimator, we found juvenile CCI-injured Tie2-Fc (2.6$\pm$ 0.15 mm^3; n=6) mice to have a significantly larger lesion volume compared to control juvenile CCI-injured FC (1.51$\pm$ 0.11 mm^3; n=3) mice (Figure 13C). These data demonstrate that disruption

of Ang-Tie2 signaling through Tie2-Fc soluble proteins in juvenile mice following CCI-injury have a larger lesion volume compared to juvenile CCI-injured mice that received control FC injections.

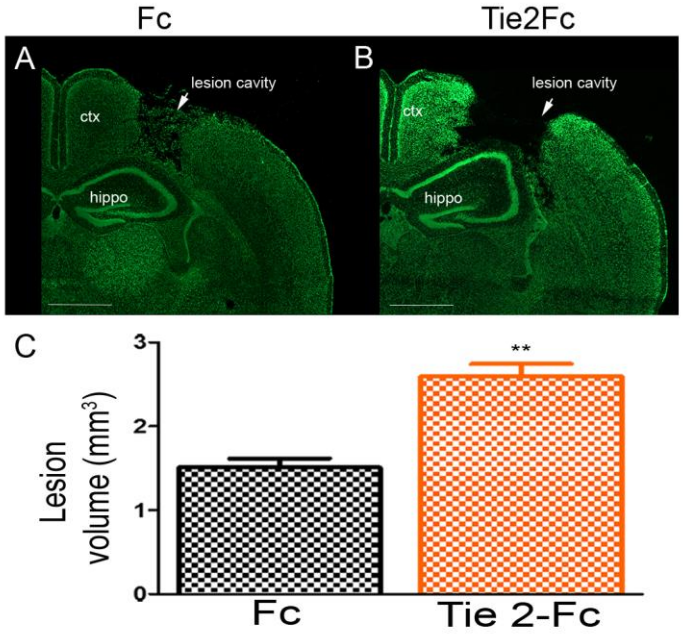

Figure 13. Comparison of Lesion Volume at 2 days post-CCI between juvenile FC treated and juvenile Tie2-Fc treated mice. Nissl stained sections collected at 2 days post-CCI from juvenile control treated Fc (A) and juvenile treatment treated Tie2-FC (B) brains show juvenile FC treated brains have less tissue loss compared to juvenile Tie2 treated brains. Quantified analysis (C) of lesion volume using Caveleri Estimator. Bar graph displays significant smaller lesion volume (mm^3) in Fc treated juvenile mice compared to Tie2-FC treated juvenile mice. Dataset represented as mean +/- SEM. $^{**}P<0.001$. CTX- cortex; hippo- hippocampus. (Juvenile Fc n= 3) (Juvenile Tie2Fc = 6). Scale bar 1mm.

Discussion

Insights into differential age-dependent responses and recovery to cerebral ischemic conditions have prompted its investigation in the stroke field and are now starting to emerge as an important determinant of TBI outcome (*4, 60*). The current study shows that juvenile mice at P21 have less cortical tissue loss following CCI injury compared to adult mice and this overt neuroprotection in the juvenile brain can be attenuated by blocking the endothelial cell (EC) specific Angiopoietin-Tie2 signaling cascade. These results identify an age-dependent mechanism and response of the juvenile vasculature that confers tissue protection following CCI injury. Our data conflicts with another finding that demonstrates significant cortical tissue loss in P21 mice after CCI injury (*8*). This discrepancy may be due to the strains of mice used or differences in the severity of CCI injury. Variability in tissue recovery has been demonstrated by studies in the TBI field that have shown strain related genetic differences exist in rats that are subjected to lateral fluid percussion injury (*61*). Furthermore, the initial severity of the impact is a strong predictor of outcome in the clinical and experimental settings, suggesting more severe injuries can cause greater initial tissue loss and irreversible damage that may force the tissue to a point of no return (*62-65*).

In the present study, we utilized P21 mice, which have been previously shown to model the adolescent human brain (*4, 66*). We have identified that this murine age, P21, is better protected from CCI injury and demonstrate that the vasculature's acute response within the juvenile brain confers this protection. This is evidenced by early and sustained improvements in CBF to the area of injury that was not observed in adult CCI-injured mice (Figure 2G). Clinical evidence suggests that while depressed levels of CBF leads to a poor prognosis, the early restoration of blood flow is linked to improvements in motor and neurological function (*67, 68*). We found in the

experimental setting that juvenile CCI-injured mice showed no deficit in motor recovery or hippocampal learning and memory when tested with the rotarod and novel object recognition behavioral tasks, respectively; while adult CCI-injured mice saw a motor and an acute memory deficit (Figure 12). We show that the increase and sustained levels of CBF in our P21 model is further supported by the increased diameter sizes of vessels found on the surface of the brain and the abundance of $CD31^+$ microvessels found within the peri-lesion in juvenile CCI-injured mice that was not observed in adult CCI-injured mice (Figure 3 and Figure 7; respectively). Overall we found that juvenile CCI-injured mice had significantly larger diameter collateral vessels and SMA^+ surface vessels compared to adult CCI-injured mice. These findings are consistent with studies that looked at pial arterioles in juvenile pigs after fluid percussion injury and found these surface vessels to be larger after injury and constrict less, increasing overall CBF compared to newborn pigs which were observed to have the opposite effect after injury (*5*). Taken together these studies demonstrate a conserved age-dependent mechanism across species of the juvenile pial arteriole response to TBI. Furthermore, findings within the stroke literature show that the extent of collateral vessel remodeling confers greater tissue protection after ischemic injury (*47, 69*). While future studies will need to further investigate the cellular mechanisms of collateral remodeling in TBI, our studies show juvenile collateral vessels respond to CCI by increasing in diameter, therefore, may enhance the CBF we observed in these mice. Furthermore, the preservation of the number and non-apoptotic morphology of $CD31^+$ cells found in the peri-lesion of juvenile CCI-injured mice compared to adult CCI-injured mice contributes to supplying the vulnerable neuronal tissue with blood.

Our findings also indicate an age protective role of BBB permeability in juvenile CCI-injured mice. We demonstrate that the BBB is less permeable in juvenile CCI-injured mice as we

observed a significant reduction of Evan's Blue into the tissue compared to adult- CCI injured mice (Figure 9). Juvenile CCI-injured mice also trended to have an up-regulation of TJ proteins, claudin-5 and occludin-1 from extracted ECs after CCI injury. In line with this finding, stroke studies have also reported an age-dependent BBB resistance to hypoxic ischemic injury in juvenile rats compared to younger rats (*4*). Thus, we began to wonder what the developmental differences were in regard to BBB function with respect to age. Studies have shown that while the BBB is established during embryogenesis in rodents with expression of tight junction proteins and associated pericytes, these vessels are void of astrocytes (*35, 70, 71*). Staining with GFAP shows with age, astrocyte end feet increasingly become associated with the vessels further establishing the fully functional BBB by adolescence or at P21 when rodents are weaned (*70*). During TBI, when there is physical disruption of the barrier, neonatal mice may actually be more susceptible to injury because their BBB is missing an integral structural component, astrocyte end feet coverage compared to more mature brains, which would have this astrocyte-vessel association. Prolonged, increased permeability of the BBB leaves the brain vulnerable to molecules that exacerbate tissue loss (*4*). BBB integrity has also been shown to decline with increased age due to the cellular stresses of aging that allow ECs to lose tight contact with one another (*72*). Thus, to begin to address the difference in BBB permeability in our studies between juvenile and adult CCI-injured mice, we focused on EC- specific signaling pathways.

While other studies have looked at gene expression changes within the cortex after TBI injury, our study is unique in the sense that we specifically looked at how ECs were responding to CCI-injury in an age-dependent manner as we isolated ECs through $CD31^+$ magnetic bead separation (*14*). Specifically, we were interested in the Angiopoietin-Tie2 signaling cascade as this signaling pathway is predominately EC specific. The importance of Ang-Tie2 signaling for

the survival of ECs has been demonstrated by developmental studies that have shown deletion or early inactivation of Tie2 results in embryonic lethality or pronounced vascular deficits, respectively (*73, 74*). These vascular deficits include reduction in the integrity of blood vessels and loss of ECs (*74-76*). Furthermore, *in-vitro* studies have shown that Ang-1-Tie2 signaling protects ECs from apoptosis through downstream activation of PI-3, which then goes to activate Akt mediated anti-apoptotic signals (*77, 78*). Thus we were interested if Ang-Tie2 signaling would have a robust response in juvenile mice after CCI-injury compared to adult mice to confer this tissue protection.

To test the role of the Ang-Tie2 axis, we administered soluble Tie2-Fc recombinant proteins immediately after juvenile CCI-injury through tail vein injections. Fc soluble proteins were administered to another subset of juvenile CCI-injured mice to act as our control. We found that by blocking the Ang-Tie2 signaling cascade with Tie2-Fc, the overt neuroprotection we saw in juvenile- CCI injured mice was attenuated (Figure 13). This finding is supported by an elegant study in the stroke field, which demonstrated that activation of Tie2 using AKB- 9785, which causes Tie2 phosphorylation, after MCA occlusion in adult mice, resulted in significant tissue protection which was not observed when Tie2 was not phosphorylated in a normal injury setting (*17*). Furthermore, the authors imply Tie2 phosphorylation has a positive role on BBB integrity as they observed less IgG staining in AKB-9785 treated (Tie2 phosphorylated) brains compared to non-treated brains after MCA occlusion (*17*). To test how Tie2 phosphorylation may be regulating BBB function, the authors cultured ECs in the presence of Ang-2, which caused EC permeability; however, the addition of AKB- 9785 and subsequent phosphorylation of Tie2 resulted in ECs overcoming the permeability effects of Ang-2, suggesting a role of Tie2 activation in strengthening the integrity of BBB (*17*).

While we saw a significant increase of Ang-1 expression in the $CD31^-$ fraction in juvenile CCI-injured mice compared to adult CCI-injured mice, our findings are consistent with other reports that have shown Ang-1 is expressed by pericytes and astrocytes and we were not surprised that we did not see Ang-1 expression in the $CD31^+$ EC fraction (*21, 79*) (Figure 11). Pericytes and astrocytes constitutively express Ang-1 to provide vessel stabilization and further recruitment of mural cells to maintain the integrity of the BBB (*80, 81*). We speculate that in juvenile mice while the BBB has pericyte coverage and newly associated astrocyte endfeet surrounding ECs, CCI-injury causes an age-related release of Ang-1 from pericytes and astrocytes onto the Tie2 receptor, causing phosphorylation. This increase in expression of Ang-1 would cause a robust response from the ECs in stimulating pro-survival signals through the downstream Akt pathway, promoting vessel integrity and supplying blood to the underlying tissue. In addition, Ang-1 phosphorylation of Tie-2 would aid against BBB permeability by further strengthening the association of adjacent ECs (*17, 82-84*). While we have identified a key developmental age that has better protection from CCI-injury conferred by Ang-Tie2 binding, future studies will be needed to address our incomplete understanding of age-dependent responses of the BBB to injury. Further understanding age-related differences of the immune system to CCI-injury is another important part of tissue survival (*71, 85, 86*). Studies have found age-dependent responses of particular immune cells after CCI-injury (*8*). Interestingly, $CD45^+$ leukocytes and $GR\text{-}1^+$ granulocytes have been found to have an age-dependent elevated response in P21 mice compared to adult mice following CCI-injury (*8, 87*). While early immune cell activation is important for tissue recovery, a pro-longed inflammatory response interferes with repair mechanisms further complicating the recovery process (*88*).

Future work will look to further address the complicated cascade of mechanisms that may confer protection; however, in this study we have demonstrated an age-dependent role of the Ang-Tie2 axis following CCI injury. Understanding how the vasculature responds to trauma in a juvenile brain, where BBB vulnerability is reduced and vessels are responsive to injury cues by enlarging in diameter, will be critical in better understanding the pathogenesis after childhood TBI. Developing specific age therapeutics is an important step in treating TBI taking into account brain maturation stages that may require differential treatment to stimulate tissue protection and limit BBB permeability.

References

1. T. K. Andrews, F. D. Rose, D. A. Johnson, Social and behavioural effects of traumatic brain injury in children. *Brain Inj* **12**, 133-138 (1998).
2. M. Rutter, Psychological sequelae of brain damage in children. *Am J Psychiatry* **138**, 1533-1544 (1981).
3. C. D. Marquez de la Plata *et al.*, Impact of age on long-term recovery from traumatic brain injury. *Arch Phys Med Rehabil* **89**, 896-903 (2008).
4. K. Muramatsu, A. Fukuda, H. Togari, Y. Wada, H. Nishino, Vulnerability to cerebral hypoxic-ischemic insult in neonatal but not in adult rats is in parallel with disruption of the blood-brain barrier. *Stroke* **28**, 2281-2288; discussion 2288-2289 (1997).
5. W. M. Armstead, Age-dependent cerebral hemodynamic effects of traumatic brain injury in newborn and juvenile pigs. *Microcirculation* **7**, 225-235 (2000).
6. Y. R. Sophie Su, A. Veeravagu, G. Grant, in *Translational Research in Traumatic Brain Injury*, D. Laskowitz, G. Grant, Eds. (Boca Raton (FL), 2016).
7. D. Sun *et al.*, Cell proliferation and neuronal differentiation in the dentate gyrus in juvenile and adult rats following traumatic brain injury. *J Neurotrauma* **22**, 95-105 (2005).
8. W. Tong, T. Igarashi, D. M. Ferriero, L. J. Noble, Traumatic brain injury in the immature mouse brain: Characterization of regional vulnerability. *Experimental Neurology* **176**, 105-116 (2002).
9. D. O. Ajao *et al.*, Traumatic brain injury in young rats leads to progressive behavioral deficits coincident with altered tissue properties in adulthood. *J Neurotrauma* **29**, 2060-2074 (2012).
10. P. D. Adelson, M. J. Whalen, P. M. Kochanek, P. Robichaud, T. M. Carlos, Blood brain barrier permeability and acute inflammation in two models of traumatic brain injury in the immature rat: a preliminary report. *Acta Neurochir Suppl* **71**, 104-106 (1998).
11. S. Bake, A. Selvamani, J. Cherry, F. Sohrabji, Blood brain barrier and neuroinflammation are critical targets of IGF-1-mediated neuroprotection in stroke for middle-aged female rats. *PLoS One* **9**, e91427 (2014).
12. M. Giraud *et al.*, Early Blood Brain Barrier Changes in Acute Ischemic Stroke: A Sequential MRI Study. *J Neuroimaging* **25**, 959-963 (2015).
13. J. M. Null, W. A. Null, Modulators of IgG penetration through the blood-brain barrier: Implications for Alzheimer's disease immunotherapy. *Hum Antibodies*, (2016).
14. T. Babikian *et al.*, Molecular and physiological responses to juvenile traumatic brain injury: focus on growth and metabolism. *Dev Neurosci* **32**, 431-441 (2010).
15. M. D. Ginsberg *et al.*, Uncoupling of local cerebral glucose metabolism and blood flow after acute fluid-percussion injury in rats. *Am J Physiol* **272**, H2859-2868 (1997).
16. W. M. Armstead, C. D. Kurth, Different cerebral hemodynamic responses following fluid percussion brain injury in the newborn and juvenile pig. *J Neurotrauma* **11**, 487-497 (1994).
17. S. Gurnik *et al.*, Angiopoietin-2-induced blood-brain barrier compromise and increased stroke size are rescued by VE-PTP-dependent restoration of Tie2 signaling. *Acta Neuropathol* **131**, 753-773 (2016).

18. N. Nourhaghighi, K. Teichert-Kuliszewska, J. Davis, D. J. Stewart, S. Nag, Altered expression of angiopoietins during blood-brain barrier breakdown and angiogenesis. *Lab Invest* **83**, 1211-1222 (2003).
19. M. Oudega, Molecular and cellular mechanisms underlying the role of blood vessels in spinal cord injury and repair. *Cell Tissue Res* **349**, 269-288 (2012).
20. H. Beck, T. Acker, C. Wiessner, P. R. Allegrini, K. H. Plate, Expression of angiopoietin-1, angiopoietin-2, and tie receptors after middle cerebral artery occlusion in the rat. *Am J Pathol* **157**, 1473-1483 (2000).
21. L. Eklund, P. Saharinen, Angiopoietin signaling in the vasculature. *Exp Cell Res* **319**, 1271-1280 (2013).
22. L. Eklund, B. R. Olsen, Tie receptors and their angiopoietin ligands are context-dependent regulators of vascular remodeling. *Exp Cell Res* **312**, 630-641 (2006).
23. U. Fiedler *et al.*, Angiopoietin-2 sensitizes endothelial cells to TNF-alpha and has a crucial role in the induction of inflammation. *Nat Med* **12**, 235-239 (2006).
24. D. M. Lai *et al.*, Angiopoietin-like protein 1 decreases blood brain barrier damage and edema following focal cerebral ischemia in mice. *Neurochem Int* **52**, 470-477 (2008).
25. H. Kim *et al.*, Dexamethasone coordinately regulates angiopoietin-1 and VEGF: a mechanism of glucocorticoid-induced stabilization of blood-brain barrier. *Biochem Biophys Res Commun* **372**, 243-248 (2008).
26. S. Nag, J. L. Manias, A. Kapadia, D. J. Stewart, Molecular Changes Associated with the Protective Effects of Angiopoietin-1 During Blood-Brain Barrier Breakdown Post-Injury. *Mol Neurobiol*, (2016).
27. M. Deschauer *et al.*, Molecular and biochemical investigations in fumarase deficiency. *Mol Genet Metab* **88**, 146-152 (2006).
28. S. N. McGill, N. A. Ahmed, N. V. Christou, Endothelial cells: role in infection and inflammation. *World J Surg* **22**, 171-178 (1998).
29. S. L. Andersen, Trajectories of brain development: point of vulnerability or window of opportunity? *Neurosci Biobehav Rev* **27**, 3-18 (2003).
30. N. Herschkowitz, J. Kagan, K. Zilles, Neurobiological bases of behavioral development in the first year. *Neuropediatrics* **28**, 296-306 (1997).
31. B. Crain, C. Cotman, D. Taylor, G. Lynch, A quantitative electron microscopic study of synaptogenesis in the dentate gyrus of the rat. *Brain Res* **63**, 195-204 (1973).
32. J. De Felipe, P. Marco, A. Fairen, E. G. Jones, Inhibitory synaptogenesis in mouse somatosensory cortex. *Cereb Cortex* **7**, 619-634 (1997).
33. P. R. Huttenlocher, Synaptic density in human frontal cortex - developmental changes and effects of aging. *Brain Res* **163**, 195-205 (1979).
34. C. Englert *et al.*, Crossing the blood-brain barrier: Glutathione-conjugated poly(ethylene imine) for gene delivery. *J Control Release* **241**, 1-14 (2016).
35. J. Xu, E. A. Ling, Studies of the ultrastructure and permeability of the blood-brain barrier in the developing corpus callosum in postnatal rat brain using electron dense tracers. *J Anat* **184 (Pt 2)**, 227-237 (1994).
36. M. L. Prins, D. A. Hovda, Developing experimental models to address traumatic brain injury in children. *J Neurotrauma* **20**, 123-137 (2003).
37. D. S. DeWitt, D. S. Prough, Traumatic cerebral vascular injury: the effects of concussive brain injury on the cerebral vasculature. *J Neurotrauma* **20**, 795-825 (2003).

38. P. M. Kochanek *et al.*, Cerebral blood flow at one year after controlled cortical impact in rats: assessment by magnetic resonance imaging. *J Neurotrauma* **19**, 1029-1037 (2002).
39. J. W. Lighthall, Controlled cortical impact: a new experimental brain injury model. *J Neurotrauma* **5**, 1-15 (1988).
40. D. I. Shreiber *et al.*, Experimental investigation of cerebral contusion: histopathological and immunohistochemical evaluation of dynamic cortical deformation. *J Neuropathol Exp Neurol* **58**, 153-164 (1999).
41. T. Brickler *et al.*, Nonessential Role for the NLRP1 Inflammasome Complex in a Murine Model of Traumatic Brain Injury. *Mediators Inflamm* **2016**, 6373506 (2016).
42. G. Baumann, L. Travieso, D. J. Liebl, M. H. Theus, Pronounced hypoxia in the subventricular zone following traumatic brain injury and the neural stem/progenitor cell response. *Exp Biol Med (Maywood)* **238**, 830-841 (2013).
43. M. H. Theus, J. Ricard, J. R. Bethea, D. J. Liebl, EphB3 limits the expansion of neural progenitor cells in the subventricular zone by regulating p53 during homeostasis and following traumatic brain injury. *Stem Cells* **28**, 1231-1242 (2010).
44. J. O. Ojo *et al.*, Chronic Repetitive Mild Traumatic Brain Injury Results in Reduced Cerebral Blood Flow, Axonal Injury, Gliosis, and Increased T-Tau and Tau Oligomers. *J Neuropathol Exp Neurol* **75**, 636-655 (2016).
45. R. A. Defazio *et al.*, A protocol for characterizing the impact of collateral flow after distal middle cerebral artery occlusion. *Transl Stroke Res* **2**, 112-127 (2011).
46. M. H. Theus, J. Ricard, S. J. Glass, L. G. Travieso, D. J. Liebl, EphrinB3 blocks EphB3 dependence receptor functions to prevent cell death following traumatic brain injury. *Cell Death Dis* **5**, e1207 (2014).
47. D. S. Liebeskind, Stroke: the currency of collateral circulation in acute ischemic stroke. *Nat Rev Neurol* **5**, 645-646 (2009).
48. F. O. Lima *et al.*, The pattern of leptomeningeal collaterals on CT angiography is a strong predictor of long-term functional outcome in stroke patients with large vessel intracranial occlusion. *Stroke* **41**, 2316-2322 (2010).
49. P. Meier *et al.*, Beneficial effect of recruitable collaterals: a 10-year follow-up study in patients with stable coronary artery disease undergoing quantitative collateral measurements. *Circulation* **116**, 975-983 (2007).
50. A. Perrein *et al.*, Cerebral vasospasm after traumatic brain injury: an update. *Minerva Anestesiol* **81**, 1219-1228 (2015).
51. N. F. O'Brien, K. E. Reuter-Rice, S. Khanna, B. M. Peterson, K. B. Quinto, Vasospasm in children with traumatic brain injury. *Intensive Care Med* **36**, 680-687 (2010).
52. Y. Xiong, A. Mahmood, M. Chopp, Animal models of traumatic brain injury. *Nature Reviews Neuroscience* **14**, 128-142 (2013).
53. L. He *et al.*, Analysis of the brain mural cell transcriptome. *Sci Rep* **6**, 35108 (2016).
54. M. Tsacopoulos, P. J. Magistretti, Metabolic coupling between glia and neurons. *J Neurosci* **16**, 877-885 (1996).
55. R. B. Banati, Neuropathological imaging: in vivo detection of glial activation as a measure of disease and adaptive change in the brain. *Br Med Bull* **65**, 121-131 (2003).
56. S. Chen, J. D. Pickard, N. G. Harris, Time course of cellular pathology after controlled cortical impact injury. *Exp Neurol* **182**, 87-102 (2003).
57. M. V. Sofroniew, H. V. Vinters, Astrocytes: biology and pathology. *Acta Neuropathol* **119**, 7-35 (2010).

58. U. Scherbel *et al.*, Differential acute and chronic responses of tumor necrosis factor-deficient mice to experimental brain injury. *Proc Natl Acad Sci U S A* **96**, 8721-8726 (1999).
59. M. K. Baskaya, A. Dogan, A. M. Rao, R. J. Dempsey, Neuroprotective effects of citicoline on brain edema and blood-brain barrier breakdown after traumatic brain injury. *J Neurosurg* **92**, 448-452 (2000).
60. C. Zhu *et al.*, Age-dependent regenerative responses in the striatum and cortex after hypoxia-ischemia. *J Cereb Blood Flow Metab* **29**, 342-354 (2009).
61. W. M. Reid *et al.*, Strain-related differences after experimental traumatic brain injury in rats. *J Neurotrauma* **27**, 1243-1253 (2010).
62. B. van Baalen *et al.*, Traumatic brain injury: classification of initial severity and determination of functional outcome. *Disabil Rehabil* **25**, 9-18 (2003).
63. P. K. Yip, A. Malaspina, Spinal cord trauma and the molecular point of no return. *Mol Neurodegener* **7**, 6 (2012).
64. P. M. Washington *et al.*, The effect of injury severity on behavior: a phenotypic study of cognitive and emotional deficits after mild, moderate, and severe controlled cortical impact injury in mice. *J Neurotrauma* **29**, 2283-2296 (2012).
65. V. Anderson *et al.*, Childhood brain insult: can age at insult help us predict outcome? *Brain* **132**, 45-56 (2009).
66. J. Dobbing, J. Sands, Comparative aspects of the brain growth spurt. *Early Hum Dev* **3**, 79-83 (1979).
67. Y. Inoue *et al.*, Changes in cerebral blood flow from the acute to the chronic phase of severe head injury. *J Neurotrauma* **22**, 1411-1418 (2005).
68. T. W. Langfitt, W. D. Obrist, T. A. Gennarelli, M. J. O'Connor, C. A. Weeme, Correlation of cerebral blood flow with outcome in head injured patients. *Ann Surg* **186**, 411-414 (1977).
69. M. B. Maas *et al.*, Collateral vessels on CT angiography predict outcome in acute ischemic stroke. *Stroke* **40**, 3001-3005 (2009).
70. E. M. Cornford, M. E. Cornford, Nutrient transport and the blood-brain barrier in developing animals. *Fed Proc* **45**, 2065-2072 (1986).
71. B. D. Semple, K. Blomgren, K. Gimlin, D. M. Ferriero, L. J. Noble-Haeusslein, Brain development in rodents and humans: Identifying benchmarks of maturation and vulnerability to injury across species. *Prog Neurobiol* **106-107**, 1-16 (2013).
72. G. Onyszchuk, Y. Y. He, N. E. Berman, W. M. Brooks, Detrimental effects of aging on outcome from traumatic brain injury: a behavioral, magnetic resonance imaging, and histological study in mice. *J Neurotrauma* **25**, 153-171 (2008).
73. P. C. Maisonpierre *et al.*, Angiopoietin-2, a natural antagonist for Tie2 that disrupts in vivo angiogenesis. *Science* **277**, 55-60 (1997).
74. C. Suri *et al.*, Requisite role of angiopoietin-1, a ligand for the TIE2 receptor, during embryonic angiogenesis. *Cell* **87**, 1171-1180 (1996).
75. D. J. Dumont *et al.*, Dominant-negative and targeted null mutations in the endothelial receptor tyrosine kinase, tek, reveal a critical role in vasculogenesis of the embryo. *Genes Dev* **8**, 1897-1909 (1994).
76. N. Jones, D. J. Dumont, Tek/Tie2 signaling: new and old partners. *Cancer Metastasis Rev* **19**, 13-17 (2000).

77. C. D. Kontos *et al.*, Tyrosine 1101 of Tie2 is the major site of association of p85 and is required for activation of phosphatidylinositol 3-kinase and Akt. *Mol Cell Biol* **18**, 4131-4140 (1998).
78. N. Jones *et al.*, Identification of Tek/Tie2 binding partners. Binding to a multifunctional docking site mediates cell survival and migration. *J Biol Chem* **274**, 30896-30905 (1999).
79. H. G. Augustin, G. Y. Koh, G. Thurston, K. Alitalo, Control of vascular morphogenesis and homeostasis through the angiopoietin-Tie system. *Nat Rev Mol Cell Biol* **10**, 165-177 (2009).
80. S. Dohgu, F. Takata, Y. Kataoka, Brain pericytes regulate the blood-brain barrier function. *Nihon Yakurigaku Zasshi* **146**, 63-65 (2015).
81. N. N. Haj-Yasein *et al.*, Glial-conditional deletion of aquaporin-4 (Aqp4) reduces blood-brain water uptake and confers barrier function on perivascular astrocyte endfeet. *Proc Natl Acad Sci U S A* **108**, 17815-17820 (2011).
82. H. Shimoda *et al.*, Abnormal recruitment of periendothelial cells to lymphatic capillaries in digestive organs of angiopoietin-2-deficient mice. *Cell Tissue Res* **328**, 329-337 (2007).
83. A. Armulik *et al.*, Pericytes regulate the blood-brain barrier. *Nature* **468**, 557-561 (2010).
84. E. Isasi, L. Barbeito, S. Olivera-Bravo, Increased blood-brain barrier permeability and alterations in perivascular astrocytes and pericytes induced by intracisternal glutaric acid. *Fluids Barriers CNS* **11**, 15 (2014).
85. B. Maier, H. L. Laurer, S. Rose, W. A. Buurman, I. Marzi, Physiological levels of pro- and anti-inflammatory mediators in cerebrospinal fluid and plasma: a normative study. *J Neurotrauma* **22**, 822-835 (2005).
86. M. J. Bell *et al.*, Interleukin-6 and interleukin-10 in cerebrospinal fluid after severe traumatic brain injury in children. *J Neurotrauma* **14**, 451-457 (1997).
87. D. Anthony *et al.*, CXC chemokines generate age-related increases in neutrophil-mediated brain inflammation and blood-brain barrier breakdown. *Curr Biol* **8**, 923-926 (1998).
88. A. Erturk *et al.*, Interfering with the Chronic Immune Response Rescues Chronic Degeneration After Traumatic Brain Injury. *J Neurosci* **36**, 9962-9975 (2016).

Chapter 3:

Model and Strain-Dependent Effects on Adult Cerebral Pial Collateral Remodeling following Traumatic Brain Injury

Thomas R Brickler[1], Kisha Gresham[1], Alexander Winemiller[2], Stefanie Robel[2] and Michelle H Theus[1]

[1]The Department of Biomedical Sciences and Pathobiology, Virginia-Maryland Regional College of Veterinary Medicine, 215 Duck Pond Drive, Blacksburg, VA, 24061 USA

[2]Virgnia Tech Carillion Research Institute, College of Medicine, 2 Riverside Circle, Roanoke, VA 24016 USA

Abstract

Traumatic brain injury (TBI) is a major health concern worldwide and a pathological feature of TBI is immediate reduced levels of cerebral blood flow (CBF) that directly contribute to mortality and morbidity. While there are different severities of TBI that range from mild, moderate, to severe, any injury to the brain can trigger fluctuations in CBF that can then further impair functional output and cause irreversible damage to the brain. To better understand the underlying pathology of changes in CBF after trauma and potential avenues for therapeutic potential, animal models have been developed to replicate many aspects of TBI. While arteriole remodeling has been highly studied in the context of ischemic diseases such as stroke, few studies have investigated the extent of large arteriole remodeling in the context of TBI. Here we examine arteriole remodeling in collateral vessels in two different models of TBI and in two different species of mice. Adult CD1 and C57BL/6 mice were subject to either cortical controlled impact (CCI) injury, which replicates moderate head injury, or repetitive weight drop model injury, which replicates mild concussive injuries, followed by blood perfusion scans to observe changes in CBF

over the time course of the injuries. We use a technique called vessel painting that selectively labels the arteriole network to address remodeling of the surface arteriole collaterals after TBI and found that arteriole remodeling is both model and species dependent. We observed that CCI resulted in impaired collateral remodeling in both strains that correlated with no changes in blood flow perfusion or tissue perseveration between CD1 and C57BL/6 mice. In contrast, following mTBI, we found that the collateral vessels in C57BL/6 mice were larger after injury compared to sham control and CD1 mice. These findings suggest that surface arteriole remodeling is both strain and model dependent following TBI.

Introduction

Traumatic brain injury (TBI) is an acquired neurological condition resulting from sudden head trauma leading to a decline in cognition and behavior (*1-5*). TBI is often classified as mild to moderate to severe depending on the extent of the primary mechanical injury (*6-8*). There is little known about the mechanism(s) underlying the effects of mild or moderate hits to the brain due to the restrictive assessments (cognitive or imaging) used to evaluate this type of non-fatal injury (*9-12*). Thus, laboratory models of these types of injuries allow us to better understand the biological outcome of the brain (*13-20*). Two established models to help assess the brain's response to trauma are the cortical controlled impactor (CCI) (*21-24*) and the closed-skull mild repetitive weight drop model (rmTBI) (*20, 25-28*). The CCI model causes a focal cortical lesion that is accompanied by pathological features of human brain injury that correlate with severity (*21, 22, 29*). Pathological hallmarks of this injury include hemorrhaging (*30, 31*), neuronal cell loss (*32-34*), and ischemia to and around the area of injury (*35-37*). In a single closed-skull injury that causes a concussive injury to the brain, minor immunohistochemical changes are observed (*9, 10, 18, 26*) wherein repeated mTBIs diffuse axonal injury accompanied with mild astrocytic reactivity can be observed with no apparent neuronal loss (*9, 38-40*). While single concussions present with acute cognitive dysfunction (*41, 42*), repetitive concussions cause an increase in neurological deficits over time (*43-46*).

Targeted treatment is limited to the secondary or delayed, non-mechanical damage mediated by a multidimensional cascade of events including changes in cerebral blood flow and oxygenation (*47, 48*). Disruption of the arteriole vascular network contributes to an ischemic milieu which mediates neuronal tissue loss and impedes prospective repair strategies (*49-54*). Interestingly, pial arteriole collaterals (i.e. natural by-pass vessels) have been linked to tissue preservation, where both pre-existing density and post-injury enlargement are known to play an

important role in the pathophysiology of cerebral ischemia (*55*). Cerebral collateral vessels, also known as leptomeningeal anastomoses, provide an alternative route around vascular obstructions and are vital in restoring and re-routing blood flow to affected tissue regions (*56*).

While numerous clinical attempts to increase angiogenesis (neovascularization of the pre-existing capillary network) in individuals with ischemic disease by administration of growth factors have mixed results (*57, 58*), the notion of improving the extent of arteriole collateral circulation has recently garnered increased attention. Rodent studies have provided significant insight into collateral function, including the observation that several murine strains such as C57BL/6 possess greater numbers of pre-existing collaterals, which help regulate cerebral blood flow following vascular occlusion and reduce tissue damage compared to strains with fewer collaterals (*59*). While having greater numbers of collaterals that form during development can prevent progressive stroke-induced damage occurring in adulthood, tissue reperfusion can also be enhanced by their post-injury remodeling (*60*). Arteriogenesis occurs by enlargement of native collaterals or by *de novo* formation of arterioles (*61-64*). This putative tissue-saving adaptation has also been shown to be strain dependent (*59, 65*), however, to-date no studies have analyzed this effect following brain trauma. Our current investigation, therefore, aimed to establish whether collateral remodeling is affected by mechanical tissue trauma using moderate controlled cortical impact (CCI) and mild repetitive TBI model in two different strains of mice, inbred C57BL/6, and outbred CD1. We found consistent with others that C57BL/6 mice have more collaterals compared to CD1 mice (*59, 66*). We also found that while there is no change in collateral size in the CCI model comparing sham to injured animals, the closed head weight drop model causes a significant increase in collateral diameter size in the C57BL/6 mice suggesting a head severity dependent and

species dependent remodeling of collateral vessels. The potential of immediate restoration of blood flow after TBI is an important area of investigation to prevent irreversible damage.

Materials and Methods

Animals. All mice were generated and housed in an AAALAC approved, virus/antigen-free facility with a 12 h light-dark cycle; food and water *ad libitum*. CD1 and C57BL/6 mice were purchased from Charles Rivers and Jackson lab, respectively, and bred until desired numbers were generated for experimentation. All experiments were conducted in accordance with the NIH Guide for the Care and Use of Laboratory Animals and were conducted under the approval of the Virginia Tech Institutional Animal Care and Use Committee (IACUC; #15-063) and the Virginia Maryland Regional College of Veterinary Medicine.

CCI Injury. Male CD1 and C57/BL6 mice at 2-4 months were anesthetized with ketamine and xylazine intraperitoneal (i.p.) injection and positioned in a stereotaxic frame (*67-69*). Body temperature was monitored with a rectal probe and maintained at 37°C with a controlled a heating pad (homeothermic blanket system; Harvard Apparatus). A 5mm craniotomy was made using a portable drill over the right parietal-temporal cortex (−2.5 mm A/P and 2.0 mm lateral from bregma). Injury was induced by moderate CCI using the *e*CCI- 6.3 device (Custom Design & Fabrication; 3mm impounder) at a velocity of 3.5 m/s, depth of 1.0 mm, and 150 ms impact duration (*68, 69*). Sham controls received anesthesia, skin incisions and sutures only. Following injury, the incision was closed using Vetbond tissue adhesive (3M, St. Paul, MN, USA) and the animals were placed into a heated cage to maintain body temperature for 1 h post-injury followed by daily monitoring for 4 days post-injury.

Weight Drop. Male CD1 and C57/BL6 mice at 2-4 months were anesthetized with ketamine and xylazine intraperitoneal (i.p.) injection and placed chest-down on a foam cushion. The mouse is quickly positioned so its head is directly under the path of the falling weight over midline lambda. The weight is released down the cylinder at a height of 36 inches, where it impacts the skull. A thin metal disk is placed on the exposed skull to prevent skull cracking. Body temperature is maintained at 37°C with a controlled a heating pad (homeothermic blanket system; Harvard Apparatus) and monitored with a rectal probe. The mouse is then placed onto a stereotactic frame where blood flow imaging takes place and returned to a holding cage to recover. Methods were repeated every 45 mins per animal until the mouse received a total of three hits.

Blood Flow Analysis. Cerebral blood flow measurement was conducted using LDI (Moor LDI 5061 and Moor Software Version 5.3, from Moor Instruments) as previously described (*70*). Mice were anesthetized and kept at 37.0 $\pm$ 0.5ºC body temperature. For the CCI injury group, the measurements were performed before surgery, directly after impact, and 4 days post- injury. Tissue perfusion is quantified with a region of interest (ROI) defined around the area of injury. Corresponding areas in contralateral hemispheres and sham were similarly surveyed. For the rmTBI group, the measurements were performed before surgery, directly after injury, 45mins before and post subsequent injuries. Tissue perfusion is quantified with a region of interest (ROI) defined as an oval around the caudal most area of the cortex reaching into both hemispheres. Corresponding areas in contralateral hemispheres and sham were similarly surveyed. Shams acted as internal controls and the valid pixel (VP) and mean pixel (MP) of ROIs of each hemisphere of sham animals was averaged. The ratio of injured animal's corresponding hemispheres to sham hemispheres was used to plot the time-course.

Vessel Painting. Vessel painting on post-natal and CCI-injured mice was modified from previous studies (*70, 71*). Briefly, mice were injected s.c. with heparin (2,000 units/kg), and sodium nitroprusside (SNP, 0.75 mg/kg) five minutes prior to euthanization using an overdose of isoflurane. When breathing stopped, the chest cavity was opened and then cardiac perfused using a Gilson MiniPuls3 peristaltic perfusion pump (Gilson Scientific, Bedfordshire, UK). Using a continuous infusion, 6-10 ml of 1x phosphate buffered saline (PBS) containing 20 units/ml heparin was perfused to flush blood from the cerebrovascular system, then 10 ml DiI (0.01µg/ml, Invitrogen)– 4% sucrose–PBS-heparin mixture was perfused to label the vasculature (0.7 ml/min for P1, 1.0 ml/min P7 and 2ml/min for P21 and adult flow rate), and finally, 4% cold paraformaldehyde (PFA) was perfused to fix the tissue. After perfusion, brains were carefully removed from the skull and placed in PFA overnight. Fixed brains were imaged at multiple image planes at 4x magnification on an upright fluorescence microscope (BX-51, Olympus America), using mosaic tile imaging from StereoInvestigator software (MBF, Williston, VT). Scaled mosaic images were imported into ImageJ, then the total number of intra- and inter-tree collaterals were identified between and within the MCA, ACA, and PCA artery branches and quantified using the counting tool in ImageJ on each scaled mosaic image. Pial collateral diameters were also individually assessed on the scaled mosaic images using ImageJ by averaging four independent diameters along the collateral length.

Quantification of collateral number and diameter. Collateral number and diameter was obtained from vessel painted, imaged brains at 4x magnification and analyzed in StereoInvestigator (MicroBrightField, Williston, VT, USA). The number of collaterals between the MCA, ACA, and PCA trees were counted. Once collaterals were identified, and the scaling for the images was set,

diameters were measured using the measure line tool. Two measurements were taken for each collateral and averaged to give the closest estimated size of the vessel.

Immunostaining. Brains were transferred into a 30% sucrose solution to cryopreserve for three days and then embedded in tissue freezing medium. Ten serial, coronal sections (30µm in thickness) were collected, from a cryostat (Thermo Fisher Cryostar NX50). For immunostaining, sections were blocked in 2% FISH gel with 0.1% Triton for 3 hours and incubated in primary antibody in block at 4°C. Green fluorescent NISSL 1/200 (Invitrogen N21480) was diluted 1:100 and added for one hour at room temperature. Rabbit anti-Glial Fibrillary Acidic Protein (GFAP): 1/200 (Cell Signaling 12389S) was diluted 1:100 and added overnight at 4C. Sections were washed 4 times with 1X PBS and GFAP slides were incubated with anti-rabbit Alexa Fluor 488-conjugated secondary antibodies (Molecular Probes, Carlsbad, CA) for 1h at RT.

Confocal Image Analysis

In order to analyze images taken on Zeiss LSM 880 confocal laser scanning microscope, three series coronal sections per brain were imaged using z-stack at 20X and 40X magnification. To analyze z-stacks as one image rather than several images individually, we used Fiji by ImageJ (NIH) (*72*) to project the z-stack images into a 2D plane.

Evaluation of lesion volume. Lesion volume was assessed by a blinded investigator using Caveleri Estimator from StereoInvestigator (MicroBrightField, Williston, VT, USA) and an Olympus BX51TRF motorized microscope (Olympus America, Center Valley, PA, USA). Lesion volume (mm^3) was determined as previously described (*67*). Briefly, volume analysis was performed by

estimating the area of tissue loss in the ipsilateral cortical hemisphere for five coronal serial sections at or around the epicenter (−1.1 to -2.6 mm posterior from bregma) of injury. Nissl stained serial sections were viewed under fluorescent illumination (GFP) at a magnification of 4x. A random sampling scheme was used that estimates every 10th section from rostral to caudal, yielding five total sections to be analyzed. A randomly placed grid with 100 µm spaced points was placed over the ipsilateral hemisphere and the area of the lesion was marked within each grid. Lesion boundaries were identified by loss of NISSL staining, pyknotic neurons, and tissue hemorrhage. The marked areas, using grid spacing, was then used to estimate total tissue volume based on section thickness, section interval, and total number of sections within the Caveleri program, StereoInvestigator. Data is represented as the volume of tissue loss or lesion volume (mm^3) for juvenile and adult mice.

Evaluation of $GFAP^+$ Cells. GFAP reactivity was assessed by a blinded investigator. Images of sham and mTBI injured serial sections were collected on confocal microscopy under fluorescent illumination (GFP) at a magnification of 10x. The images were then analyzed in Zenlight 2012. A region of interest (ROI) was placed around the Dentate Gyrus and hippocampus and intensity was taken. Another ROI was taken with no staining to subtract for the background.

Statistical analysis. Data was graphed using GraphPad Prism, version 4 (GraphPad Software, Inc., San Diego, CA). Student's two-tailed t-test was used for comparison of two experimental groups. Multiple comparisons were done using one-way and two-way ANOVA where appropriate followed by Tukey test for multiple pairwise examinations. Changes were identified as significant

if P was less than 0.05. Mean values were reported together with the standard error of the mean (SEM).

Results

Analysis of pial collateral number and diameter following moderate controlled cortical impact (CCI) injury

To assess whether strain related differences in collateral density and remodeling occur following CCI injury, we vessel painted CD1 mice and C57BL/6 mice four days after CCI-injury to count and measure collateral vessels (Figure 1). In agreement with other published reports (*59, 66*) we found that C57BL/6 sham-injured mice had significantly more collateral vessels on the contralateral (31.6±2.16; n=5) and ipsilateral (30.4±2.70) sides of injury compared to CD1 sham-injured mice on the contralateral (10.67±2.67; n=6) and ipsilateral (9.5±2.49) injury sides (Figure 1A and 1B). Following CCI injury, C57BL/6 CCI-injured (16.6±2.32; n=5) mice had a significant reduction in the number of collaterals compared to C57BL/6 sham-injured mice; however, C57BL/6 CCI-injured mice still had significantly more collateral vessels compared to CD1 CCI-injured mice (3.33±0.99; n=6) (Figure 1B). Not surprisingly, on the contralateral side of injury, both CD1 CCI-injured (9.67±1.78) and C57BL/6 CCI-injured (35.6±0.51) mice do not lose collateral vessels compared to non-injured sham controls (Figure 1A).

We next assessed the diameter of these identified collateral vessels between the two strains to determine if these collateral vessels responded differently to CCI-injury (Figure 1C and 1D). Interestingly, we found that C57BL/6- sham-injured mice had significantly larger diameter collateral vessels on the contralateral (20.40±0.91µm; n=8) and ipsilateral (21.55±1.6µm) sides of injury compared to the contralateral (16.36±0.70µm; n=8) and ipsilateral (17.63±0.40µm) sides of

CD1 sham-injured mice (Figure 1C and 1D). No significant changes in collateral diameter were found in both strains following CCI-injury (Figure 1C and 1D).

To assess how density and diameter of collateral vessels may be different between the two strains in CCI, we separated collaterals based on diameter ranges (0-20 µm; 21-25 µm; 26-30 µm; 31-39 µm; 40 µm) (Figure 1E and 1F). We found that on the contralateral side of injury, within the 21-25 µm range, C57BL/6 sham-injured (2.67± 0.76; n=6) and C57BL/6 CCI-injured (2.67± 0.62; n=6) mice had significantly more collaterals compared to CD1 sham-injured (0.25± 0.16; n=8) and CD1 CCI-injured (0.60±0.60; n=5) mice, respectively (Figure 1E). On the ipsilateral side of injury, CD1 CCI-injured (1.6± 0.40) mice lost a significant amount of collaterals in the 0-20 µm range compared to CD1 sham-injured (4.38± 1.09) mice (Figure 1F). C57BL/6 sham-injured (3.17± 0.70) mice had significantly more collaterals in the 21-25 µm range compared to CD1 sham-injured (0.38± 0.26) mice (Figure 1F). Representative vessel painted whole mount images from CD1 and C57BL/6 sham-injured and CD1 and C57BL/6 CCI-injured mice show the loss of collateral vessels in both strains after CCI-injury compared to sham-injury (Figure 1G- 1J). These findings suggest that moderate CCI injury does not induce collateral remodeling in both CD1 and C57BL/6 mouse strains. Interestingly, we did find that C57BL/6 sham-injured collateral vessels were larger in diameter compared to CD1 mice.

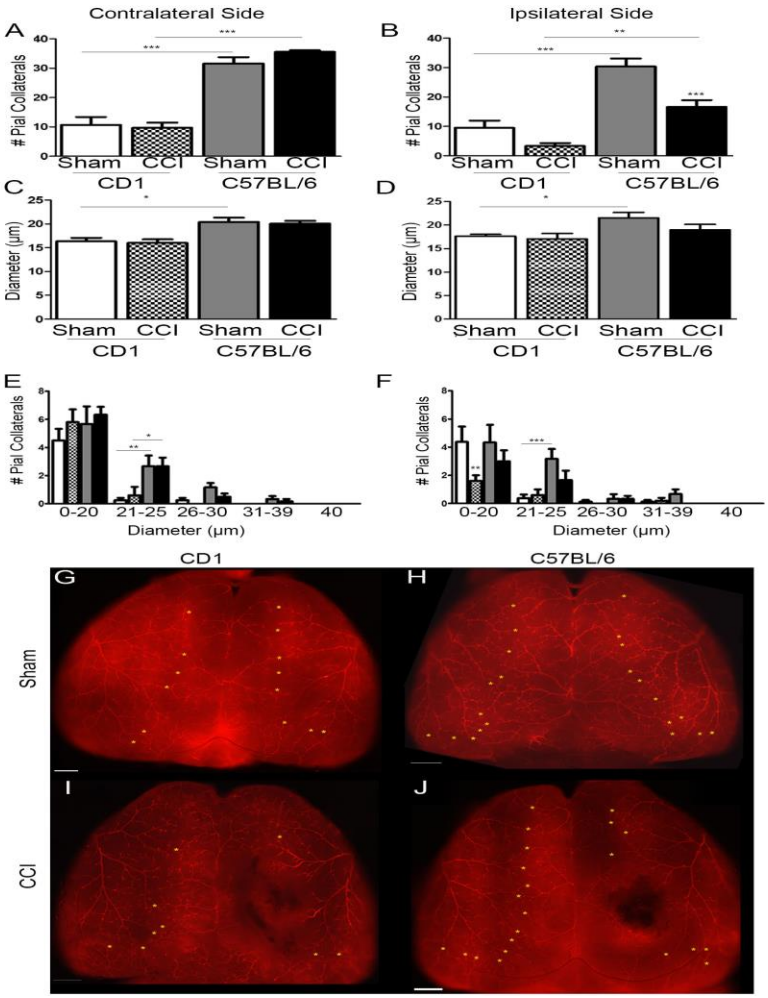

Figure 1. Pial collateral density and diameter in CD1 and C57BL/6 mice following CCI injury. Bar graph (A) shows that on the contralateral side of injury, C57BL/6 sham and CCI-injured mice have significantly more collateral vessels compared to CD1 sham and CCI-injured mice. Bar graph (B) shows on the ipsilateral side of injury both CD1 and C57BL/6 CCI-injured mice loose collateral vessels compared to sham-injured controls. C57BL/6 CCI-injured mice have significantly more collateral vessels compared to CD1 CCI-injured mice. Bar graphs (C-D) show on the contralateral and ipsilateral side of injury, C57BL/6 sham-injured mice have significantly larger collateral diameter compared to CD1 sham-injured mice. After CCI injury there is no significant change in diameter among the groups. Bar graph (E) represents breakdown of

collateral vessel diameters and shows C57BL/6 sham and CCI -injured mice have significantly more collateral vessels within the 21-25 µm range compared to CD1 sham and CCI-injured mice. Bar graph (F) shows on the ipsilateral side of injury, CD1 CCI-injured mice significantly lose the number of collaterals that lie within 0-20 µm range compared to CD1 sham-injured mice. C57BL/6 sham-injured mice have significantly more collateral vessels within the 21-25 µm range compared to CD1 sham-injured mice. Vessel painted whole mount images show the collateral vessels among CD1 sham-injured (G) and C57BL/6-sham-injured (H) and the loss of collateral vessels in CD1 CCI-injured (I) and C57BL/6 CCI-injured (J) mice. Asterisks mark individual collateral vessels. Dataset represented as mean +/- SEM. $^{***}P<0.0001$; $^{**}P<0.001$; $^{*}P<0.05$. (CD1 sham and injury n= 8 and n=5 per group); (C57BL/6 sham and injury n= 8 and n= 6 per group). Scale bar 1mm.

Analysis of pial collateral number and diameter following repetitive mild traumatic brain injury (mTBI)

We next wanted to assess if strain differences in collateral density and remodeling occur following a mild repetitive model of TBI using the weight drop model. Similar to the CCI-injury studies, we vessel painted C57BL/6 and CD1 mice four days after mTBI-injury to count and measure collateral vessels (Figure 2). We found that C57BL/6 sham-injured mice had significantly more collateral vessels on the left (18.6$\pm$1.21; n=5) and right (21.68$\pm$1.31) hemispheres compared to CD1 sham left (10$\pm$1.53; n=4) and right (13.3$\pm$2.33) hemispheres (Figure 2A and 2B). After repetitive mTBI, there was no change in collateral number between mTBI and sham-injured controls. C57BL/6 mTBI mice had significantly more collaterals on the left (21.6$\pm$1.70; n=9) and

right (23.71±0.75) compared to CD1 mTBI mice on the left (13±1.0; n=7) and right (13.3±0.88) hemispheres (Figure 2A and 2B).

We next wanted to determine if remodeling occurred in this mild model of TBI by measuring the diameter of identified collateral vessels. We found that C57BL/6 sham-injured mice have significantly larger diameter collateral vessels on the left (21±0.70µm; n=5) and right (21.68±1.31µm) hemispheres compared to CD sham-injured left (16.82±0.89µm; n=6) and right (17.44±0.66µm) hemispheres (Figures 2C and 2D). Interestingly, C57BL/6 mTBI mice had significantly larger collateral vessel diameters on the left (25.56±1.18µm; n=6) and right (25.59±0.71µm) hemispheres compared to C57BL/6 sham-injured mice. The increase in diameter seen in the C57BL/6 mTBI strain was also significantly larger compared to CD1 mTBI left (18.16±0.90µm; n=7) and right (18.40±0.66µm) hemispheres (Figure 2C and 2D).

To assess how density and diameter of collateral vessels may be different between the two strains in mTBI, we separated collaterals based on diameter ranges (0-20 µm; 21-25 µm; 26-30 µm; 31-39 µm; 40 µm) (Figure 2E and 2F). On the left hemisphere we found that both CD1 mTBI (4.87± 0.80; n=7) mice and C57BL/6 mTBI (3.3± 1.02; n=6) mice had a significant reduction in the number of collateral vessels within the 0-20 µm compared to sham-injured control strains (6.67± 0.72; n=6 and 6.4±1.36; n=7; respectively). While the subsequent ranges of diameters (21-25 µm; 26-30 µm) had similar densities of collateral vessels between the strains, we found within the 31-39 µm range, C57BL/6 mTBI (2± 0.37) mice had significantly more collateral vessels compared to CD1 mTBI (0.17± 0.17) mice (Figure 2E). On the right hemisphere, CD1 sham-injured (5.33± 0.72) and CD1 mTBI (4.57± 0.78) mice had significantly more collaterals within the 0-20µm range compared to C57BL/6 sham-injured (3.4±0.75) and C57BL/6 mTBI (1.83±0.54) mice, respectively (Figure 1F). C57BL/6 mTBI (3.8±0.60) mice had significantly more collateral

vessels within the 21-25µm range compared to C57BL/6 sham-injured (2.0±0.45) controls. In addition, C57BL/6 mTBI (3.8± 0.60; 1.83± 0.31; 1.83±0.54) mice had significantly more collateral vessels within the 21-25µm, 26-30µm, and 31-39µm compared to CD1-mTBI (1.0±0.54; 0.14± 0.14; 0) mice (Figure 2F). On both the left and right hemispheres C57BL/6 mTBI mice had collateral vessels that reached the 40 µm range that was absent in CD1 mTBI and sham-injured mice. Confocal images of individual collateral vessels stained with DiI through our vessel staining technique showed CD1 sham-injured collaterals to be smaller compared to C57BL/6 sham-injured collaterals (Figure 2G and 2I; respectively). There were no observable changes in diameter in CD1 sham-injured and CD1 mTBI vessels (Figure 2G and 2H; respectively). Interestingly, C57BL/6 mTBI collaterals appeared larger compared to C57BL/6 sham-injured and CD1 mTBI mice (Figure 2J; 2I; 2H, respectively). This data demonstrates mTBI causes an increase in diameter of collateral vessels in the C57BL/6 strain that is not observed in the CD1 strain.

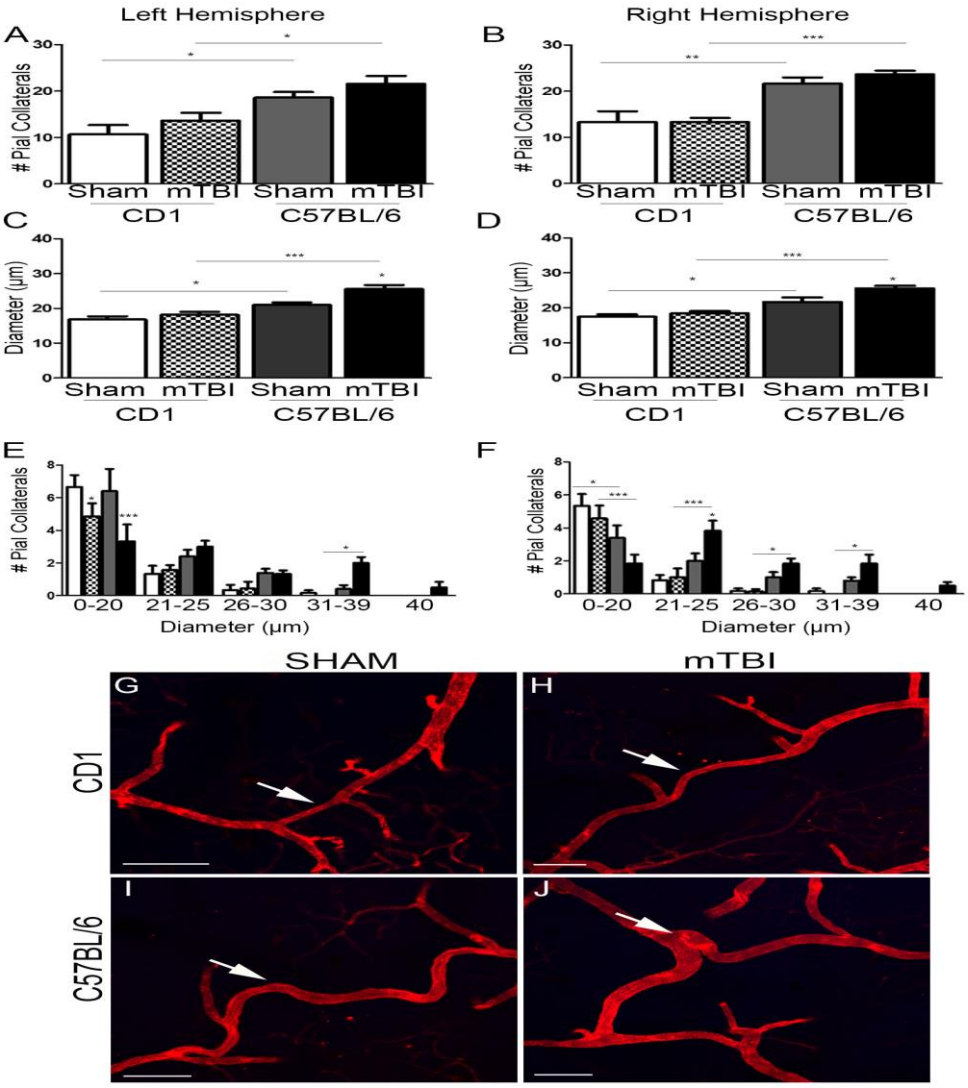

Figure 2. Pial collateral density and diameter in CD1 and C57BL/6 mice following repetitive mTBI. Bar graphs (A-B) show that on the left and right hemispheres, C57BL/6 sham-injured and mTBI strain have significantly more collateral vessels compared to CD1 sham-injured and mTBI mice following repetitive mTBI. Bar graphs (C-D) show on the left and right hemispheres, C57BL/6 sham-injured mice have significantly larger collateral diameters compared to CD1 sham-injured mice. After repetitive mTBI, C57BL/6 mTBI mice have significantly larger diameter compared to C57BL/6 sham-injured mice and CD1 mTBI mice. Bar graph (E)

represents the breakdown of collateral vessel diameters on the left hemisphere. After repetitive mTBI, both strains see a reduction in collateral number within the 0-20µm compared to sham-injured control strains. C57BL/6 mTBI mice have significantly more collateral vessels within the 31-39µm range compared to CD1 mTBI mice. Bar graph (F) represents the breakdown of collateral vessel diameters on the right hemisphere. CD1 sham-injured and mTBI mice have significantly more collateral vessels within the 0-20µm range compared to C57BL/6 sham-injured and mTBI mice, respectively. At the 21-25µm, 26-30µm, and 31-39µm range, C57BL/6 mTBI mice have more collaterals compared to CD1 mTBI mice. Representative confocal vessel painted images show collateral vessel diameter differences. CD1 sham-injured (G) strain collateral vessels appear smaller compared to C57BL/6 sham-injured (I) strain. No change in diameter is observed CD1 mTBI (H) strain. C57BL/6 mTBI (J) strain display increase in collateral diameter. Dataset represented as mean +/- SEM. $^{***}P<0.0001$; $^{**}P<0.001$; $^{*}P<0.05$. (CD1 sham and injury n= 6 and n=7 per group); (C57BL/6 sham and injury n= 5 and n= 6 per group). Scale bar 1mm.

Cerebral blood flow (CBF) analysis using Moor Laser Doppler Imaging following moderate CCI injury and repetitive mTBI

To assess whether strain differences in collateral density and remodeling correlated with changes in cerebral blood flow (CBF), we measured CBF via Moor Laser Doppler analysis following CCI injury and repetitive mTBI (Figure 3). In the CCI model, the perfusion units (PFU) were quantified using the same sized region of interest (ROI) around the focal area of injury and measurements were made relative to pre-scans for each animal. First, both strains of mice were subjected to moderate CCI injury and CBF was assessed immediately (0 minutes) and at 5-30

minutes during a repeat scan, followed by analysis at 4 days post-injury. The quantified data shows a similar loss in CBF in the ipsilateral cortex of CD1 (54.5 ± 3.6% of Pre-CCI scan) and C57BL/6 mice (58.9 ± 1.3% of Pre-CCI scan) immediately following CCI injury (Figure 3A). No significant difference was found between the CBF of CD1 and C57BL/6 at this time or up to 30m post-injury. CBF was then assessed at 4 days post-CCI, which also showed no significant difference between CD1 (67.1 ± 7.1% of Pre-CCI scan) compared to C57BL/6 mice (66.8 ± 9.1% of Pre-CCI scan) (Fig. 1B). No significant change in CBF was observed following sham surgery at the indicated time points (data not shown).

Next, we evaluated whether the extent of injury severity impacted changes in CBF and whether this effect is differentially regulated between the two strains of mice. In the mTBI model, the perfusion units (PFU) were quantified using a region of interest (ROI) which included the entire right and left cortical hemispheres. Measurements for each animal were made relative to the average sham control strain's same ROI. Using repetitive mTBI, CBF was evaluated immediately and at 45 minutes following each consecutive mTBI (Fig. 3C and 3D; black arrows) and a final assessment at 4 days post-mTBI. The quantified data shows a similar trend of CBF loss and reperfusion after subsequent hits between the two strains. We found that after each successive hit, there was no significant change in CBF compared to CBF prior to the hit. Representative blood flow scans so no real change in CBF between C57BL/6 strain and CD1 strain (Figure 3E). Taken together there were no changes in CBF between the strains following CCI-injury or repetitive mTBI.

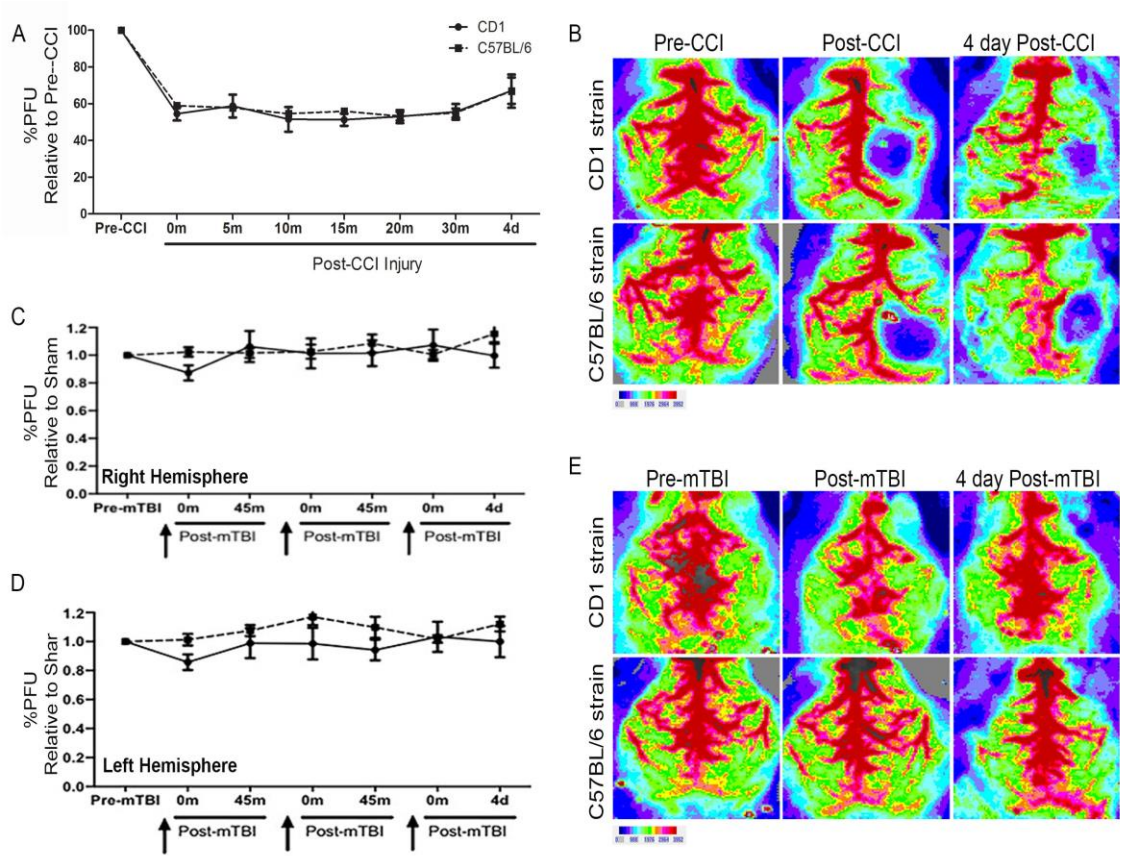

Figure 3. Acute changes in cerebral blood flow (CBF) following CCI and mTBI in CD1 and C57BL/6 mice. Quantitative analysis (A) using relative intensity shows there is no change in blood flow restoration to the area of injury following CCI. Relative intensity (B) of blood flow analysis using the Laser Doppler Imager shows CD1 and C57BL/6 have similar responses and recovery of blood flow perfusion. Quantitative analysis (C-D) using relative intensity shows there is no change in blood flow restoration to the area of injury following repetitive mTBI. Relative intensity (E) of blood flow analysis using the Laser Doppler Imager shows CD1 and C57BL/6 have similar responses and recovery of blood flow perfusion. (CD1 sham and injury n= 5 and n=7 per group); (C57BL/6 sham and injury n= 5 and n= 7 per group).

Analysis of tissue damage following CCI and mTBI.

To assess whether strain differences in collateral density and remodeling and changes in CBF correlated with lesion volume, we observed neural tissue damage following 4-days post-CCI injury (Figure 4). Serial sections were subjected to NISSL staining and lesion boundaries were demarcated by the loss of NISSL stain, pyknotic neurons, and tissue hemorrhage (Figure 4A and 4B). Using the Caveleri estimator, we found no significant difference in lesion volume between CD1 mice ($3.37 \pm 0.18 mm^3$) and C57BL/6 mice ($3.45 \pm 0.03 mm^3$) four days after CCI injury (Figure 4E). We next subjected repetitive mTBI sections to NISSL staining and found no loss of NISSL stain, pyknotic neurons or signs of tissue hemorrhage between the two strains (Figure 4C and 4D).

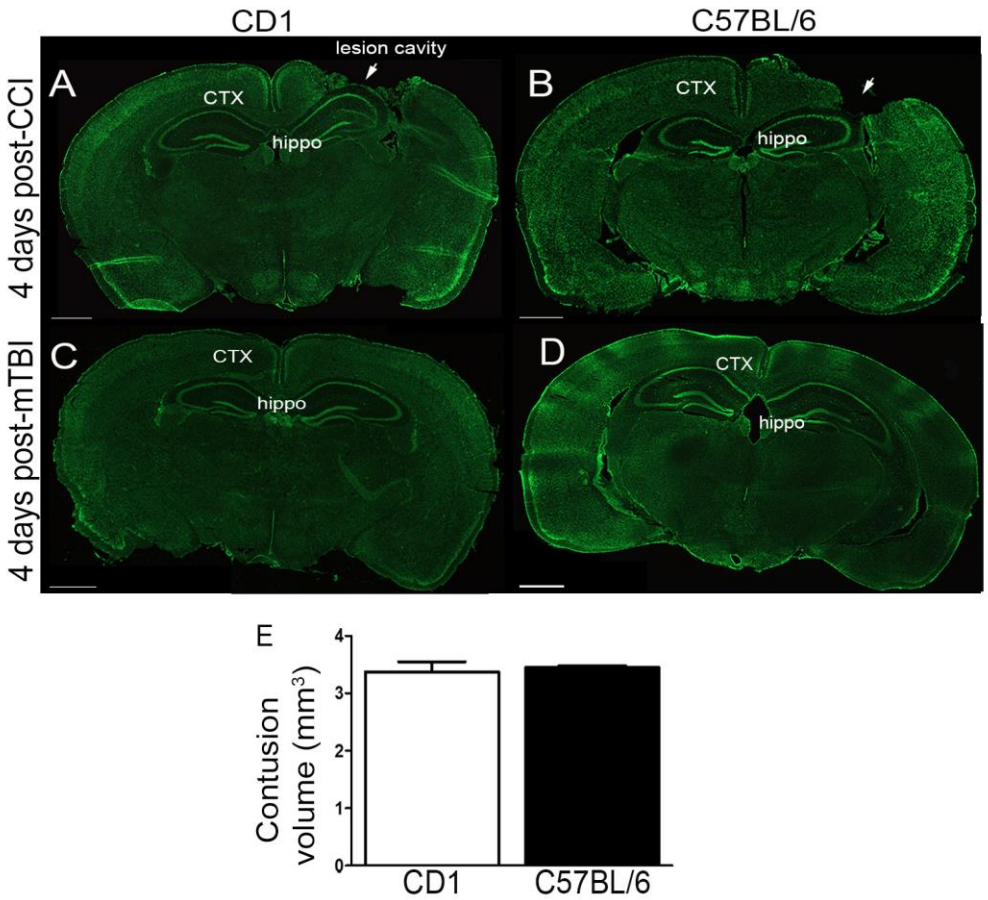

Figure 4. Strain effects on acute neural tissue loss following CCI injury and repeated mTBI. Nissl stained sections collected at 4d post-CCI from CD1 (A) and C57BL/6 (B) mice show no significant change in lesion volume. Quantified analysis (E) of lesion volume using Caveleri Estimator. Bar Graph display non-significant change in lesion volume (mm^3) at 4 d between CD1 and C57BL/6 strains. Nissl Stained sections collect at 4d post repeated mTBI from CD1 (C) and C57BL/6 (D) show no overt histological damage or focal lesion in the cortex or hippocampus. CTX- cortex, hippo- hippocampus. Dataset represented as mean +/- SEM. (CD1 and C57BL/6 n=4). Scale bar 1mm.

Analysis of astrogliosis following repetitive mTBI

As astrocytes have been shown to be tightly associated with blood vessels, we were interested in assessing the role astrocytes may be playing after repetitive mTBI. To do this, we evaluated patterns of GFAP expression in the cortex and hippocampus between the CD1 and C57BL/6 strain. Vessel painted coronal sections were used to visualize penetrating DiI^+ blood vessels and co-labeled with GFAP to observe blood vessel/astrocyte interactions (Figure 5). We observed that CD1 and C57BL/6 sham-injured mice had similar phenotypes with no to very few $GFAP^+$ cells found around penetrating vessels (Figure 5A and 5C). However, after mTBI injury, both strains of mice had an increase of $GFAP^+$ cells around penetrating vessels relative to sham controls (Figure 5B and 5D). Interestingly, CD1 mTBI strain had an observable increase in $GFAP^+$ cells in around DiI^+ vessels compared to C57BL/6 mTBI strain (Figure B^1 and D^1, respectively). A similar phenotype of increased $GFAP^+$ cells after mTBI injury was also observed in the hippocampus between the two strains compared to sham-injured mice (Figure 5E-I). To quantify our observations, we then analyzed the mean intensity of GFAP stained serial sections between CD1 and C57BL/6 strains at 4 days- post mTBI within the dentate gyrus where we observed the greatest increase of $GFAP^+$ cells (Figure 5J). We found that CD1 sham-injured (59.32 ± 15.94) and C57BL/6 sham-injured (59.34 ± 16.98) strains have similar relative mean intensities of $GFAP^+$ cells. Following mTBI injury both CD1 (260.8 ± 62.49) and C57BL/6 (114 ± 27.65) mice saw an increase in the relative mean intensity of $GFAP^+$ cells relative to sham controls. However, CD1 injured mice had a significant increase in the relative mean intensity of $GFAP^+$ cells compared to CD1 sham and injured C57BL/6 mice. These results suggest that mice subject to repetitive mTBIs revealed evidence of mild reactive astrogliosis within the hippocampus and cortex of penetrating

vessels. In contrast, no gliosis was observed in sham animals. Interestingly, GFAP reactivity occurred to a greater extent in CD1 mice compared to C57BL/6 mice.

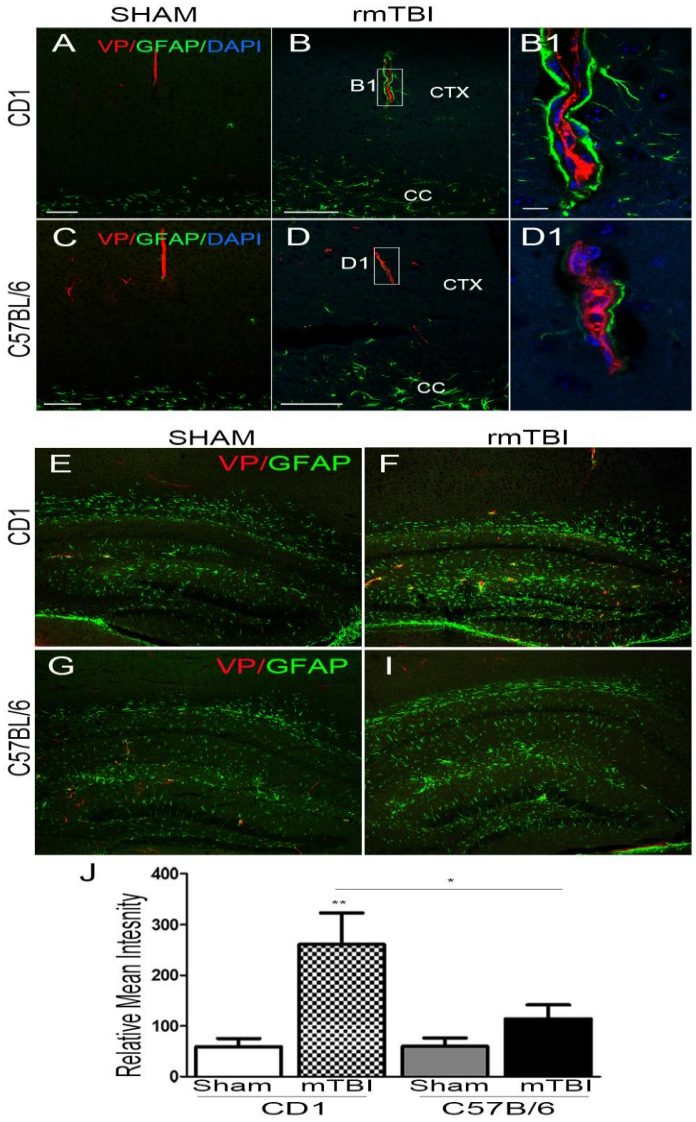

Figure 5. Strain effects on acute astrogliosis following repeated mTBI. GFAP stained sections collected at 4d post- mTBI from CD1 sham (A) and C57BL/6 sham-injured (C) strains show comparable staining of $GFAP^+$ cells in and around DiI^+ penetrating blood vessels. CD1- mTBI (B) and C57BL/6 mTBI (D) strains appear to have an increase of $GFAP^+$ staining relative to sham controls. Higher magnification of CD1 mTBI strain (B^1) and C57BL/6 mTBI strain (D^1)

reveals GFAP$^+$ cells around DiI$^+$ vessel with greater staining of GFAP$^+$ cells in CD1 mTBI strain. GFAP staining of the hippocampus reveals observable similar staining of GFAP$^+$ cells between CD1 sham (E) and C57BL/6 sham-injured (G) mice. mTBI injury appears to cause an increase of GFAP$^+$ staining between CD1 (F) and C57BL/6 (I) relative to shams. Quantified analysis (J) displays relative mean intensity of GFAP$^+$ within the hippocampus. Bar graph displays a significant increase in GFAP intensity in CD1 mTBI strain relative to sham-injured C57BL/6 – mTBI strain. Dataset represented as mean +/- SEM. $^{**}P<0.001$; $^{*}P<0.05$. (CD1 sham and injury n= 5 and n=3 per group); (C57BL/6 sham and injury n= 4 and n= 5 per group). Scale bar 20 µm.

Discussion

Insights into linking pial arteriole collateral responses, the pre-existing density, and post-injury enlargement, with tissue preservation following vascular occlusion have prompted its investigation in ischemic diseases such as hind-limb ischemia and stroke; however, the collateral response has not been addressed in the context of TBI (*66, 73-75*). The current study demonstrates a model-dependent and strain-dependent role on the remodeling extent of pial arteriole collateral vessels after TBI. We have found that when we subjected the C57BL/6 strain and CD1 strain to repetitive mTBI using the weight drop model, C57BL/6 mice have larger diameter collateral vessels compared to injured CD1 mice, highlighting a murine strain response difference to mTBI (Figure 2). Histological differences in GFAP reactivity that found GFAP expression to be increased in CD1 compared to C57BL/6 mice after repetitive mTBI also provide evidence of strain differences to repetitive mTBI at the cellular level (Figure 5). Furthermore, when we subjected the C57BL/6 strain and CD1 strain to moderate TBI using the CCI-injury model, collateral remodeling was not observed in either strain, suggesting a model-dependent response to collateral remodeling

(Figure 1). This impaired collateral response following CCI-injury is further supported with no significant changes in blood flow reperfusion to the area of injury and no significant differences in lesion volume between the two strains (Figure 3A and Figure 4, respectively). These results are the first to identify a strain and model dependent response of pial arteriole collaterals in the context of TBI. Our findings are further supported by studies in hind-limb ischemia that demonstrate genetic differences in pre-existing collateral numbers are observed between mouse strains that mediate tissue recovery after injury and these differences in collateral numbers are also evident in the brain (*66*). For example, genome-wide microarray analysis between C57BL/6 and BALB/c mice revealed differences in expression of VEGF-A that was attributed to a larger pre-existing collateral density that conferred better tissue perfusion and protection after hind-limb ischemia in the C57BL/6 that expressed higher levels of VEGF-A (*66*). Strain-related differences have also been known to exist in TBI as variability in tissue recovery after lateral fluid percussion injury has been attributed to the genetic differences seen in rats (*76*). Understanding these genetic differences in rodent species is important as clinical studies have shown collateral response is varied among the human population and their response to ischemic disease (*77, 78*).

In the present study, we utilized the murine C57BL/6 strain and CD1 strain. C57BL/6 mice have been previously shown to have significantly more collateral vessels compared to Balb/c mice, which have been observed to have very few collateral vessels (*59*). In addition, C57BL/6 mice have been shown to have larger collateral vessel diameters compared to Balb/c mice (*59*). Consistent with these studies, we have found C57BL/6 mice to have significantly more collateral vessels with overall larger diameter compared to the CD1 strain (Figure 1A-B and Figure 2A-B).

Experimental and clinical evidence in the stroke field has shown that the pre-existing number of collateral vessels can dictate tissue recovery and outcome following stroke, (*55, 56,*

79). Although the pathological response of TBI is initiated by a force applied to the brain, it shares a common disease characteristic to that of stroke, which is cerebral ischemia (*80*). Studies have shown within minutes following CCI-injury, there is a significant loss of perfusion at the impact site, which reaches ischemic conditions (*21, 51, 81, 82*). Taken together these studies prompted us to explore the extent of collateral remodeling in CCI-injury. We demonstrate that CCI-injury induces a loss of collateral vessels at and around the impact site in both strains relative to sham controls (Figure 1A and 1B). We visualized collateral vessels using vessel painting that selectively labels the arteriole network using a fluorescent lipophilic cationic dye (DiI) that is administered into the left ventricle during cardiac perfusion 4 days post-CCI injury (*71*) (Figure 1G-J). Interestingly, although C57BL/6 CCI-injured mice had significantly more remaining collateral vessels compared to CD CCI-injured mice, this did not confer tissue protection (Figure 4A-B and 4E). Furthermore, collateral diameters did not change in either strain relative to sham controls after CCI-injury (Figure 1D). In addition, this impaired collateral remodeling exhibited by the two strains following CCI-injury, we also did not observe changes in blood flow perfusion to the area of injury (Figure 3). There have been numerous studies which have shown collateral vessel remodeling to dictate the outcome of ischemic stroke; however, our understanding of the collateral response after hemorrhagic stroke is greatly understudied (*56, 66, 83*). Hemorrhagic stroke occurs when a weakened vessel ruptures and bleeds into the surrounding tissue (*84-86*). Interestingly, a retrospective clinical study on patients that have suffered ischemic stroke or hemorrhagic stroke found that collateral numbers could dictate the outcome of patients with ischemic stroke, but could not predict the outcome in hemorrhagic stroke patients (*87*). The pathological response of a ruptured/weakened blood vessels that subsequently bleeds into the surrounding tissue during a hemorrhagic stroke is similar to how the vessels would respond after CCI-injury (*21, 51, 84, 85*).

Collateral vessel remodeling is triggered by mechano-receptors in endothelial cells (ECs) that sense increases in fluid shear stress (FSS) that cause an outward remodeling of the vessel (*88*). Thus, we speculate the focal impact of the CCI injury not only ruptures blood vessels upon contact, but the dispersal of blood in all directions weakens the surrounding ECs walls, reminiscent of hemorrhagic stroke (*21, 51, 84-86*). Thus, we predict that the bleeding from vessel walls and the craniotomy that is necessary to induce this focal injury lowers the overall FSS pressure sensed by the ECs of collateral vessels, causing them not to remodel (*88, 89*). In the context of CCI-injury having a greater density of collateral vessel does not confer tissue protection as seen in ischemic stroke (*56, 66, 83*).

Clinical studies have shown that concussive injuries can cause mild reductions of blood flow or even increases of blood flow after injury (*90-92*). As we were interested in collateral remodeling, we wanted to mimic ischemic stroke as close as we could, in the context of TBI. Despite these unknown CBF fluctuations after mTBI, what can be agreed upon is that the injured brain is highly vulnerable to ischemic conditions (*90*). Recent studies have shown that repetitive injuries can induce decreases in CBF, which is absent after a single hit, thus we decided to look at collateral remodeling in the repetitive weight drop model (*93, 94*). Our studies indicate that following repetitive mTBI using the weight drop model, the C57BL/6 strain is observed to have an outward remodeling of collateral vessels relative to non-injured mice (Figure 2C-D). This collateral vessel remodeling after repetitive mTBI also appears to be strain dependent as we did not observe collateral vessel diameter changes in the CD1 strain between injured and non- injured mice (Figure 2C-D). This overall increase in diameter of collateral vessels that we observed in the repetitive mTBI injured C57BL/6 strain was not observed in the CD1 strain. Although we did not observe changes in CBF to correlate with increases in diameter in the C57BL/6 strain, this may be

attributed to our experimental design. Both strains received multiple doses of ketamine prior to each hit, which has been shown to increase the overall effects of CBF (*95*). Thus, we may have picked up a ketamine-induced increase of CBF in our CD1 strain. In addition, we did not observe neuronal loss in the cortex or other brain regions, using NISSL stained coronal sections, in either strain after repetitive mTBI injury and this finding is supported by other studies that have used a similar repetitive mTBI model and did not observe neuronal tissue loss (*9, 20, 38*). Not surprising, there was no loss of collateral vessels after repetitive mTBI injury in both strains relative to sham-injured controls as the weight drop model has been shown to mimic axonal diffuse injury after a concussion (*96, 97*) (Figure 2A and 2B). While there are no studies that address the FSS pressure across the cerebral vasculature after closed-head injuries, we can infer that pressure gradients are increased in all cells types by studies that looked at the biomechanical forces of the brain after blast injury (*98*). This study found that the sudden acceleration and deceleration of forces experienced by the brain, for example, the soft brain tissue hitting the hard skull, could generate enough force to increase the shear stress across the brain; therefore, increasing the intracranial pressure (*98*). This shear stress of axonal stretching was seen greatest on the cortex where the force was applied and countercoup (*98*). From these studies, we can infer a similar scenario occurs in our repetitive weight drop model that causes an increase in intracranial pressure experienced by the surface collateral vessels. This increase in shear stress produces enough force across the vasculature to cause collateral vessels to outwardly remodel in the C57BL/6 strain as this strain has been shown to have an interconnected vascular network through the number of these collateral vessels. Conversely, the CD1 strain does not have an intricate collateral network, so the pressure experienced by the blood vessels could be lost (Figure 2G-J).

Previous research has shown that after repetitive mTBI there is an increase of GFAP reactivity, measured by mean GFAP staining intensity that is most evident in the hippocampus, although there is no hippocampal cell loss (*9*). Our findings support this as we observed an increase in GFAP reactivity in the hippocampus in both strains following repetitive mTBI (Figure 5E-J). Interestingly, we also found a strain related difference in GFAP reactivity as the CD1 strain had more $GFAP^+$ cells within the dentate gyrus compared to the C57BL/6 strain (Figure 5E-I). Previous studies in immunology support this finding as studies have shown strain background plays a role in the inflammatory response (*99, 100*). In addition, astrocytes help bridge the neurovascular unit as they help regulate the microcirculatory response and help make up the blood brain barrier (BBB) (*101-104*). Interestingly, as astrocytes help regulate the permeability of the BBB, which is needed in physiological settings, in the context of the pathological setting, studies have found that in order to protect neurons from injury, reactive astrocytes restrict immune cells from entering the brain (*105*).

Collateral vessel remodeling is dependent on infiltrating monocytes and macrophages to help stimulate vessel growth (*106, 107*). We speculate the tight association of reactive astrocytes on blood vessels in the CD1 strain after repetitive mTBI may dampen the collateral response by preventing monocytes and macrophages from entering the brain to stimulate remodeling. Conversely, less reactive astrocyte association with the blood vessel as we have seen in the C57BL/6 strain after repetitive mTBI would allow monocytes and macrophages to enter the brain to stimulate the collateral remodeling process. Collectively, these findings further confirm the response and repair of the cerebral vasculature to different severities of TBI, while highlighting a model and strain dependent role of collateral remodeling following TBI.

References

1. D. S. DeWitt, L. W. Jenkins, D. S. Prough, Enhanced vulnerability to secondary ischemic insults after experimental traumatic brain injury. *New Horiz* **3**, 376-383 (1995).
2. J. A. Langlois, R. W. Sattin, Traumatic brain injury in the United States: research and programs of the Centers for Disease Control and Prevention (CDC). *J Head Trauma Rehabil* **20**, 187-188 (2005).
3. J. A. Langlois, W. Rutland-Brown, M. M. Wald, The epidemiology and impact of traumatic brain injury: a brief overview. *J Head Trauma Rehabil* **21**, 375-378 (2006).
4. M. Schwarzbold *et al.*, Psychiatric disorders and traumatic brain injury. *Neuropsychiatr Dis Treat* **4**, 797-816 (2008).
5. B. E. Masel, D. S. DeWitt, Traumatic brain injury: a disease process, not an event. *J Neurotrauma* **27**, 1529-1540 (2010).
6. A. I. R. Maas, N. Stocchetti, R. Bullock, Moderate and severe traumatic brain injury in adults. *Lancet Neurology* **7**, 728-741 (2008).
7. J. F. Malec *et al.*, The mayo classification system for traumatic brain injury severity. *J Neurotrauma* **24**, 1417-1424 (2007).
8. B. L. Fischer *et al.*, Neural activation during response inhibition differentiates blast from mechanical causes of mild to moderate traumatic brain injury. *J Neurotrauma* **31**, 169-179 (2014).
9. B. Mouzon *et al.*, Repetitive mild traumatic brain injury in a mouse model produces learning and memory deficits accompanied by histological changes. *J Neurotrauma* **29**, 2761-2773 (2012).
10. A. C. McKee *et al.*, Chronic traumatic encephalopathy in athletes: progressive tauopathy after repetitive head injury. *J Neuropathol Exp Neurol* **68**, 709-735 (2009).
11. A. Costanza *et al.*, Review: Contact sport-related chronic traumatic encephalopathy in the elderly: clinical expression and structural substrates. *Neuropathol Appl Neurobiol* **37**, 570-584 (2011).
12. J. J. Bazarian *et al.*, Diffusion tensor imaging detects clinically important axonal damage after mild traumatic brain injury: a pilot study. *J Neurotrauma* **24**, 1447-1459 (2007).
13. P. D. Adelson, Animal models of traumatic brain injury in the immature: A review. *Experimental and Toxicologic Pathology* **51**, 130-136 (1999).
14. N. Marklund, L. Hillered, Animal modelling of traumatic brain injury in preclinical drug development: where do we go from here? *Brit J Pharmacol* **164**, 1207-1229 (2011).
15. W. T. O'Connor, A. Smyth, M. D. Gilchrist, Animal models of traumatic brain injury: A critical evaluation. *Pharmacol Therapeut* **130**, 106-113 (2011).
16. Y. Xiong, A. Mahmood, M. Chopp, Animal models of traumatic brain injury. *Nature Reviews Neuroscience* **14**, 128-142 (2013).
17. L. Y. Xu, Animal model of repetitive mild traumatic brain injury for human traumatic axonal injury and chronic traumatic encephalopathy. *Neural Regeneration Research* **10**, 1731-1732 (2015).
18. Y. Shitaka *et al.*, Repetitive closed-skull traumatic brain injury in mice causes persistent multifocal axonal injury and microglial reactivity. *J Neuropathol Exp Neurol* **70**, 551-567 (2011).

19. J. O. Ojo *et al.*, Chronic Repetitive Mild Traumatic Brain Injury Results in Reduced Cerebral Blood Flow, Axonal Injury, Gliosis, and Increased T-Tau and Tau Oligomers. *J Neuropathol Exp Neurol* **75**, 636-655 (2016).
20. M. J. Kane *et al.*, A mouse model of human repetitive mild traumatic brain injury. *J Neurosci Methods* **203**, 41-49 (2012).
21. C. E. Dixon, G. L. Clifton, J. W. Lighthall, A. A. Yaghmai, R. L. Hayes, A controlled cortical impact model of traumatic brain injury in the rat. *J Neurosci Methods* **39**, 253-262 (1991).
22. J. W. Lighthall, Controlled cortical impact: a new experimental brain injury model. *J Neurotrauma* **5**, 1-15 (1988).
23. D. H. Smith *et al.*, A Model of Parasagittal Controlled Cortical Impact in the Mouse - Cognitive and Histopathologic Effects. *J Neurotraum* **12**, 169-178 (1995).
24. J. W. Lighthall, H. G. Goshgarian, C. R. Pinderski, Characterization of axonal injury produced by controlled cortical impact. *J Neurotrauma* **7**, 65-76 (1990).
25. I. Khalin *et al.*, A mouse model of weight-drop closed head injury: emphasis on cognitive and neurological deficiency. *Neural Regen Res* **11**, 630-635 (2016).
26. S. M. DeFord *et al.*, Repeated mild brain injuries result in cognitive impairment in B6C3F1 mice. *J Neurotrauma* **19**, 427-438 (2002).
27. C. E. Creeley, D. F. Wozniak, P. V. Bayly, J. W. Olney, L. M. Lewis, Multiple episodes of mild traumatic brain injury result in impaired cognitive performance in mice. *Acad Emerg Med* **11**, 809-819 (2004).
28. Y. Yoshiyama *et al.*, Enhanced neurofibrillary tangle formation, cerebral atrophy, and cognitive deficits induced by repetitive mild brain injury in a transgenic tauopathy mouse model. *J Neurotrauma* **22**, 1134-1141 (2005).
29. E. D. Hall *et al.*, Spatial and temporal characteristics of neurodegeneration after controlled cortical impact in mice: more than a focal brain injury. *J Neurotrauma* **22**, 252-265 (2005).
30. S. L. Smith, E. D. Hall, Mild pre- and posttraumatic hypothermia attenuates blood-brain barrier damage following controlled cortical impact injury in the rat. *J Neurotrauma* **13**, 1-9 (1996).
31. P. M. Kochanek *et al.*, Severe controlled cortical impact in rats: assessment of cerebral edema, blood flow, and contusion volume. *J Neurotrauma* **12**, 1015-1025 (1995).
32. C. Woertgen, R. D. Rothoerl, A. Brawanski, Neuron-specific enolase serum levels after controlled cortical impact injury in the rat. *J Neurotrauma* **18**, 569-573 (2001).
33. A. M. Palmer *et al.*, Traumatic brain injury-induced excitotoxicity assessed in a controlled cortical impact model. *J Neurochem* **61**, 2015-2024 (1993).
34. R. H. Singleton, H. Q. Yan, W. Fellows-Mayle, C. E. Dixon, Resveratrol attenuates behavioral impairments and reduces cortical and hippocampal loss in a rat controlled cortical impact model of traumatic brain injury. *J Neurotrauma* **27**, 1091-1099 (2010).
35. R. M. Bryan, Jr., L. Cherian, C. Robertson, Regional cerebral blood flow after controlled cortical impact injury in rats. *Anesth Analg* **80**, 687-695 (1995).
36. R. L. Sutton, L. Lescaudron, D. G. Stein, Unilateral cortical contusion injury in the rat: vascular disruption and temporal development of cortical necrosis. *J Neurotrauma* **10**, 135-149 (1993).

37. M. L. Forbes *et al.*, Assessment of cerebral blood flow and CO2 reactivity after controlled cortical impact by perfusion magnetic resonance imaging using arterial spin-labeling in rats. *J Cereb Blood Flow Metab* **17**, 865-874 (1997).
38. H. L. Laurer *et al.*, Mild head injury increasing the brain's vulnerability to a second concussive impact. *J Neurosurg* **95**, 859-870 (2001).
39. K. Uryu *et al.*, Repetitive mild brain trauma accelerates Abeta deposition, lipid peroxidation, and cognitive impairment in a transgenic mouse model of Alzheimer amyloidosis. *J Neurosci* **22**, 446-454 (2002).
40. V. Conte *et al.*, Vitamin E reduces amyloidosis and improves cognitive function in Tg2576 mice following repetitive concussive brain injury. *J Neurochem* **90**, 758-764 (2004).
41. J. A. Creed, A. M. DiLeonardi, D. P. Fox, A. R. Tessler, R. Raghupathi, Concussive brain trauma in the mouse results in acute cognitive deficits and sustained impairment of axonal function. *J Neurotrauma* **28**, 547-563 (2011).
42. J. Bleiberg, D. Warden, Duration of cognitive impairment after sports concussion. *Neurosurgery* **56**, E1166 (2005).
43. M. Franzblau *et al.*, Vascular damage: a persisting pathology common to Alzheimer's disease and traumatic brain injury. *Med Hypotheses* **81**, 842-845 (2013).
44. M. Fujita, E. P. Wei, J. T. Povlishock, Intensity- and interval-specific repetitive traumatic brain injury can evoke both axonal and microvascular damage. *J Neurotrauma* **29**, 2172-2180 (2012).
45. P. M. Washington, S. Villapol, M. P. Burns, Polypathology and dementia after brain trauma: Does brain injury trigger distinct neurodegenerative diseases, or should they be classified together as traumatic encephalopathy? *Exp Neurol* **275 Pt 3**, 381-388 (2016).
46. J. O. Ojo *et al.*, Repetitive mild traumatic brain injury augments tau pathology and glial activation in aged hTau mice. *J Neuropathol Exp Neurol* **72**, 137-151 (2013).
47. K. Zweckberger *et al.*, Effect of early and delayed decompressive craniectomy on secondary brain damage after controlled cortical impact in mice. *J Neurotrauma* **23**, 1083-1093 (2006).
48. R. Boursereau, A. Donadieu, F. Dabertrand, D. Dubayle, J. L. Morel, Blood brain barrier precludes the cerebral arteries to intravenously-injected antisense oligonucleotide. *Eur J Pharmacol* **747**, 141-149 (2015).
49. K. Kenney *et al.*, Cerebral Vascular Injury in Traumatic Brain Injury. *Exp Neurol* **275 Pt 3**, 353-366 (2016).
50. C. L. Ho, C. M. Wang, K. K. Lee, I. Ng, B. T. Ang, Cerebral oxygenation, vascular reactivity, and neurochemistry following decompressive craniectomy for severe traumatic brain injury. *J Neurosurg* **108**, 943-949 (2008).
51. D. S. DeWitt, D. S. Prough, Traumatic cerebral vascular injury: the effects of concussive brain injury on the cerebral vasculature. *J Neurotrauma* **20**, 795-825 (2003).
52. A. M. Andrews, E. M. Lutton, S. F. Merkel, R. Razmpour, S. H. Ramirez, Mechanical Injury Induces Brain Endothelial-Derived Microvesicle Release: Implications for Cerebral Vascular Injury during Traumatic Brain Injury. *Front Cell Neurosci* **10**, 43 (2016).
53. K. W. Wang *et al.*, Simvastatin attenuates the cerebral vascular endothelial inflammatory response in a rat traumatic brain injury. *Ann Clin Lab Sci* **44**, 145-150 (2014).

54. G. X. Yu *et al.*, Traumatic brain injury in vivo and in vitro contributes to cerebral vascular dysfunction through impaired gap junction communication between vascular smooth muscle cells. *J Neurotrauma* **31**, 739-748 (2014).
55. O. Y. Bang, M. Goyal, D. S. Liebeskind, Collateral Circulation in Ischemic Stroke: Assessment Tools and Therapeutic Strategies. *Stroke* **46**, 3302-3309 (2015).
56. H. C. Alves, F. T. Pacheco, A. J. Rocha, Collateral blood vessels in acute ischemic stroke: a physiological window to predict future outcomes. *Arq Neuropsiquiatr* **74**, 662-670 (2016).
57. S. Grundmann *et al.*, A new intra-arterial delivery platform for pro-arteriogenic compounds to stimulate collateral artery growth via transforming growth factor-beta1 release. *J Am Coll Cardiol* **50**, 351-358 (2007).
58. P. Gupta, N. Khurana, T. Singh, D. Gupta, K. K. Dhingra, Bone marrow angiogenesis in aplastic anemia--a study of CD 34 and VEGF expression in bone marrow biopsies. *Hematology* **14**, 16-21 (2009).
59. D. Chalothorn, J. E. Faber, Strain-dependent variation in collateral circulatory function in mouse hindlimb. *Physiol Genomics* **42**, 469-479 (2010).
60. Y. Akamatsu *et al.*, Impaired leptomeningeal collateral flow contributes to the poor outcome following experimental stroke in the Type 2 diabetic mice. *J Neurosci* **35**, 3851-3864 (2015).
61. J. E. Lahteenvuo *et al.*, Vascular endothelial growth factor-B induces myocardium-specific angiogenesis and arteriogenesis via vascular endothelial growth factor receptor-1- and neuropilin receptor-1-dependent mechanisms. *Circulation* **119**, 845-856 (2009).
62. G. L. Semenza, Vasculogenesis, angiogenesis, and arteriogenesis: mechanisms of blood vessel formation and remodeling. *J Cell Biochem* **102**, 840-847 (2007).
63. I. Buschmann, W. Schaper, Arteriogenesis Versus Angiogenesis: Two Mechanisms of Vessel Growth. *News Physiol Sci* **14**, 121-125 (1999).
64. P. Carmeliet, Mechanisms of angiogenesis and arteriogenesis. *Nat Med* **6**, 389-395 (2000).
65. S. P. Deosarkar *et al.*, A Novel Dynamic Neonatal Blood-Brain Barrier on a Chip. *PLoS One* **10**, e0142725 (2015).
66. D. Chalothorn, J. A. Clayton, H. Zhang, D. Pomp, J. E. Faber, Collateral density, remodeling, and VEGF-A expression differ widely between mouse strains. *Physiol Genomics* **30**, 179-191 (2007).
67. M. H. Theus, J. Ricard, S. J. Glass, L. G. Travieso, D. J. Liebl, EphrinB3 blocks EphB3 dependence receptor functions to prevent cell death following traumatic brain injury. *Cell Death Dis* **5**, e1207 (2014).
68. G. Baumann, L. Travieso, D. J. Liebl, M. H. Theus, Pronounced hypoxia in the subventricular zone following traumatic brain injury and the neural stem/progenitor cell response. *Exp Biol Med (Maywood)* **238**, 830-841 (2013).
69. M. H. Theus, J. Ricard, J. R. Bethea, D. J. Liebl, EphB3 limits the expansion of neural progenitor cells in the subventricular zone by regulating p53 during homeostasis and following traumatic brain injury. *Stem Cells* **28**, 1231-1242 (2010).
70. B. Okyere *et al.*, Endothelial-Specific EphA4 Negatively Regulates Native Pial Collateral Formation and Re-Perfusion following Hindlimb Ischemia. *PLoS One* **11**, e0159930 (2016).

71. R. A. Defazio *et al.*, A protocol for characterizing the impact of collateral flow after distal middle cerebral artery occlusion. *Transl Stroke Res* **2**, 112-127 (2011).
72. C. A. Schneider, W. S. Rasband, K. W. Eliceiri, NIH Image to ImageJ: 25 years of image analysis. *Nat Methods* **9**, 671-675 (2012).
73. J. L. Lucitti *et al.*, Formation of the collateral circulation is regulated by vascular endothelial growth factor-A and a disintegrin and metalloprotease family members 10 and 17. *Circ Res* **111**, 1539-1550 (2012).
74. O. Y. Bang *et al.*, Impact of collateral flow on tissue fate in acute ischaemic stroke. *J Neurol Neurosurg Psychiatry* **79**, 625-629 (2008).
75. C. W. Lee *et al.*, Temporal patterns of gene expression after acute hindlimb ischemia in mice: insights into the genomic program for collateral vessel development. *J Am Coll Cardiol* **43**, 474-482 (2004).
76. W. M. Reid *et al.*, Strain-related differences after experimental traumatic brain injury in rats. *J Neurotrauma* **27**, 1243-1253 (2010).
77. J. A. Sherman, A. Hall, D. J. Malenka, E. D. De Muinck, M. Simons, Humoral and cellular factors responsible for coronary collateral formation. *Am J Cardiol* **98**, 1194-1197 (2006).
78. R. Vogel *et al.*, Collateral-flow measurements in humans by myocardial contrast echocardiography: validation of coronary pressure-derived collateral-flow assessment. *Eur Heart J* **27**, 157-165 (2006).
79. J. Liu *et al.*, Vascular remodeling after ischemic stroke: mechanisms and therapeutic potentials. *Prog Neurobiol* **115**, 138-156 (2014).
80. T. Babikian *et al.*, Molecular and physiological responses to juvenile traumatic brain injury: focus on growth and metabolism. *Dev Neurosci* **32**, 431-441 (2010).
81. D. S. DeWitt, D. S. Prough, C. L. Taylor, J. M. Whitley, Reduced cerebral blood flow, oxygen delivery, and electroencephalographic activity after traumatic brain injury and mild hemorrhage in cats. *J Neurosurg* **76**, 812-821 (1992).
82. D. C. Engel *et al.*, Changes of cerebral blood flow during the secondary expansion of a cortical contusion assessed by 14C-iodoantipyrine autoradiography in mice using a non-invasive protocol. *J Neurotrauma* **25**, 739-753 (2008).
83. D. S. Liebeskind, Stroke: the currency of collateral circulation in acute ischemic stroke. *Nat Rev Neurol* **5**, 645-646 (2009).
84. M. R. Goldstein, L. Mascitelli, F. Pezzetta, Hemorrhagic stroke in the Stroke Prevention by Aggressive Reduction in Cholesterol Levels study. *Neurology* **72**, 1448; author reply 1448-1449 (2009).
85. V. L. Feigin, C. M. Lawes, D. A. Bennett, C. S. Anderson, Stroke epidemiology: a review of population-based studies of incidence, prevalence, and case-fatality in the late 20th century. *Lancet Neurol* **2**, 43-53 (2003).
86. D. T. Winkler *et al.*, Spontaneous hemorrhagic stroke in a mouse model of cerebral amyloid angiopathy. *J Neurosci* **21**, 1619-1627 (2001).
87. E. M. Fanou *et al.*, Effect of Collaterals on Clinical Presentation, Baseline Imaging, Complications, and Outcome in Acute Stroke. *AJNR Am J Neuroradiol* **36**, 2285-2291 (2015).
88. W. Cai, W. Schaper, Mechanisms of arteriogenesis. *Acta Biochim Biophys Sin (Shanghai)* **40**, 681-692 (2008).

89. M. Heil, W. Schaper, Influence of mechanical, cellular, and molecular factors on collateral artery growth (arteriogenesis). *Circ Res* **95**, 449-458 (2004).
90. E. C. Junger *et al.*, Cerebral autoregulation following minor head injury. *J Neurosurg* **86**, 425-432 (1997).
91. S. Strebel, A. M. Lam, B. F. Matta, D. W. Newell, Impaired cerebral autoregulation after mild brain injury. *Surg Neurol* **47**, 128-131 (1997).
92. J. Becelewski, K. Pierzchala, [Cerebrovascular reactivity in patients with mild head injury]. *Neurol Neurochir Pol* **37**, 339-350 (2003).
93. J. Thompson, W. Sebastianelli, S. Slobounov, EEG and postural correlates of mild traumatic brain injury in athletes. *Neurosci Lett* **377**, 158-163 (2005).
94. E. M. Buckley *et al.*, Decreased microvascular cerebral blood flow assessed by diffuse correlation spectroscopy after repetitive concussions in mice. *J Cereb Blood Flow Metab* **35**, 1995-2000 (2015).
95. H. Van Aken, J. Van Hemelrijck, Influence of anesthesia on cerebral blood flow and cerebral metabolism: an overview. *Agressologie* **32**, 303-306 (1991).
96. A. Marmarou *et al.*, A new model of diffuse brain injury in rats. Part I: Pathophysiology and biomechanics. *J Neurosurg* **80**, 291-300 (1994).
97. M. A. Foda, A. Marmarou, A new model of diffuse brain injury in rats. Part II: Morphological characterization. *J Neurosurg* **80**, 301-313 (1994).
98. M. S. Chafi, G. Karami, M. Ziejewski, Biomechanical assessment of brain dynamic responses due to blast pressure waves. *Ann Biomed Eng* **38**, 490-504 (2010).
99. K. L. Lambertsen, R. Gregersen, B. Finsen, Microglial-macrophage synthesis of tumor necrosis factor after focal cerebral ischemia in mice is strain dependent. *J Cereb Blood Flow Metab* **22**, 785-797 (2002).
100. J. L. Hoover-Plow *et al.*, Strain and model dependent differences in inflammatory cell recruitment in mice. *Inflamm Res* **57**, 457-463 (2008).
101. J. I. Alvarez, T. Katayama, A. Prat, Glial influence on the blood brain barrier. *Glia* **61**, 1939-1958 (2013).
102. Z. G. Zhang *et al.*, Correlation of VEGF and angiopoietin expression with disruption of blood-brain barrier and angiogenesis after focal cerebral ischemia. *J Cereb Blood Flow Metab* **22**, 379-392 (2002).
103. N. Nourhaghighi, K. Teichert-Kuliszewska, J. Davis, D. J. Stewart, S. Nag, Altered expression of angiopoietins during blood-brain barrier breakdown and angiogenesis. *Lab Invest* **83**, 1211-1222 (2003).
104. L. Eklund, P. Saharinen, Angiopoietin signaling in the vasculature. *Exp Cell Res* **319**, 1271-1280 (2013).
105. M. V. Sofroniew, Reactive astrocytes in neural repair and protection. *Neuroscientist* **11**, 400-407 (2005).
106. E. Fung, A. Helisch, Macrophages in collateral arteriogenesis. *Front Physiol* **3**, 353 (2012).
107. J. M. van Golde *et al.*, Impaired collateral recruitment and outward remodeling in experimental diabetes. *Diabetes* **57**, 2818-2823 (2008).

Chapter 4:
Non-essential Role for the NLRP1 Inflammasome Complex following Traumatic Brain Injury

Thomas Brickler, Kisha Gresham, Irving C. Allen, Armand Meza, Sheryl Coutermarsh-Ott, Tere M. Williams, Daniel E. Rothschild and Michelle H. Theus

The Department of Biomedical Sciences and Pathobiology, Virginia-Maryland Regional College of Veterinary Medicine, 215 Duck Pond Drive, Blacksburg, VA, 24061 USA

Abstract

Traumatic brain injury (TBI) elicits the immediate production of pro-inflammatory cytokines which participate in regulating the immune response. While the mechanisms of adaptive immunity in secondary injury are well-characterized, the role of the innate response is unclear. Recently, the NLR inflammasome has been shown to become activated following TBI, causing processing and release of interleukin-1β (IL-1β). The inflammasome is a multi-protein complex consisting of nucleotide-binding domain and leucine-rich repeat containing proteins (NLR), caspase-1 and apoptosis-associated speck-like protein (ASC). ASC has been shown to be upregulated after TBI and is critical in coupling the proteins during complex formation resulting in IL-1β cleavage. To directly test whether inflammasome activation contributes to acute TBI-induced damage, we assessed IL-1β, IL-18 and IL-6 expression, contusion volume, hippocampal cell death and motor behavior recovery in *Nlrp1*$^{-/-}$, *Asc*$^{-/-}$ and wild type mice after controlled cortical impact (CCI) injury. Although IL-1β expression is significantly attenuated in the cortex of *Nlrp1*$^{-/-}$ and *Asc*$^{-/-}$ mice following CCI injury, no difference in motor recovery, cell death or contusion volume is observed compared to wild type. These findings indicate that inflammasome activation does not significantly contribute to acute neural injury in the mouse CCI model.

Introduction

Mechanical trauma to the CNS results in the disruption of the cellular microenvironment leading to massive necrotic and apoptotic loss of neuronal and glia populations. The progressive cascade of secondary events, including ischemia, inflammation, excitotoxicity and free radial release contribute to neural tissue damage. Activation of the innate immune response including microglia, peripheral-derived macrophages and astrocytes (1-3), can lead to the expression of pro-inflammatory cytokines, chemokines and reactive oxygen species, thereby triggering the inflammatory responses in the central nervous system (CNS). Recently, the initiation of such a response following tissue injury was shown to involve a multi-protein complex called the inflammasome (4). This cytosolic complex enables the activation of pro-inflammatory caspases, mainly caspase-1 (5, 6) resulting in a potent inflammatory response. Inflammasome complexes generally have three main components: an NLR protein; the enzyme caspase-1; and an adaptor protein that facilitates the interaction between the two. The NOD-like receptors (NLRs) are critical in this process and members of the inflammasome forming NLR subfamily recruit the adapter apoptosis-associated speck-like protein (ASC) to activate caspase-1. Currently, at least 8 different NLR proteins are well characterized as being capable of inflammasome formation under a diverse range of stimuli. In the brain, the inflammasome forming NLRs NLRP1, NLRP2, and NLRP3 have each been shown to modulate caspase-1 activation and the subsequent processing of IL-1β and IL-18, primarily from glia cells (7-10). The CNS is particularly sensitive to IL-1β and IL-18 signaling since multiple neural cell types express receptors for these cytokines (11-13). In addition, activated caspase 1 can mediate a form of necrotic cell death known as pyroptosis (14-16), making it a potential candidate for cell death signaling within neurons following injury. Therefore, induction of the NLR-mediated inflammasome complex could contribute to the pro-inflammatory

milieu as well as neuronal pyroptosis following immunopathogenic conditions such as traumatic brain injury (TBI). Interestingly, recent studies have demonstrated assembly of the NLRP1 and NLRP3-inflammasome complex including increased expression of ASC, activation of caspase 1 and processing of IL-1β in a rat model of TBI (8, 9). Furthermore, therapeutic administration of anti-ASC neutralizing antibodies was shown to reduce the innate immune response and significantly decrease contusion volume in the same model (9). These studies suggest that inflammasome activation plays a critical role in acute neural injury and that pyropotosis may be a key element of neuronal cell death following brain trauma.

To better understand the role of the NLRP1 inflammasome complex in TBI-induced damage, we sought to evaluate the effects of NLRP1 and ASC gene deletion on cortical tissue loss in a murine model of controlled cortical impact (CCI) injury. This model produces a well-demarcated cortical lesion that mimics the contusions commonly observed in TBI patients. Because the pathophysiological sequela of TBI is dependent on impact severity and location, we investigated whether the absence of inflammasome activation impacts the histopathological outcome using this distinct model. The overall goal of this study was to assess the role of the NLR inflammasome following CCI injury by quantifying IL1- β, IL18 expression and determine whether inflammasome disruption impacts cortical contusion volume and motor recovery in wild type, *Nlrp1*$^{-/-}$ and *Asc*$^{-/-}$ mice.

Materials and methods

Animals/Ethics Statement

The generation and characterization of *Nlrp1*$^{-/-}$ and *Asc*$^{-/-}$ mice have been previously described (17, 18). All mice were maintained on the C57Bl/6 background and all animals were

genotyped using standard PCR analysis prior to each study. All experiments were conducted in accordance with the NIH Guide for the Care and Use of Laboratory Animals and were conducted under the approval of the Virginia Tech Institutional Animal Care and Use Committee (IACUC; #12-081) and the Virginia Maryland Regional College of Veterinary Medicine.

CCI Injury.

Male mice ages 2-4 months were anesthetized with ketamine and xylazine by intraperitoneal (i.p.) injection and positioned in a stereotaxic frame (19, 20). Body temperature was monitored with a rectal probe and maintained at 37°C with a controlled heating pad set. A 5mm craniotomy was made using a portable drill over the right parietal-temporal cortex (−2.5 mm A/P and 2.0 mm lateral from bregma). Injury was induced by moderate CCI using the *e*CCI- 6.3 device (Custom Design & Fabrication; 4mm impounder) at a velocity of 3.5 m/s, depth of 0.5 mm, and 150 ms impact duration (19, 20). Sham controls received anesthesia, skin incisions and sutures only. Following injury, the incision was closed using Vetbond tissue adhesive (3M, St. Paul, MN, USA) and the animals were placed into a heated cage to maintain body temperature for 1 h post injury. At 1, 3 or 14 days post-CCI injury, mice were anesthetized and brain tissue removal was performed following decapitation. Fresh frozen tissue was embedded in OCT and sectioned at 30 um thick. Five serial coronal sections were (300um apart) stained for NISSL substance (21). Rotarod behavior assessment was performed as previously described (21).

Evaluation of contusion volume

Lesion or contusion volume was assessed by a blinded investigator using Caveleri Estimator from StereoInvestigator (MicroBrightField, Williston, VT, USA) and an Olympus

BX51TRF motorized microscope (Olympus America, Center Valley, PA, USA). Contusion volume (mm^3) was determined as previously described (21). Briefly, volume analysis was performed by estimating the area of tissue loss in the ipsilateral cortical hemisphere for five coronal serial sections at or around the epicenter (−1.1 to -2.6 mm posterior from bregma) of injury. Nissl stained serial sections were viewed under brightfield illumination at a magnification of 4x. A random sampling scheme was used that estimates every 10th section from rostral to caudal, yielding five total sections to be analyzed. A randomly placed grid with 100 µm spaced points was placed over the ipsilateral hemisphere and the area of contusion was marked within each grid. Contusion boundaries were identified by loss of NISSL staining, pyknotic neurons and tissue hemorrhage. The contoured areas, using grid spacing, was then used to estimate total tissue volume based on section thickness, section interval and total number of sections within the Caveleri program, StereoInvestigator. Data is represented as volume of tissue loss or contusion volume (mm^3) for wild type, *Nlrp1*$^{-/-}$ and *Asc*$^{-/-}$ mice.

Evaluation of protein Cytokine levels in cortical tissue samples

Protein was isolated from cortical tissue samples of wild type, *Nlrp1*$^{-/-}$ and *Asc*$^{-/-}$ mice at 1 day post-CCI injury as previously described (21). Briefly, fresh brain tissue was dissected in L15 (Gibco) media on ice and homogenized in RIPA buffer (pH 7.5, 1% NP-40, 1% sodium-deoxycholate, 0.1% SDS, 0.15 M NaCl, 2 mM EDTA and 0.01 M sodium phosphate) in the presence of Complete protease inhibitor cocktail (Roche, Florence, SC, USA) and phosphatase inhibitor cocktail 2 (Sigma-Aldrich, St. Louis, MO, USA). Supernatant was collected by centrifuging at 14 000 × *g* for 30 min at 4 °C and the Lowry assay was used for the determination of protein concentration (Pierce, Rockford, IL, USA). Protein samples were then tested for IL-1β,

IL-18, and IL-6 expression levels using ELISA (BD Biosciences), as previously described (22). Final concentrations of each cytokine were calculated based on internal standard controls and represented as pg/ml then normalized to the amount of protein (mg) loaded per well of the ELISA and represented at (pg/ml)/mg for each sample. This is a standard procedure to account for differences in starting protein levels that could significantly influence the final concentration of each cytokine (23-25).

Meta-data Analysis

The microarray data was generated following a metadata analysis or data mining of publically available datasets using a publically accessible microarray meta-analysis NextBio search engine; Available: http://www.nextbio.com/b/search/ba.nb. The data analysis was performed from the following datasets (human: GSE2392, 1432, 10612, 12837, 12305 12679; mouse: GSE17256, 10246, 9566, 11288; TBI study: GSE2392**).**

Statistical analysis.

Data was graphed using GraphPad Prism, version 4 (GraphPad Software, Inc., San Diego, CA). Student's two-tailed t test was used for comparison of two experimental groups. Multiple comparisons were done using one-way and two-way ANOVA where appropriate followed by Tukey test for multiple pairwise examinations. Changes were identified as significant if P was less than 0.05. Mean values were reported together with the standard deviation (SD).

Results

NLRP1 inflammasome activation does not contribute to acute cortical damage after CCI injury

Inflammasome complex formation has been shown to play a critical role in initiating inflammation in a variety of settings (26), though our understanding of its role in neuroinflammation is limited. Here, we sought to analyze the effects of inflammasome disruption on acute neural tissue damage and cytokine production following TBI. Specifically, we evaluated injury outcome in *Nlrp1*$^{-/-}$ and *Asc*$^{-/-}$ mice, using the controlled cortical impact (CCI) model (19-21), at 3 days post-injury. Serial sections were subjected to NISSL staining and contusion boundaries were demarcated by loss of NISSL stain, pyknotic neurons and tissue hemorrhage. Using the Caveleri estimator, we found no significant difference in contusion volume (F=1.37, P=0.3) among wild type (4.22 $\pm$ 0.97mm^3; n=8), *Nlrp1*$^{-/-}$ (3.70 $\pm$ 1.12mm^3 n=7) and *Asc*$^{-/-}$ (4.57 $\pm$ 1.43mm^3; n=5) mice at 3 days post-CCI (Figure 1A-1C and 1G) or 14 days (F=1.07; P=0.49); (3.113 $\pm$ 0.85mm^3 n=8; 3.0 $\pm$ 1.2mm^3 n=5; 3.76 $\pm$ 0.66mm^3 n=5; respectively) (Figure 1D-1F) post-CCI injury. These results indicate that genetic ablation of specific genes known to be involved in the formation of the NLR inflammasome complex has no effect on neural tissue loss in the cortex following acute TBI. We also performed Rotarod behavioral analysis to test whether motor deficit and recovery was affected by inflammasome disruption following CCI-injury. Mice were pre-trained on the Rotarod 4 days prior to CCI-injury then subjected to motor assessment at 3, 7 and 14 days post-sham or -CCI injury. Time to fall was record then normalized to the average baseline time for each mouse. No differences between groups was seen following sham injury for each time points tested (Figure 1H). Although motor deficits were observed following CCI-injury, no difference between groups was observed in motor ability at 3 days (wild type 60.07% $\pm$ 18.4 n=9; *Nlrp1*$^{-/-}$ 55.7% $\pm$ 9.1 n=5; *ASC*$^{-/-}$ 45.44% $\pm$ 10.5 n=5) compared to baseline, or at any other

time point tested (Figure 1I). These data correlate with contusion volume estimates and confirm that inflammasome disruption has no effect on neural tissue loss or motor function after CCI-injury.

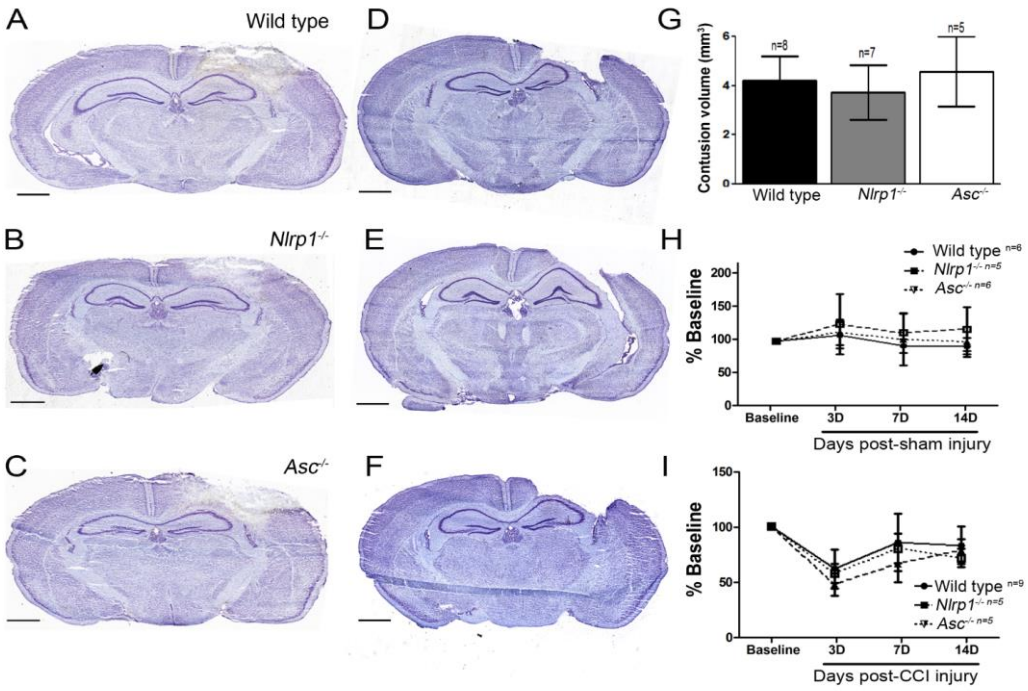

Figure 1. Genetic disruption of the NLRP1 inflammasome complex has no effect on contusion volume and motor deficits following CCI-injury. Using Caveleri estimator on Nissl stained sections collected from (A, D) Wild type, (B, E) *Nlrp1*$^{-/-}$, and (C, F) *Asc*$^{-/-}$ brains at 3 and 14 days post-injury, respectively, shows no significant change in contusion volume (mm^3). D) Bar graph represents mean contusion volume $\pm$ SD in wild type, *Nlrp1*$^{-/-}$ and *Asc*$^{-/-}$ mice (n=5-8 per group). Rotarod assessment or motor function was performed in each group and demonstrate no significant difference between sham-injured mice (H) or CCI-injured mice (I). n=5-9 per group; represented as mean $\pm$ SD.

Next, we investigated the protein expression of the pro-inflammatory cytokines IL-1β, IL-18 and IL-6 in the cortex of *Nlrp1*$^{-/-}$, *Asc*$^{-/-}$ and wild type mice following CCI injury. Following injury, we collected cortical tissue samples from the ipsilateral and contralateral hemispheres of sham and CCI-injured mice at 24 hours. Total IL-1β, IL-18, and IL-6 levels were quantified using ELISA. Our findings demonstrate that CCI injury results in a significant increase in IL-1β (1.3-fold; 78.2 $\pm$ 13.6 pg/ml per mg protein) and IL-6 (5-fold; 229.3 $\pm$ 30.9) levels in the wild type CCI-injured ipsilateral cortex compared to un-injured contralateral (IL-1β 56.8 $\pm$ 2.9; IL-6 43.3 $\pm$ 29.2) or sham-injured ipsilateral tissue (IL-1β 45.3 $\pm$ 5.7; IL-6 56.6 $\pm$ 12.9) (Figure 2A and 2C). However, ipsilateral IL-1levels are significantly attenuated in CCI-injured *Nlrp1*$^{-/-}$ (51.9 $\pm$ 6.5) and *Asc*$^{-/-}$ (56.8 $\pm$ 3.7) mice where levels reach that of un-injured wild type samples (Figure 2A). On the other hand, we observed a similar increase in IL-6 in the injured cortex of wild type, *Nlrp1*$^{-/-}$ and *Asc*$^{-/-}$ mice (Figure 2C). Ipsilateral IL-6 levels are slightly reduced in *Nlrp1*$^{-/-}$ (172.6 $\pm$ 34.9) but not *Asc*$^{-/-}$ (197.4 $\pm$ 29.7) compared to wild type. Interestingly, no significant difference in IL-18 levels was found following CCI-injury although a reduced trend in all ipsilateral samples is observed (Figure 2B). We find that disruption of the NLRP1 inflammasome complex leads to an attenuation of IL-1β production, an end-product of the inflammasome complex, while having minimal effects on IL-6 following CCI injury. These data indicate that IL-1β does not significantly contribute to the neural tissue injury in this model. We further characterized the histopathological changes induced by CCI injury in wild type (Figure 2D), *Nlrp1*$^{-/-}$ (Figure 2E) and *Asc*$^{-/-}$ (Figure 2F) using H & E staining. For each strain of mice we found a well-demarcated area of necrosis, hemorrhage and loss of neuropil at 3 days post-CCI injury. In all sections tested, the surrounding devitalized brain tissue was vacuolated and contained numerous necrotic neurons (Figure 2 insets; thin arrows), low numbers of macrophages containing phagocytized erythrocytes and cellular

debris (Figure 2 insets; arrowheads), and numerous neutrophils present in the peri-lesion site and perivascular spaces (Figure 2 insets; thick arrows). No overt differences in the pathological phenotype was observed between the strains of mice following CCI injury.

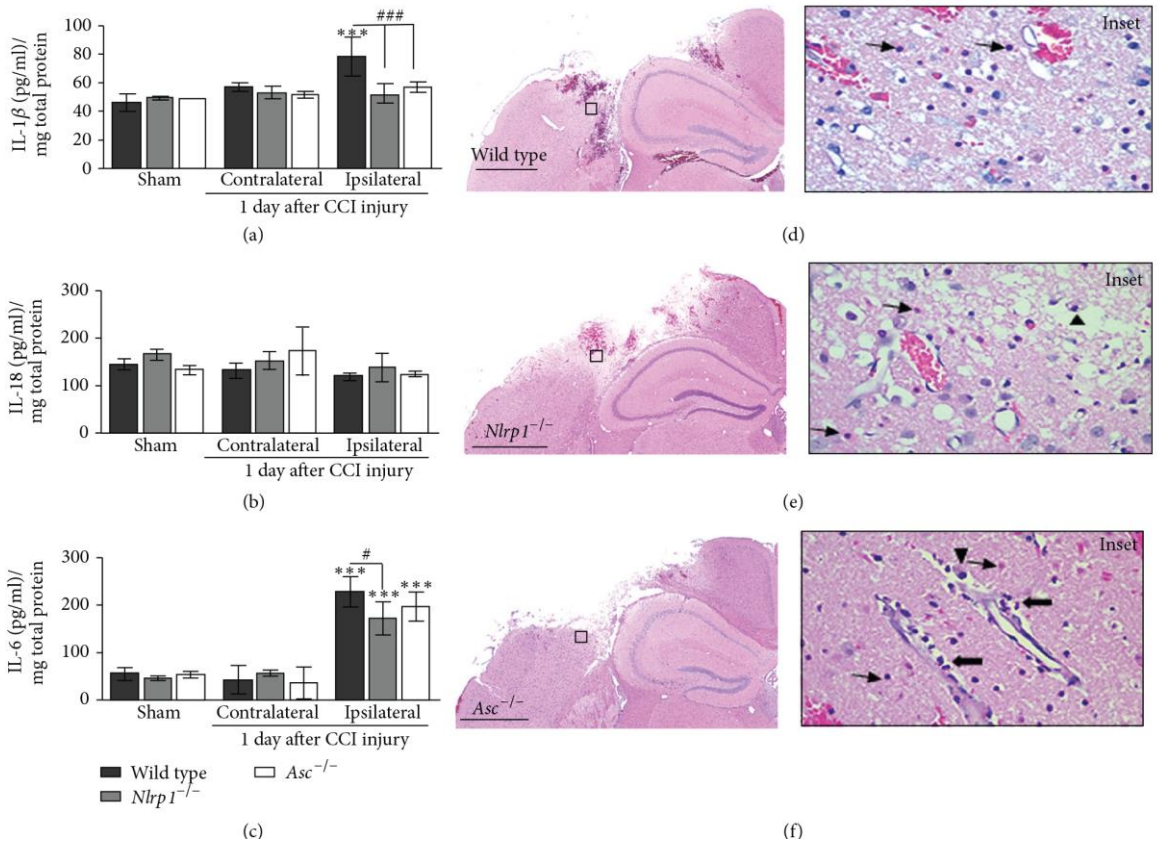

Figure 2. Cytokine protein expression and Histopathology in wild type, NLRP$^{-/-}$ and ASC$^{-/-}$ mice. Quantification of IL-1β, IL-18 and IL-6 in wild type, *Nlrp1*$^{-/-}$ and *Asc*$^{-/-}$ cortical tissue samples analyzed by ELISA at 1 day post-CCI injury. A) IL-1β, a direct release product of the inflammasome signaling cascade is significantly reduced in the ipsilateral cortex of *Nlrp1*$^{-/-}$ and *Asc*$^{-/-}$ compared to wild type cortex. B) No significant differences were observed in IL-18 levels at 1 day post-injury. C) IL-6 is increased in wild type, *Nlrp1*$^{-/-}$ and *Asc*$^{-/-}$ mice following trauma with

a slight attenuation in *Nlrp1*$^{-/-}$ ipsilateral cortex compared to wild type. *P<0.05; **P<0.01; ***P<0.001 compared to the contralateral and sham-injured cortical control samples. $^{\#}$P<0.05; $^{\#\#\#}$P<0.001 compared to wild type ipsilateral cortex. D) H&E staining on coronal brain sections from wild type, E) *Nlrp* $^{-/-}$ and F) *ASC* $^{-/-}$ mice shows no difference in histopathological outcome. Prominent cellular features present in all sections include large numbers of necrotic neurons (thin arrows), few macrophages (arrowheads) and neutrophils (thick arrows); insets. Scale bar= 1mm. n=4-5 per group; represented as mean $\pm$ SD.

Hippocampal dysfunction and cell loss is a hallmark of TBI (21, 27-29). In addition to cortical tissue loss, we also evaluated cell death in the dentate gyrus (DG) of wild type, *Nlrp1*$^{-/-}$ and *Asc*$^{-/-}$ mice (Figure 3). Serial coronal sections were stained with TUNEL and optical fractionator, StereoInvestigator was used to quantify the total number of TUNEL-positive cells in the contralateral and ipsilateral DG at 3 days post-CCI. In all three strains, our analysis revealed a similar increase in cell death in the ipsilateral DG compared to contralateral, however, no significant difference was observed (Figure 3A) between wild type (1507.7 $\pm$ 1221.2), *Nlrp1*$^{-/-}$ (1840.6 $\pm$ 862.3) and *Asc*$^{-/-}$ (1635.8 $\pm$ 315.8) mice in the ipsilateral DG (Figure B, C and D, respectively).

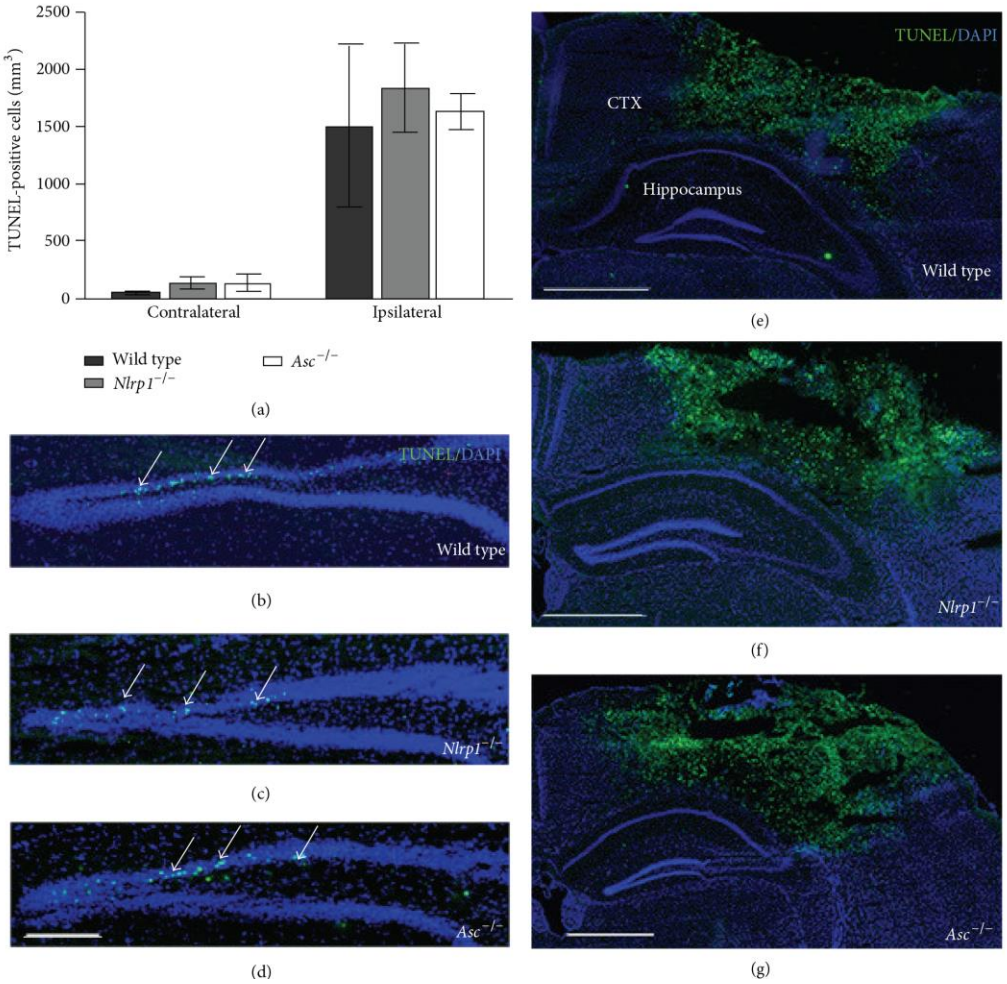

Figure 3. TUNEL analysis in the dentate gyrus of wild type, NLRP$^{-/-}$ and ASC$^{-/-}$ mice. (A) Quantification of TUNEL-positive cells in the ipsilateral and contralateral dentate gyrus (DG) 3 days followings CCI injury. Increased cell death is observed in the ipsilateral compared to contralateral DG in all groups, however, no significant difference in TUNEL is observed between wild type, *Nlrp1*$^{-/-}$ and *Asc*$^{-/-}$ mice following trauma. Representative immunofluorescence images of TUNEL (green)-DAPI (blue) co-labeled cells in the ipsilateral DG of (B) Wild type, (C) *Nlrp1*$^{-/-}$ and (C) *Asc*$^{-/-}$ mice. Images from 4x magnification; scale bar=1mm. n=4-5 per group; represented as mean $\pm$ SD.

Meta-analysis of NLRP1, ASC and IL-1β gene expression

To expand upon these findings, we sought to evaluate cell-specific expression in murine and human samples using a data mining bioinformatics approach. NLRP1, ASC and IL-1β expression was analyzed in immune and neural cell types using a publically accessible microarray meta-analysis search engine (Nextbio website. Available: http://www.nextbio.com/b/search/ba.nb.), as previously described (30). This analysis revealed highly variable levels between select cell populations relevant to the immune response compared to neural tissue. Overall, human *NLRP1, ASC and IL-1β* show greater than median cell expression in the naïve peripheral blood (PB) cells known to respond to trauma. These include neutrophils, macrophages and monocytes (Figure 4A-4C), with the exception of *IL-1β*, which has the highest level of expression in human microglial cells (Figure 4C). Brain-derived cell types show lower than median expression levels of these genes suggesting the greatest activity occurs in response to immune activation. *Nlrp1 (Nlrp1a; Nlrp1b; and Nlrp1c)* (Figure 4D) expression data has not been added to the datasets evaluated using this method. However, similar results to the human findings were obtained for *Asc* and *Il1-b* in naïve C57Bl/6 mice (Figure 4E and 4F; respectively), with the exception of neutrophils that express these genes in the bone marrow but not PB (data not shown).

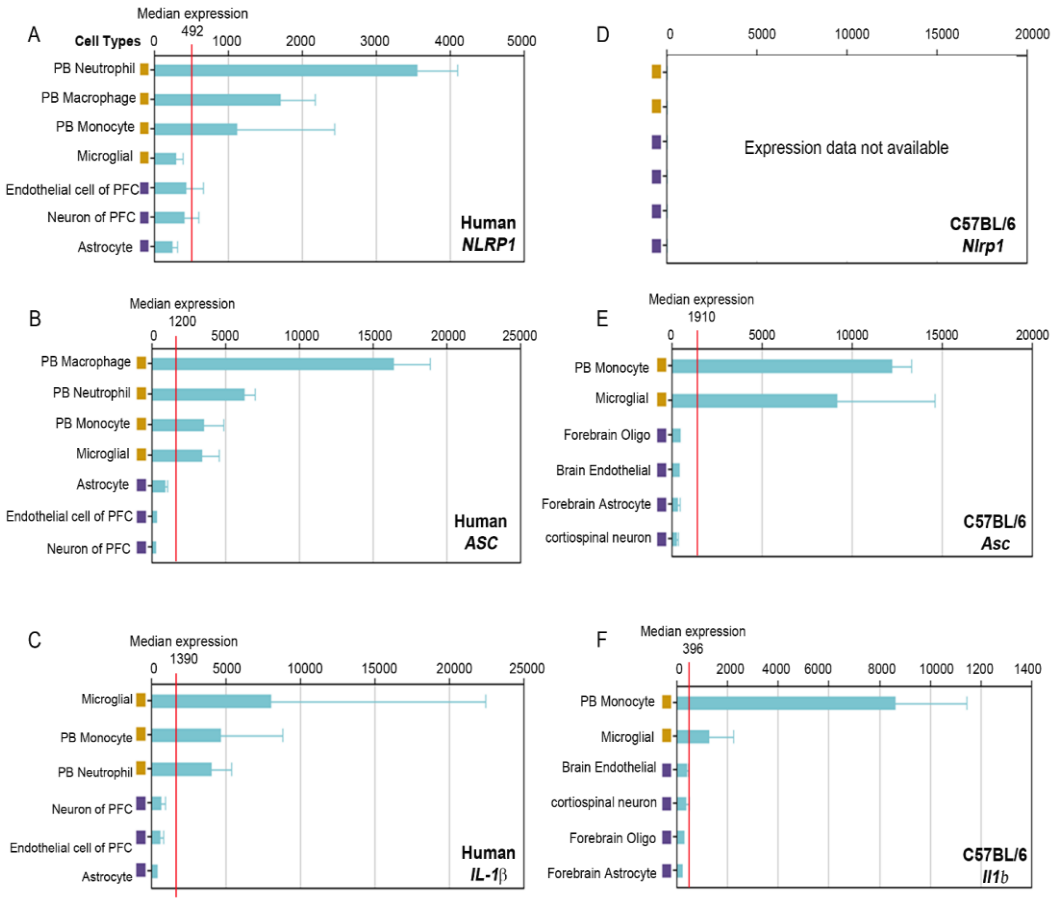

Figure 4. Cell specific gene expression of *NLRP1*, *ASC* and *IL-1β* in human and murine tissue. Expression of human **A)** *NLRP1*, **B)** *ASC* and **C)** *IL-1β* in relevant immune and neural system cell types was compiled using a publically accessible microarray meta-analysis search engine (Nextbio website: http://www.nextbio.com/b/search/ba.nb. Accessed 2014 Sept. 8). Expression of mouse **D)** *Nlrp1*, **E)** *Asc* and **F)** *Il1b* from the C57Bl/6 strain can be directly compared to the human expression profile in specific immune and neural cells. No gene expression data was available for *Nlrp1 (Nlrp1a, Nlrp1b, and Nlrp1c)* at the time the search engine was accessed. PB, peripheral blood; PFC, prefrontal cortex.

Finally, we compared our ELISA data with previous microarray obtained from murine cortical tissue samples following sham- and CCI injury at 4-72 hrs post-trauma using meta-analysis (31). At each time point tested from the datasets GSE2392, no change was observed in gene expression for *Nlrp1* or *Asc* between sham and injury levels (Figure 5). However, in agreement with our ELISA results the microarray metadata shows an increase in *Il1b* (1.8 fold) and *Il6* expression (2.54 fold) at 24 hr post-CCI injury (Figure 5A and 5C; respectively). Likewise, *Il1a* (data not shown; 8 hr post-injury) and the *Il1r1* (Figure 5) is also increased during acute trauma. Interestingly, at this time there was also an observed decrease (-1.28 fold) in Il18 expression. We also observed that *Ccl2* expression consistently showed the highest fold increase at each time point tested (5.78, 17.2, 8.86 and 5.59 fold; respectively). These results emphasize the trauma-induced changes seen in the inflammasome-related pathways at the transcription level.

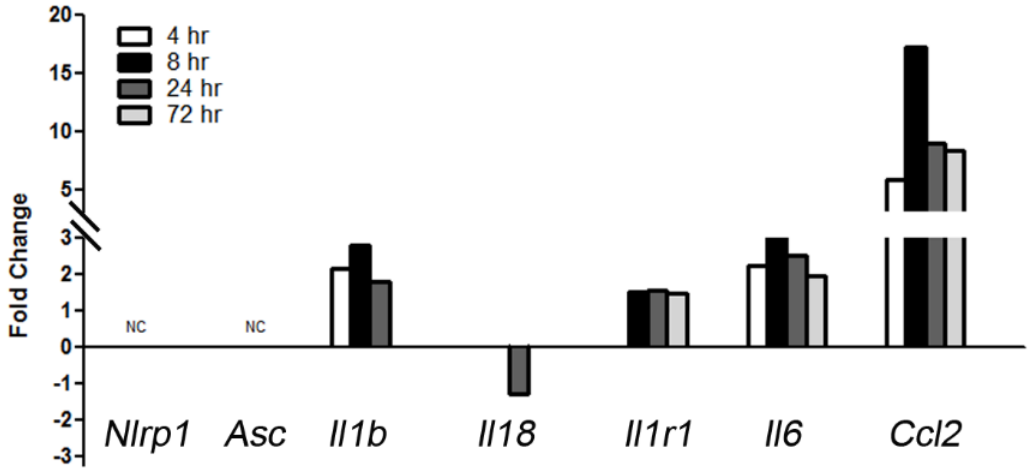

Figure 5. Time course of gene expression in the murine parietal cortex after CCI injury. Expression of several inflammasome related genes was compiled using the meta-analysis system. Cortical tissue samples from sham and CCI-injured mice were subjected to microarray analysis

(31). Changes in expression are represented as fold change from un-injured levels. No change in *Nlrp1* or *Asc* was detected, while greater expression is noted for *Il1b*, *Il1r1*, *Il6* and *Ccl2* at 4, 8, 24 or 72 hrs after trauma. Conversely, there was a reduced fold change (-1.28) in the expression of *Il18* at 24 hours post-CCI injury.

Discussion

New insights into the role of the innate NLR inflammasome complex during acute inflammation have prompted its investigation in the pathogenesis of numerous neurological diseases, including TBI (32, 33). The current study shows that genetic deletion of NLRP1 (*Nlrp1a, Nlrp1b and Nlrp1c*) or ASC, essential proteins for the assembly of the NLRP1 inflammasome complex, has no direct effect on cortical tissue loss, hippocampal cell death or motor behavior deficits. In this present study, we utilized the Rotarod as a measure of functional recovery following CCI injury in the motor cortex. This technique measures aspects of motor impairment that are not evident by either the beam-balance or beam-walking tasks in our model. For this reason our current experiments focused on the Rotarod, which is the most robust, sensitive and efficient index for assessing motor impairment produced by CCI injury (34). Although we find a significant attenuation of IL-1β in *Nlrp1*$^{-/-}$ or *Asc*$^{-/-}$ mice, histopathological changes seen following cortical trauma were similar to that found in wild type mice. These results are the first to identify a non-essential role for the NLR inflammasome in injury outcome following cortical brain trauma using a genetic approach. Our data is not consistent with previous findings that demonstrate significant protection following administration of ASC neutralizing antibodies in the rat lateral fluid percussion injury (FPI) model of TBI (9). This discrepancy may be due to species differences between rats and mice or possible variations in the cytokine profile induced between the CCI and

fluid percussion TBI models. Likewise, recent studies indicate that mouse and rat genetic factors may also mediate some of this variability (35). It is also possible that other compensatory mechanisms may be associated with TBI progression in the *Nlrp1*$^{-/-}$ and *Asc*$^{-/-}$ mice, which are completely devoid of NLRP1 inflammasome function from birth. The discrepancies observed in our model versus the prior study in rats underscore the need for further investigation to develop additional mechanistic insight into the role of the NLRP1 inflammasome following traumatic brain injury.

In the present study, we utilized NLRP1 and ASC gene targeted knockout mice, which have been previously shown to prevent NLRP1-mediated inflammasome complex formation during acute inflammation (17, 18). We demonstrate attenuated inflammasome function in the *Nlrp1*$^{-/-}$ and *Asc*$^{-/-}$ mice, as evidenced by reduction of IL-1β following acute CCI injury. Interestingly, IL18 levels were unaffected in the cortex after trauma (Figure 2B). In fact, we observed a trend towards reduced IL-18 levels in wild type, *Nlrp1*$^{-/-}$ and *Asc*$^{-/-}$ mice indicating that non-inflammasome regulated pathways may be acting to suppress IL-18 induction in response to cortical impact. This is further supported by our meta-analysis that also shows reduced expression of *Il-18* at the transcription level (Figure 5). Overall, we find abolishing IL-1B expression in the absence of ASC and Nlrp1 does not correlate with changes in lesion volume or behavioral outcome after controlled cortical impact. Therefore, in order to identify key cytokines that may play a more central role, we further analyzed IL-6, as this cytokine has been largely implicated in tissue damage and progression of cavity formation. IL-6 generation has also been shown to be significantly modulated by several NLRs and is often dysregulated in NLR deficient mice in other models beyond the nervous system (36-38). Compared to the ~2-fold increase in IL-1β, there was a ~6-fold increase in IL-6 expression after TBI implying this protein, among others, are more central to

the inflammatory response in brain trauma. NLRP1 has not previously been shown to regulate IL-6 and the small reduction seen in the cortical tissue samples of TBI-injured *Nlrp1*$^{-/-}$ mice (Figure 2C) is somewhat surprising. We do not believe such minimal changes would impact the overall downstream effects on IL-6 production. However, it is possible that earlier induction (6-12hrs) of IL-6 is unaffected, which is also critical for stimulating the inflammatory milieu and progression of injury.

ASC, NLRP1 and IL-1β are expressed in neurons, glial, vascular endothelial and peripheral-derived immune cells (36, 37) and have been shown to be up-regulated after TBI (8, 9). These immune mediators play a vital role in activating the inflammatory response, which is a necessary component of repair and healing (38, 39). However, acute inflammation also exacerbates tissue damage in the brain for which IL-1 has been implicated as a major player (40, 41). Previous studies in ischemic stroke have demonstrated that exogenous IL-1 administration can exacerbate neuronal injury (42) while inhibition of caspase-1 or IL-1 receptor antagonism provides protection (43, 44). Deletion of IL-1 α and IL-1 β also can significantly reduce ischemic injury in mice (45). Furthermore, current clinical trials of IL-1 receptor antagonist are underway in patients who suffer acute stroke (46). However, our studies indicate that attenuation of IL-1β does not correlate with neuroprotection in CCI-injured *Nlrp1*$^{-/-}$ and *Asc*$^{-/-}$ mice suggesting that NLR inflammasome activation and IL-1 production does not play a significant role in neuronal damage after TBI. Injury-induced expression of IL-1 β in the current model may be too weak to participate in eliciting a majority of the immune response. Our data shows that IL-1β is minimally upregulated at 24 hr (1.3-fold increase) as compared to IL-6 (5-fold increase) suggesting that other pro-inflammatory pathways may play a more prominent role (47). For example, TNF-α expression is consistently upregulated across several TBI models in rodents including CCI, FPI and stab wound

injury, with detectable levels at 1 h post-injury, maximal concentration at 3-8 h, and a decline at 24 h post-injury (48, 49). Similarly, IL-6 is also an important mediator of neuroinflammation in the brain (50, 51) suggesting that these and other cytokine pathways may predominate following CCI injury. Indeed, human clinical studies have demonstrated that levels of TNF-α, IL-6, IL-8 and IL-10, correlate with TBI severity and rates of complication (52-55).

We conclude that disruption of the NLRP1 inflammasome has no effect on injury outcome in the mouse CCI model. Inflammasome activation and subsequent IL-1 β expression are not a limiting factor in behavioral deficits, neuronal loss in the cortex or hippocampus following acute injury. NLR inflammasome have been shown to be involved in a diverse range of conditions associated with aberrant inflammation, including many neurological and neurodegenerative conditions. While our current negative findings using a genetic approach were unexpected, they emphasize the need to further explore the clinical relevance and mechanistic details underlying the NLRP1 inflammasome in brain injury and other related central nervous system disorders.

Acknowledgements: The authors would like to thank Dr. Beverly H. Koller (UNC Chapel Hill) for kindly providing the *Nlrp1*-/- mice used in this study. We would also like to recognize the VT-PREP and VT-IMSD Programs for student support (T.M.W.) and the Virginia Maryland College of Veterinary Medicine (I.C.A.; D.R.).

References

1. Rivest S: **Regulation of innate immune responses in the brain**. *Nature reviews Immunology* 2009, **9**(6):429-439.
2. Loane DJ, Byrnes KR: **Role of microglia in neurotrauma**. *Neurotherapeutics : the journal of the American Society for Experimental NeuroTherapeutics* 2010, **7**(4):366-377.
3. Chen S, Pickard JD, Harris NG: **Time course of cellular pathology after controlled cortical impact injury**. *Exp Neurol* 2003, **182**(1):87-102.
4. Martinon F, Burns K, Tschopp J: **The inflammasome: a molecular platform triggering activation of inflammatory caspases and processing of proIL-beta**. *Molecular cell* 2002, **10**(2):417-426.
5. Chen S, Sun B: **Negative regulation of NLRP3 inflammasome signaling**. *Protein & cell* 2013, **4**(4):251-258.
6. Rathinam VA, Vanaja SK, Fitzgerald KA: **Regulation of inflammasome signaling**. *Nature immunology* 2012, **13**(4):333-342.
7. Minkiewicz J, de Rivero Vaccari JP, Keane RW: **Human astrocytes express a novel NLRP2 inflammasome**. *Glia* 2013, **61**(7):1113-1121.
8. Liu HD, Li W, Chen ZR, Hu YC, Zhang DD, Shen W, Zhou ML, Zhu L, Hang CH: **Expression of the NLRP3 inflammasome in cerebral cortex after traumatic brain injury in a rat model**. *Neurochemical research* 2013, **38**(10):2072-2083.
9. de Rivero Vaccari JP, Lotocki G, Alonso OF, Bramlett HM, Dietrich WD, Keane RW: **Therapeutic neutralization of the NLRP1 inflammasome reduces the innate immune response and improves histopathology after traumatic brain injury**. *Journal of cerebral blood flow and metabolism : official journal of the International Society of Cerebral Blood Flow and Metabolism* 2009, **29**(7):1251-1261.
10. Jha S, Srivastava SY, Brickey WJ, Iocca H, Toews A, Morrison JP, Chen VS, Gris D, Matsushima GK, Ting JP: **The inflammasome sensor, NLRP3, regulates CNS inflammation and demyelination via caspase-1 and interleukin-18**. *The Journal of neuroscience : the official journal of the Society for Neuroscience* 2010, **30**(47):15811-15820.
11. Alboni S, Montanari C, Benatti C, Sanchez-Alavez M, Rigillo G, Blom JM, Brunello N, Conti B, Pariante MC, Tascedda F: **Interleukin 18 activates MAPKs and STAT3 but not NF-kappaB in hippocampal HT-22 cells**. *Brain, behavior, and immunity* 2014, **40**:85-94.
12. Crampton SJ, Collins LM, Toulouse A, Nolan YM, O'Keeffe GW: **Exposure of foetal neural progenitor cells to IL-1beta impairs their proliferation and alters their differentiation - a role for maternal inflammation?** *Journal of neurochemistry* 2012, **120**(6):964-973.
13. Miyoshi K, Obata K, Kondo T, Okamura H, Noguchi K: **Interleukin-18-mediated microglia/astrocyte interaction in the spinal cord enhances neuropathic pain processing after nerve injury**. *The Journal of neuroscience : the official journal of the Society for Neuroscience* 2008, **28**(48):12775-12787.
14. Adamczak SE, de Rivero Vaccari JP, Dale G, Brand FJ, 3rd, Nonner D, Bullock MR, Dahl GP, Dietrich WD, Keane RW: **Pyroptotic neuronal cell death mediated by the AIM2 inflammasome**. *Journal of cerebral blood flow and metabolism : official journal*

of the International Society of Cerebral Blood Flow and Metabolism 2014, **34**(4):621-629.
15. Bergsbaken T, Fink SL, Cookson BT: **Pyroptosis: host cell death and inflammation**. *Nature reviews Microbiology* 2009, **7**(2):99-109.
16. Zhang WH, Wang X, Narayanan M, Zhang Y, Huo C, Reed JC, Friedlander RM: **Fundamental role of the Rip2/caspase-1 pathway in hypoxia and ischemia-induced neuronal cell death**. *Proceedings of the National Academy of Sciences of the United States of America* 2003, **100**(26):16012-16017.
17. Kovarova M, Hesker PR, Jania L, Nguyen M, Snouwaert JN, Xiang Z, Lommatzsch SE, Huang MT, Ting JP, Koller BH: **NLRP1-dependent pyroptosis leads to acute lung injury and morbidity in mice**. *Journal of immunology* 2012, **189**(4):2006-2016.
18. Mariathasan S, Newton K, Monack DM, Vucic D, French DM, Lee WP, Roose-Girma M, Erickson S, Dixit VM: **Differential activation of the inflammasome by caspase-1 adaptors ASC and Ipaf**. *Nature* 2004, **430**(6996):213-218.
19. Baumann G, Travieso L, Liebl DJ, Theus MH: **Pronounced hypoxia in the subventricular zone following traumatic brain injury and the neural stem/progenitor cell response**. *Exp Biol Med (Maywood)* 2013, **238**(7):830-841.
20. Theus MH, Ricard J, Bethea JR, Liebl DJ: **EphB3 limits the expansion of neural progenitor cells in the subventricular zone by regulating p53 during homeostasis and following traumatic brain injury**. *Stem Cells* 2010, **28**(7):1231-1242.
21. Theus MH, Ricard J, Glass SJ, Travieso LG, Liebl DJ: **EphrinB3 blocks EphB3 dependence receptor functions to prevent cell death following traumatic brain injury**. *Cell Death Dis* 2014, **5**:e1207.
22. Gris D, Ye Z, Iocca HA, Wen H, Craven RR, Gris P, Huang M, Schneider M, Miller SD, Ting JP: **NLRP3 plays a critical role in the development of experimental autoimmune encephalomyelitis by mediating Th1 and Th17 responses**. *Journal of immunology* 2010, **185**(2):974-981.
23. Allen IC, TeKippe EM, Woodford RM, Uronis JM, Holl EK, Rogers AB, Herfarth HH, Jobin C, Ting JP: **The NLRP3 inflammasome functions as a negative regulator of tumorigenesis during colitis-associated cancer**. *The Journal of experimental medicine* 2010, **207**(5):1045-1056.
24. Allen IC, Wilson JE, Schneider M, Lich JD, Roberts RA, Arthur JC, Woodford RM, Davis BK, Uronis JM, Herfarth HH *et al*: **NLRP12 suppresses colon inflammation and tumorigenesis through the negative regulation of noncanonical NF-kappaB signaling**. *Immunity* 2012, **36**(5):742-754.
25. Williams TM, Leeth RA, Rothschild DE, McDaniel DK, Coutermarsh-Ott SL, Simmons AE, Kable KH, Heid B, Allen IC: **Caspase-11 attenuates gastrointestinal inflammation and experimental colitis pathogenesis**. *American journal of physiology Gastrointestinal and liver physiology* 2015, **308**(2):G139-150.
26. Pedra JH, Cassel SL, Sutterwala FS: **Sensing pathogens and danger signals by the inflammasome**. *Current opinion in immunology* 2009, **21**(1):10-16.
27. Levin HS: **Cognitive function outcomes after traumatic brain injury**. *Curr Opin Neurol* 1998, **11**(6):643-646.
28. Hamm RJ, Dixon CE, Gbadebo DM, Singha AK, Jenkins LW, Lyeth BG, Hayes RL: **Cognitive deficits following traumatic brain injury produced by controlled cortical impact**. *Journal of neurotrauma* 1992, **9**(1):11-20.

29. Hall ED, Sullivan PG, Gibson TR, Pavel KM, Thompson BM, Scheff SW: **Spatial and temporal characteristics of neurodegeneration after controlled cortical impact in mice: more than a focal brain injury**. *J Neurotrauma* 2005, **22**(2):252-265.
30. Kupershmidt I, Su QJ, Grewal A, Sundaresh S, Halperin I, Flynn J, Shekar M, Wang H, Park J, Cui W *et al*: **Ontology-based meta-analysis of global collections of high-throughput public data**. *PloS one* 2010, **5**(9).
31. Natale JE, Ahmed F, Cernak I, Stoica B, Faden AI: **Gene expression profile changes are commonly modulated across models and species after traumatic brain injury**. *Journal of neurotrauma* 2003, **20**(10):907-927.
32. Walsh JG, Muruve DA, Power C: **Inflammasomes in the CNS**. *Nature reviews Neuroscience* 2014, **15**(2):84-97.
33. Fan L, Young PR, Barone FC, Feuerstein GZ, Smith DH, McIntosh TK: **Experimental brain injury induces expression of interleukin-1 beta mRNA in the rat brain**. *Brain research Molecular brain research* 1995, **30**(1):125-130.
34. Hamm RJ, Pike BR, O'Dell DM, Lyeth BG, Jenkins LW: **The rotarod test: an evaluation of its effectiveness in assessing motor deficits following traumatic brain injury**. *Journal of neurotrauma* 1994, **11**(2):187-196.
35. Mills CD, Hains BC, Johnson KM, Hulsebosch CE: **Strain and model differences in behavioral outcomes after spinal cord injury in rat**. *Journal of neurotrauma* 2001, **18**(8):743-756.
36. Lechan RM, Toni R, Clark BD, Cannon JG, Shaw AR, Dinarello CA, Reichlin S: **Immunoreactive interleukin-1 beta localization in the rat forebrain**. *Brain research* 1990, **514**(1):135-140.
37. Boutin H, Kimber I, Rothwell NJ, Pinteaux E: **The expanding interleukin-1 family and its receptors: do alternative IL-1 receptor/signaling pathways exist in the brain?** *Molecular neurobiology* 2003, **27**(3):239-248.
38. Shechter R, London A, Varol C, Raposo C, Cusimano M, Yovel G, Rolls A, Mack M, Pluchino S, Martino G *et al*: **Infiltrating blood-derived macrophages are vital cells playing an anti-inflammatory role in recovery from spinal cord injury in mice**. *PLoS medicine* 2009, **6**(7):e1000113.
39. Popovich PG, Longbrake EE: **Can the immune system be harnessed to repair the CNS?** *Nature reviews Neuroscience* 2008, **9**(6):481-493.
40. Allan SM, Tyrrell PJ, Rothwell NJ: **Interleukin-1 and neuronal injury**. *Nature reviews Immunology* 2005, **5**(8):629-640.
41. Brough D, Tyrrell PJ, Allan SM: **Regulation of interleukin-1 in acute brain injury**. *Trends in pharmacological sciences* 2011, **32**(10):617-622.
42. Yamasaki Y, Matsuura N, Shozuhara H, Onodera H, Itoyama Y, Kogure K: **Interleukin-1 as a pathogenetic mediator of ischemic brain damage in rats**. *Stroke; a journal of cerebral circulation* 1995, **26**(4):676-680; discussion 681.
43. Relton JK, Rothwell NJ: **Interleukin-1 receptor antagonist inhibits ischaemic and excitotoxic neuronal damage in the rat**. *Brain research bulletin* 1992, **29**(2):243-246.
44. Hara H, Friedlander RM, Gagliardini V, Ayata C, Fink K, Huang Z, Shimizu-Sasamata M, Yuan J, Moskowitz MA: **Inhibition of interleukin 1beta converting enzyme family proteases reduces ischemic and excitotoxic neuronal damage**. *Proceedings of the National Academy of Sciences of the United States of America* 1997, **94**(5):2007-2012.

45. Boutin H, LeFeuvre RA, Horai R, Asano M, Iwakura Y, Rothwell NJ: **Role of IL-1alpha and IL-1beta in ischemic brain damage**. *The Journal of neuroscience : the official journal of the Society for Neuroscience* 2001, **21**(15):5528-5534.
46. Emsley HC, Smith CJ, Georgiou RF, Vail A, Hopkins SJ, Rothwell NJ, Tyrrell PJ, Acute Stroke I: **A randomised phase II study of interleukin-1 receptor antagonist in acute stroke patients**. *Journal of neurology, neurosurgery, and psychiatry* 2005, **76**(10):1366-1372.
47. Namas R, Ghuma A, Hermus L, Zamora R, Okonkwo DO, Billiar TR, Vodovotz Y: **The acute inflammatory response in trauma / hemorrhage and traumatic brain injury: current state and emerging prospects**. *The Libyan journal of medicine* 2009, **4**(3):97-103.
48. Fan L, Young PR, Barone FC, Feuerstein GZ, Smith DH, McIntosh TK: **Experimental brain injury induces differential expression of tumor necrosis factor-alpha mRNA in the CNS**. *Brain research Molecular brain research* 1996, **36**(2):287-291.
49. Kita T, Liu L, Tanaka N, Kinoshita Y: **The expression of tumor necrosis factor-alpha in the rat brain after fluid percussive injury**. *International journal of legal medicine* 1997, **110**(6):305-311.
50. Shohami E, Novikov M, Bass R, Yamin A, Gallily R: **Closed head injury triggers early production of TNF alpha and IL-6 by brain tissue**. *Journal of cerebral blood flow and metabolism : official journal of the International Society of Cerebral Blood Flow and Metabolism* 1994, **14**(4):615-619.
51. Taupin V, Toulmond S, Serrano A, Benavides J, Zavala F: **Increase in IL-6, IL-1 and TNF levels in rat brain following traumatic lesion. Influence of pre- and post-traumatic treatment with Ro5 4864, a peripheral-type (p site) benzodiazepine ligand**. *Journal of neuroimmunology* 1993, **42**(2):177-185.
52. Cinat ME, Waxman K, Granger GA, Pearce W, Annas C, Daughters K: **Trauma causes sustained elevation of soluble tumor necrosis factor receptors**. *Journal of the American College of Surgeons* 1994, **179**(5):529-537.
53. Hensler T, Sauerland S, Bouillon B, Raum M, Rixen D, Helling HJ, Andermahr J, Neugebauer EA: **Association between injury pattern of patients with multiple injuries and circulating levels of soluble tumor necrosis factor receptors, interleukin-6 and interleukin-10, and polymorphonuclear neutrophil elastase**. *The Journal of trauma* 2002, **52**(5):962-970.
54. Martin C, Boisson C, Haccoun M, Thomachot L, Mege JL: **Patterns of cytokine evolution (tumor necrosis factor-alpha and interleukin-6) after septic shock, hemorrhagic shock, and severe trauma**. *Critical care medicine* 1997, **25**(11):1813-1819.
55. Narayan RK, Michel ME, Ansell B, Baethmann A, Biegon A, Bracken MB, Bullock MR, Choi SC, Clifton GL, Contant CF *et al*: **Clinical trials in head injury**. *Journal of neurotrauma* 2002, **19**(5):503-557.

Appendix

NATURE PUBLISHING GROUP LICENSE
TERMS AND CONDITIONS

Apr 27, 2017

This Agreement between Thomas Brickler ("You") and Nature Publishing Group ("Nature Publishing Group") consists of your license details and the terms and conditions provided by Nature Publishing Group and Copyright Clearance Center.

License Number	4050871301480
License date	
Licensed Content Publisher	Nature Publishing Group
Licensed Content Publication	Nature Reviews Neuroscience
Licensed Content Title	Animal models of traumatic brain injury
Licensed Content Author	Ye Xiong, Asim Mahmood and Michael Chopp
Licensed Content Date	Feb 1, 2013
Licensed Content Volume	14
Licensed Content Issue	2
Type of Use	reuse in a dissertation / thesis
Requestor type	academic/educational
Format	print and electronic
Portion	figures/tables/illustrations
Number of figures/tables /illustrations	1
High-res required	no
Figures	Figure 1, experimental set-ups for the animal models of TBI
Author of this NPG article	no
Your reference number	10.1038
Title of your thesis / dissertation	Arteriogenesis as a Therapeutic Target for Traumatic Brian Injury
Expected completion date	Apr 2017
Estimated size (number of pages)	150
Requestor Location	Thomas Brickler 1 Duckpond Drive BLACKSBURG, VA 24061 United States Attn: Thomas Brickler
Billing Type	Invoice
Billing Address	Thomas Brickler 1 Duckpond Drive BLACKSBURG, VA 24061 United States Attn: Thomas Brickler